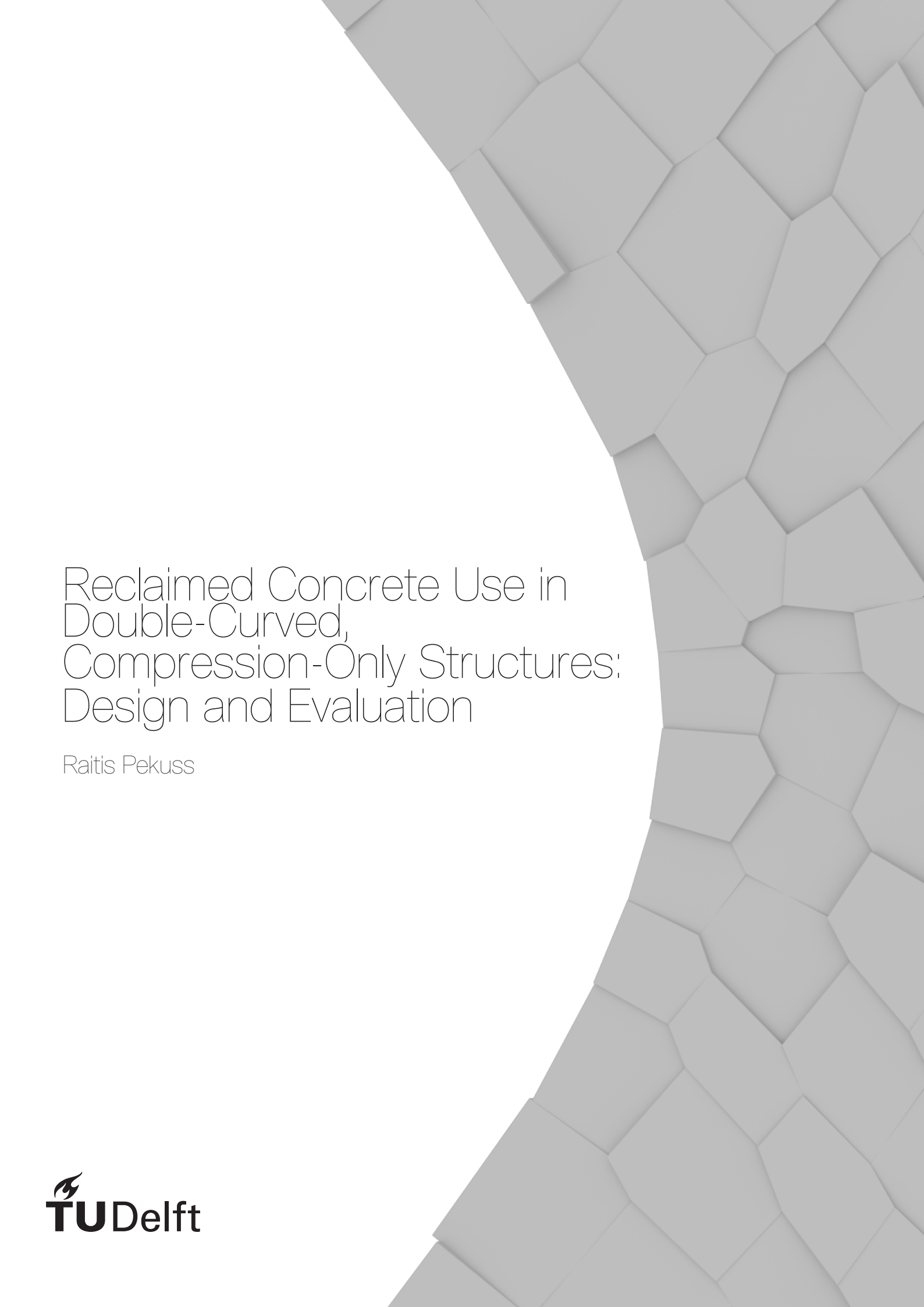

Reclaimed Concrete Use in Double-Curved, Compression-Only Structures: Design and Evaluation

Raitis Pekuss

TU Delft

Reclaimed Concrete Use in Double-Curved, Compression-Only Structures: Design and Evaluation

by

Raitis Pekuss

to obtain the degree of Master of Science
at the Delft University of Technology,
Faculty of Civil Engineering and Geosciences.

Student number:	5252962	
Project duration:	March, 2022 – December, 2023	
Thesis committee:	Dr. Mariana Popescu,	TU Delft, chair, daily supervisor
	Dr. Jeroen Coenders,	Packhunt, supervisor
	Prof.ir. Thijs Asselbergs,	TU Delft, supervisor
	Dr.ir. Roel Schipper,	TU Delft, supervisor

TU Delft

Acknowledgements

First and foremost, I want to thank my mother Ināra for her continuous support. Not a conversation has gone by during the past year without her showing interest in how I am doing with my thesis. While occasionally finding that annoying, her frequent check-ins, undoubtedly, made me feel like someone else cares about this thesis as much as I do. On top of that, I want to thank her for reminding me from an early age that “whatever happens, education is something that nobody can take away from you”. This, I believe, is a statement that I will continuously grow to appreciate more and more.

Thank you to my graduation committee. It goes without saying that conversations with them have shaped my thinking of computational design beyond the scope of this thesis. To highlight aspects that I have found particularly fond, Mariana, thank you for serving as a reliable source of insightful academic guidance, a comforting presence during moments of stress, and for being understanding with my desire to occasionally productively procrastinate. Thank you, Thijs, for reminding me of the value of a generalist approach and the importance of a good story. Jeroen, thank you for setting the standard high and introducing me to the professional world of parametric design by providing me with the opportunity to work at Packhunt. Roel, thank you for being a source of clarity and a supportive faculty presence from the first days at TU Delft.

I’m grateful that I had the opportunity to supplement my time at TU Delft with various projects. I will miss my time with the Symbiotic Urban Movement and I am thankful to the people I met there.

Thank you to my colleagues at Packhunt. My experience there has been crucial for seeing how to apply skills of computational design beyond academia. Thank you, Marianna, Twan, Marcos, Anke, and Jordy for assisting me along this part of my master’s experience.

Thank you also to Mo Smit and Peter Luescere for the discussions on circularity, Alessandro Dell’Endice for discussing my research, Michelle Capelli for sharing their work on reclaimed concrete, and Gene Kao for assistance with COMPAS.

Thank you to my peers at the Tailored Research Materiality group, especially Ewout, Nora, and Anass for their check-ins and nuanced questions, which have improved this thesis.

Finally, thank you to my friends. Thank you to U-Base, which was pivotal in allowing me to find a community in Delft. Thank you to the DD group and especially Chris for the numerous conversations over the free coffee. Thank you to Firas squared, Amey, Bernardo, Sophia, and Soley for their constant positivity and creativity spurts. Thank you to Laura and Ivo for providing a feeling of home while abroad. And finally, thank you to my main support group of Tomass, Vilhelms Dagnis, Sasha, Liene, and Alex for being there for me no matter what.

Raitis Pekuss
Delft, December 2023

Abstract

Cement production is responsible for 8% of the anthropogenic CO_2 emissions [1]. Reducing this share will be a strenuous task as the global population and urbanization rates are increasing and, therefore, the need for concrete will remain high [2], [3]. Simultaneously, despite the alarming statistic, a vast majority of demolished concrete buildings are structurally sound [4]. Therefore, this thesis aspires to push beyond the abundance of new concrete and outlines a design workflow for using reclaimed concrete. To enhance the material savings, the workflow focuses on double-curved, compression-only structures that benefit from the principles of structural geometry.

To implement the workflow, a novel stacking algorithm is designed using COMPAS [5], an open-source Python framework. It positions quadrilateral voussoirs on a funicular geometry's thrust surface in a sequential one-by-one manner. The placement is guided by three global design principles. First, a pair of opposing voussoir sides are aligned parallel to the force flow while the remaining pair, which represents the load-transferring faces, is aligned perpendicular to it. This is done to prevent sliding failure. Second, the thrust surface is confined within the middle third of the voussoir to prevent the formation of hinges and cracks. Third, voussoirs are cut into hexagonal shapes and staggering is ensured among neighboring voussoirs to create an interlocking geometry. Once a structure is completed, its stability is ensured by finding a compression-only equilibrium using the Rigid Block Equilibrium method [6].

The algorithm is then studied using various stocks with different voussoir dimensions of both regular and irregular side lengths, various deployment strategies that enable the user to customize the launch of the algorithm, and different thrust surface shapes. It is primarily assessed what fraction of the initial concrete volume can be retained in the structure. It was found that on average 47% of volume per voussoir is retained and that voussoirs of regular dimensions retain approximately 5% more of the initial volume. Minor differences exist in the results among different thrust surfaces with shapes of more uniform force flow retaining more concrete. Furthermore, smaller voussoirs mostly sized 0.7x0.7x0.2m required 20% less volume to construct a shell than a stock of 1.0x1.0x0.2m voussoirs. At the same time, the smaller stock required almost double the amount of voussoirs, thus, indicating competing goals that require the decision-making of the designer.

Next, high-level waste minimization was performed by checking if offcuts could be used to create other voussoirs from the remaining structure or if they could be returned to the stock for future placement. A pessimistic and an optimistic scenario were studied and it was found that 70-85% of initial voussoir volume can be efficiently retained within the shell and the stock.

These results served as the basis for reflecting on how the stacking algorithm influences the suggested workflow by bringing design and fabrication-specific constraints to an earlier design phase. It is described that to improve the retained volume the designer can, first, alter their way of deploying the algorithm, second, modify the input geometry, third, custom select what stock is used for placement, and, fourth, inform the contractor of the level of detail to which a building should be deconstructed and post-processed. Thus, a designer is brought closer to the construction process, and incentives for a more collaborative cross-disciplinary workflow are outlined.

Finally, suggestions are made on how to improve the functionality and efficiency of the algorithm. The primary conclusion made is to expand the criteria based on which a voussoir is selected for placement. An emphasis is directed towards using criteria such as distance-to-staggering, local radius of curvature, local force flow, and dimensions of the surrounding voussoirs to limit the offcuts that will be created to ensure complete tessellation.

Overall, this study provides a workflow that is enabled by a stacking algorithm. It outlines how to design double-curved, compression-only structures and how their design can influence the entire workflow.

“An engineer should design a structure that an architect would be ashamed to cover up”

-William F. Baker, SOM

Contents

1 Introduction

1.1. Background and motivation

The construction industry is a significant contributor to the ongoing climate crisis, which, in case the 1.5-degree threshold is reached, will expose 950 million people to heat and water stress, be responsible for 0.28 – 0.55 meters of sea level rise by 2100, among numerous other extreme weather events [7]. More specifically, four billion tons of cement are produced annually, which creates an estimated 8% of the global anthropogenic CO_2 emissions [1], [2]. This need for cement is fueled by the burgeoning rates of urbanization as the share of the population living in urban areas has risen from 29% during 1950 and will continue to do so to a projected 70% in 2050 [8]. Simultaneously, the world's population is set to increase from 2.536 billion to a projected 9.735 billion in the same time frame [3]. To relate this to the construction sector, the world is expected to use two trillion more tons of concrete by the end of 2060, which is equivalent to building a new New York City every month for the next 40 years [9]. Thus, the demand for expanding the built environment is inevitable, placing civil engineers at the forefront of fighting climate change while being partially responsible for it.

Understanding these climate trends and the negative impact the construction industry has on them, engineers and scientists must find innovative solutions to reach the world's target of net-zero emissions by 2050 to keep the average temperature increase below the 1.5-degree threshold. This is a daunting task especially as the construction industry is fragmented with many actors with personalized interests and has struggled with productivity and digitization [10].

Nevertheless, the emergence of digital fabrication tools could alter the status quo and play a role in this path towards net zero. They could automate parts of construction, optimize fabricated elements and design processes, and unlock previously impossible design strategies among other potential benefits. The World Economic Forum reports that digitization of hard-to-abate sectors, which are sectors that are particularly challenging to decarbonize due to technology and cost challenges and which include concrete production, could reduce emissions by upwards of 20% [11]. On top of that, the introduction of digital fabrication tools could provide a window to reimagine existing supply chains, collaborations, waste flows, and the materials economy at large by assisting in closing the material loops. Studies claim that a circular economy could reduce emissions from concrete production by 31% by 2050 while reducing emissions by 40% across all harder-to-abate sectors [12]. Therefore, the potential of digital fabrication tools is a core motivation for this thesis.

1.2. Research objective and scope

With the potential role of digital tools in mind, the overarching question of this thesis is how can engineers design more sustainable structures. An attempt to study this question is made through a more focused research objective:

How can reclaimed planar concrete elements be used in designing double-curved, compression-only structures?

To study this objective, a novel stacking algorithm is developed and the amount of volume of concrete retained versus discarded is studied. The algorithm is studied based on variations in:

- dimensions of the stock elements,
- regularity of the stock element dimensions,
- thrust surface shape,
- algorithm deployment strategies.

Aspects beyond the scope of this study are:

- study of how to acquire the stock,
- analysis of stock cutting patterns,
- life-cycle assessment of the designed structures,
- structural calculations of the concrete,
- construction planning of the structures including the required formwork, assembly strategies, etc.

1.3. Approach to design

Throughout this thesis, the concept of design is understood as an approach to addressing the previously proposed research objective. Therefore, design entails but is not limited to considerations regarding engineering, aesthetics, workflows, waste management, etc.

1.4. Methodology

The stacking algorithm presented in this thesis is primarily developed using COMPAS [5], [13] an open-source Python framework for the Architecture, Engineering, Fabrication, and Construction industry. This environment was chosen because it is open-source and provides vast interoperability options. More specifically, COMPAS is compatible with multiple CAD software like Rhino and Blender, runs in Windows, Mac, and Linux operating systems, can be paired with various analysis tools like Abaqus, ANSYS, etc., and provides access to various external libraries like GMSH, CGAL, and others.

For this thesis, COMPAS was primarily used within the Rhino environment and supplemented with several tools and libraries. For instance, form-finding was performed using Rhino Vault 2 [14], a COMPAS-based open-source platform for funicular form-finding that is based on the Thrust Network Analysis [15]. Force flow was found using Grasshopper and Karamba3D [16], a parametric Finite Element Analysis tool. Next, the stacking algorithm, while mostly scripted using the COMPAS framework, used commands from rhinoscriptsyntax and RhinoCommon. Data management was done with the COMPAS Network data structure, which is a geometric implementation of a graph data structure. Finally, the post-processing of the voussoirs was performed in Rhino while the verification was done using the Rigid-Block Equilibrium method [6] available via the COMPAS CRA package. The validated results were displayed using COMPAS View 2, an open-source standalone CAD viewer for the COMPAS framework. The summary of the methodology can be seen in Figure 1.1.

As most of the algorithm is developed using COMPAS, with minor tweaks, the algorithm can be shared and run without access to any proprietary software, thus future-proofing its development and democratizing access to it.

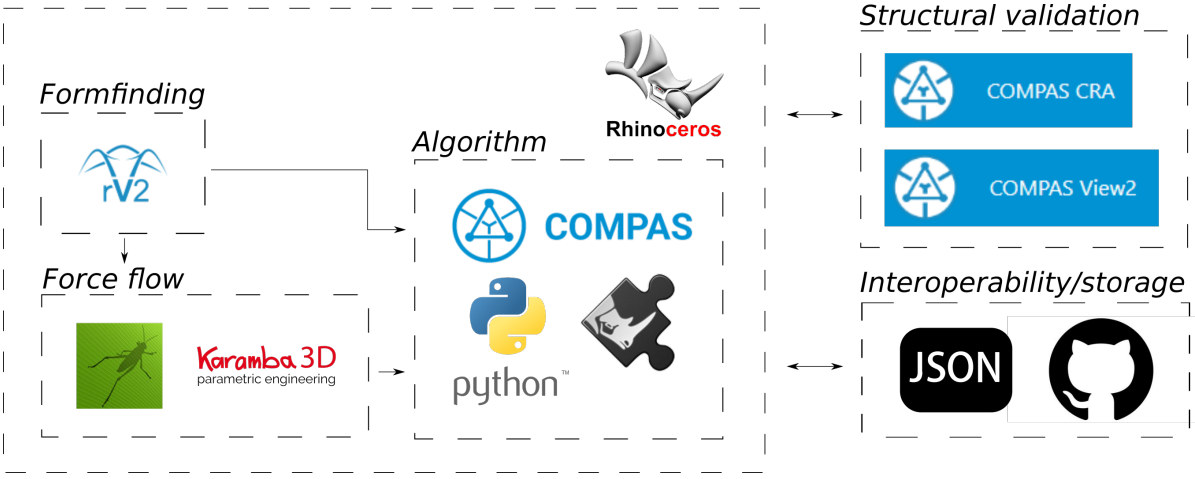

Figure 1.1: Computational methodology used in the study

1.5. Structure of the report

The following thesis is structured by first outlining the need for transitioning the construction industry to a circular economy in the section “Theoretical Framework”. The same section also elaborates on the efforts in reclaiming concrete for construction purposes, provides several examples, and suggests a link between reclaimed concrete and structural geometry. Then, the chapter “Place the Waste: tessellating funicular structures” outlines a novel design workflow for reclaiming concrete for the construction of new funicular structures. It sketches a high-level overview of the workflow from providing requirements to the disassembly process of a building to constructing funicular structures from concrete waste. In particular, the chapter describes and visually demonstrates a novel stacking algorithm in a step-by-step fashion. This algorithm is analyzed in the “Results” section by using it with various stocks, different voussoir geometries, algorithm deployment strategies, and shapes. The “Discussions” chapter compares these results, identifies how the stacking algorithm provides inputs to earlier design phases, and suggests improvements to the workflow and the algorithm. Then “Conclusions” summarizes the advantages of the suggested workflow and the algorithm, and reflects on how reclaiming concrete is a fraction of the larger effort that must be taken by the construction industry.

2

Theoretical framework

2.1. More than the sum of its parts: concrete in a circular economy

The prevalent economic model in which materials are consumed is linear. This means that products are created, used, and then discarded. While such a model proved useful in the past, it has done so at the negligence of resource limitations that cannot be ignored in the face of the ongoing climate crisis. A collective understanding is emerging that it is impossible to run a linear materials economy on a finite resource planet and, therefore, new frameworks that close the linear loop and create a circular economy, visualized in Figure 2.1, must be implemented [17].

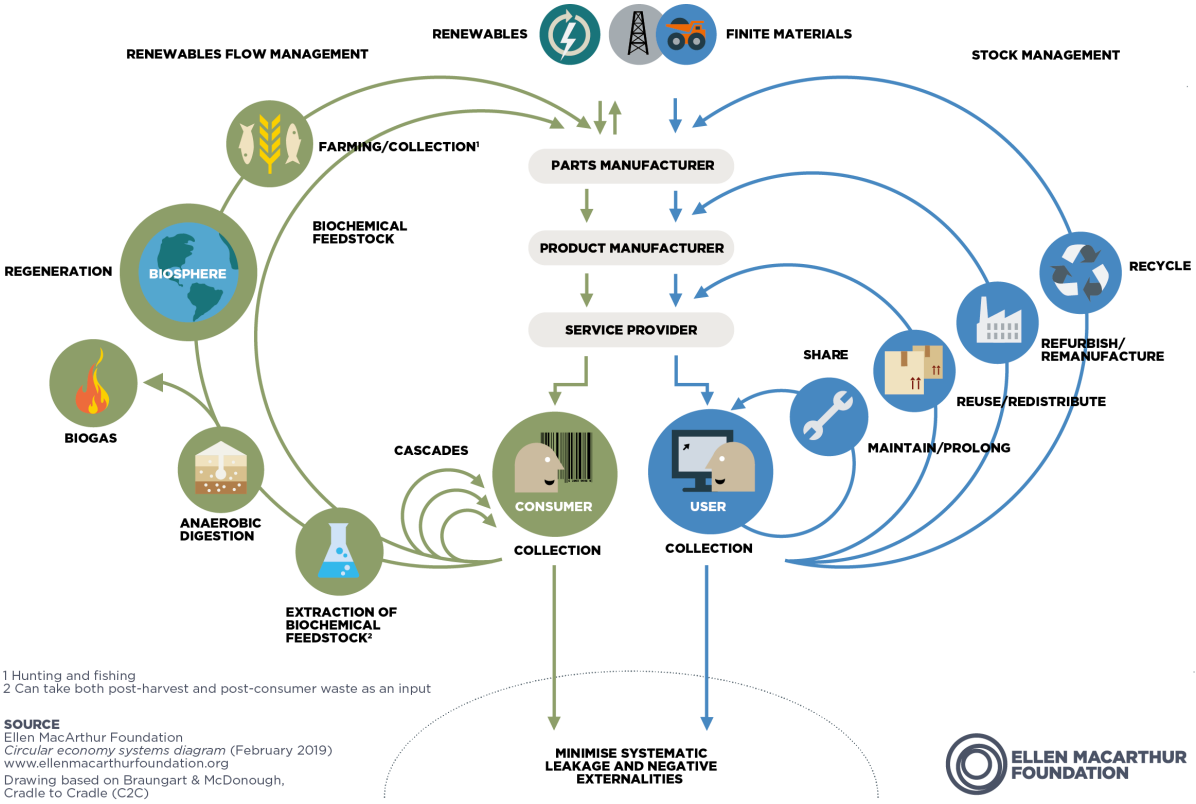

Figure 2.1: Butterfly diagram used to visualize the principles of circular economy[18]

A circular economy envisions a continuous circulation of materials through reuse, refurbishment, re-manufacturing, recycling, and composting to prevent materials as well as the resources that went into them from becoming waste. In doing so, the circular economy decouples economic growth from the constraints and wastage of using finite resources [17], [19].

The ubiquitous use of concrete and its negative impact on the environment underlines the importance of fitting into a circular economy. Currently, the most frequent use case for reclaimed concrete is to down-cycle it as back-fill for excavations or as the sub-base for road construction [20]. Other options include crushing concrete into aggregates for the process of creating new concrete, which is also the goal set by the ”Dutch Concrete Agreement” for 100% of concrete waste by 2030 [21]. Nevertheless, often such concrete mixes require an increased level of cement, thus offsetting the benefits of the recycled aggregate [22], [23].

While such solutions can be expected to improve and are certainly favorable in comparison to conventional methods of linear materials economy, circular economy, as seen in the Butterfly diagram in Figure 2.1, highlights that material value is most preserved in the smallest value circles such as sharing or reclaiming materials rather than recycling materials. This is rooted in the idea that materials, concrete including, are more than the sum of their parts. They are a composition of time, energy, and money that has gone into creating them. In fact, the areas in which the construction industry has the greatest potential of becoming circular as per the Ellen MacArthur Foundation are industrializing production processes, modularizing construction, implementing digital fabrication tools like 3D printing, and reusing building components.

To further cement the case for using reclaimed concrete it is important to highlight that most of the concrete in demolished structures is structurally sound. The average lifespan of a building prior to demolishing it is a mere 39.1 years [4]. Even more, in only 14% of cases buildings are demolished because of structural reasons. The other 86% relate to functional obsolescence and a building’s incapability to support changing functionality demands [4]. Many such buildings have been constructed using in-situ casting, which effectively turns the structure into a monolithic block and, therefore, complicates potential deconstruction. In contrast, the share that has been built using precast concrete poses an easier outlook on harvesting the concrete due to the homogeneity of precast elements as well as the fact that reclaiming can be done by effectively reversing the assembly process. Overall, such statistics point towards an untapped reservoir of resources found in construction waste that is currently sent to landfills or down-cycled.

Efforts to use reclaimed concrete exist across the industry, academia, and governments. For instance, 320 flats were constructed in Sweden using reclaimed prefabricated concrete panels [24]. In fact, a significant portion of the European housing in the 1960s and 1970s was built using large panel concrete systems and these buildings could be considered for reclaim [25] as they are approaching or have already passed their expected service lifespan. Famous examples are also found in the Netherlands that have reused prefabricated slabs, façade, roofs, and balcony elements [26]. Similarly, academic research has looked into the reuse of stadium elements [27], the reuse of cast in-situ concrete [28], and others alongside developing tools that enable designing with reclaimed elements. More specifically, the reuse of steel elements has been streamlined with a plug-in for Grasshopper called Phoenix3D that assists designers with using reclaimed steel profiles in their design [29], [30]. Such a design strategy of using claimed elements has been dubbed “form follows availability” [31]. Finally, the EU has also expressed its support for using reclaimed materials by establishing a Waste Framework Directive [32] and funding projects such as ReCreate that are aimed at studying the potential of reclaiming precast concrete [33].

2.2. Structural geometry & digital fabrication

Similar to how the most efficient strategy for a circular economy is to not demolish structures that are still functional, another approach is to use less concrete. This can be done by not just using other construction materials, which might pose their own environmental concerns, but by positioning concrete in an optimal geometric formation to take advantage of its great compression strength and avoid any bending or tensile forces. For that reason, designing compression-only structures is suggested as an additional pathway toward sustainable usage of concrete.

The design of shell structures dates back to 4000 BCE when in the Sumerian city Nippur in Babylonia the first documented tunnel vault was built [34]. Over time, the structural systems were perfected making Roman and Gothic arches a quintessential element of architecture. Notable advancement was made by Robert Hooke who postulated the idea of “Ut pendet continuum flexile, sic stabit contiguum rigidum inversum” which from Latin translates to “As hangs a flexible cable so inverted, stand the touching pieces of an arch” [35]. Almost anecdotally, Hooke initially published this idea as an anagram

because he was tired of his colleagues at the Royal Society of London publishing his ideas without crediting him. The anagram was only deciphered by the executor of Hooke's will after his passing in 1703. His idea was later famously used by Antoni Gaudi in the design of Cripta de la Colònia Güell and Sagrada Família as well as other designers to this day. Later, shell structures experienced their heyday between the 1920s and 1960s [36] before losing their appeal. When asked why so, a study from 2005 cited that the construction of concrete shells is too costly and labor-intensive [36]. However, with the advent of advanced computational modeling and digital fabrication methods, more shell structures have been created in recent years.

A famous example is the Armadillo Vault, a free-from vault that spans more than 15 meters in pure compression, has a height of 4.4 meters, a thickness between 5-12 cm, and is made up of 399 discrete limestone blocks that are held together by compression with no glue, mortar or mechanical joints [37] as seen in Figure 2.2. To design it, a novel algorithm was created for tessellating discrete funicular structures that provide users with flexibility over the design decisions and accounts for architectural, structural, and fabrication requirements in detail [38]. This project is also the main inspiration for this thesis.

Figure 2.2: Armadillo Vault - a free-form vault made of discrete elements with no adhesives or mechanical joints [37]

Another project that uses the advancements in computational modeling and digital fabrication is Striatus, an unreinforced, 3D-concrete-printed, mortar-free masonry arch bridge seen in Figure 2.3 [39]. It differs from other 3D-printed bridges by being dry-assembled. This simplifies reuse, engages the printed concrete structurally by printing layers orthogonally to the force flow instead of using the 3D printed layers as a stay-in-place formwork or post-tensioning them as well as using an unreinforced concrete mix that does not have any fibers for reinforcements. Atop the structural innovations, Striatus also proposes a computational Design-to-Production Toolchain that systematizes the workflow and simplifies collaborations among different parties to be able to achieve the previously listed benefits.

Figure 2.3: Striatus bridge made of unreinforced 3D printed masonry [40]

While incredibly impressive and relevant for making the construction industry more sustainable, both of the previously listed projects rely on using new materials. Re:Crete bridge, which spans 10 meters and is 1.2 meters high and is shown in Figure 2.4, however, uses 25 concrete blocks that have been reclaimed from a torn-down wall to form a single curvature arch bridge [28]. Importantly, the project used pre-existing cast-in-place concrete elements which have been considered more difficult to reclaim than precast members. The blocks were cut as shown in Figure **??** and mortar was filled in the joints to fill the voids. Thus the project demonstrated the viability of reclaimed concrete from not just precast, but also in-situ construction. On top of that, a life cycle assessment showed that the proposed method presents 71% less global warming potential than recycled concrete, 74% less than a comparative bridge built from steel, and only 9% more than a bridge built from timber. What's more, since the dimensions of the blocks were known, this eliminated the uncertainty in dimensional variability that exists for new structures. Therefore, the method demonstrated that certain safety factors can be reduced, resulting in a more optimized design.

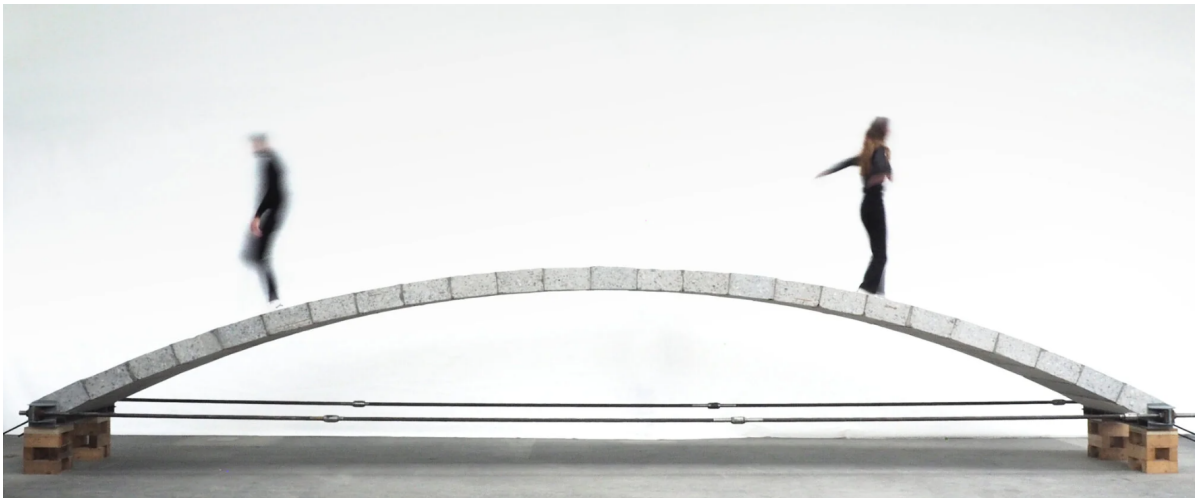

Figure 2.4: Re:Crete footbridge made of reclaimed concrete [28]

Nevertheless, bridges and shell structures are not a common typology in comparison to the concrete's use in building, therefore, questions of scalability of the described solutions arise. To address this, recent studies have suggested that shells with a raised floor on them could provide an alternative for concrete slabs in high-rises. Such a 4.5 x 4.5-meter slab, but from virgin concrete elements, has been proposed as a part of a research project ACORN in the UK and is displayed in Figure 2.6 [42]. Such a slab requires 50% less embodied carbon than an equivalent flat slab. It is worth noting that efforts towards designing thin vaulted floors have already occurred [43], nevertheless for those methods usage of reclaimed concrete is more difficult to imagine.

Figure 2.5: Sawing of the blocks for the Re:Crete bridge[41]

To summarize, the Armadillo vault and the Striatus bridge have demonstrated that computational modeling and digital fabrication tools can be combined with historical ways of building shell structures that result in stable discrete element assemblies that have a comparatively lower environmental footprint. The Re:Crete bridge builds upon this by using reclaimed planar concrete elements from complicated-to-extract cast-in-place concrete waste elements, however, it does it in only a single direction of curvature. The vaulted slab by Acorn, however, demonstrates that shell structures could be applied in a relevant building typology to scale the benefits of all of the listed projects, but used virgin concrete. Therefore, a research gap exists for creating double-curve compression-only structures from reclaimed planar concrete elements. This thesis aspires to reduce this gap.

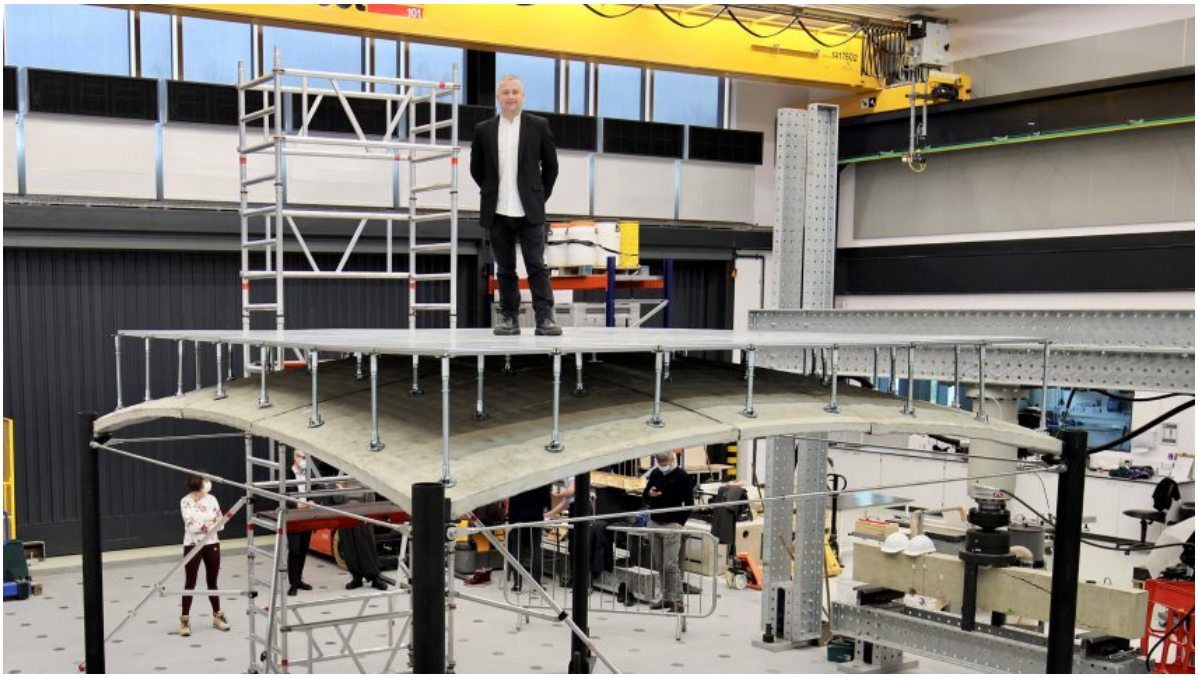

Figure 2.6: Vaulted slab by ACORN [44]

3

Place the waste: tessellating funicular structures

“As hangs a flexible cable so inverted, stand the touching pieces of an arch”

- Robert Hooke

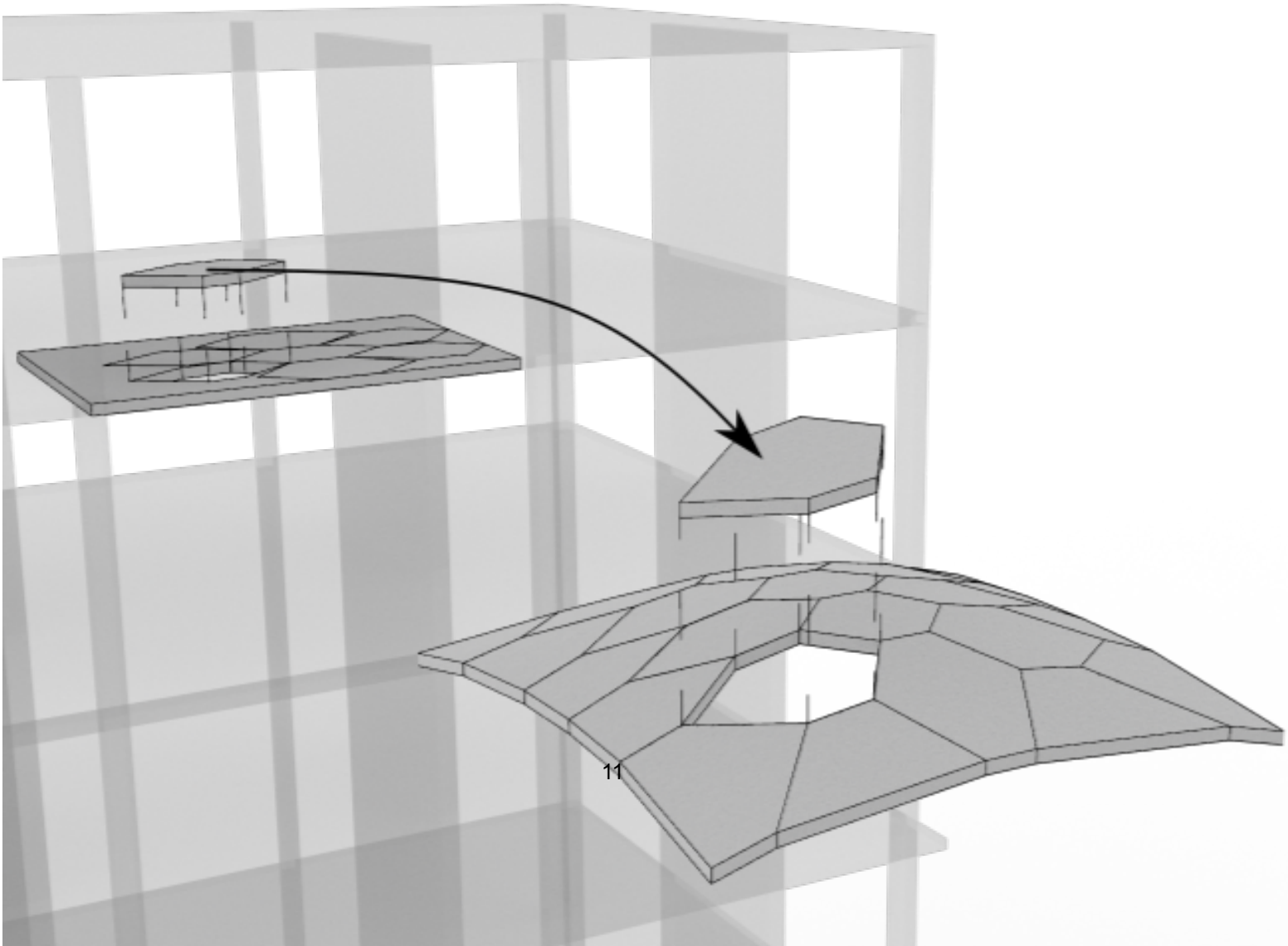

3.1. List of Terms

The following chapter introduces a novel design workflow and a stacking algorithm for using reclaimed concrete in design. To assist the reader through the algorithm, definitions of commonly used algorithm-specific terms are provided below in alphabetical order:

- Kern - middle third of a cross-section,
- Patch sides - voussoir's sides parallel to patch vectors as shown in Figure 3.1,

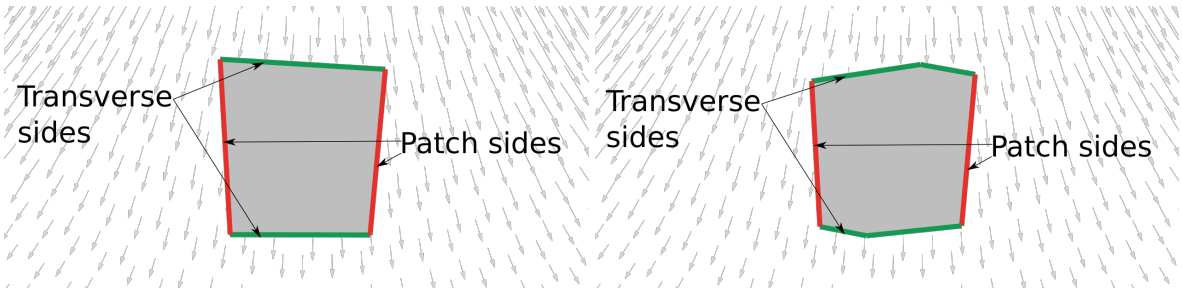

(a) Quad voussoir used upon placement (b) Hexagonal voussoir obtained in processing

Figure 3.1: Definition of a patch and transverse sides

- Patch vector - reversed average of a certain number of parametrically defined vectors from the force flow closest to the pivot point as shown in Figure 3.2.

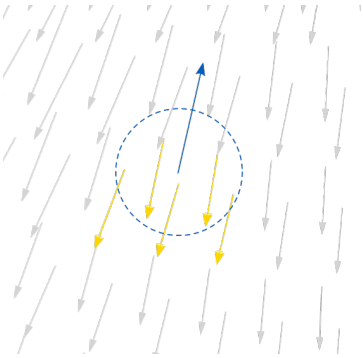

Figure 3.2: Definition of a patch vector

- Pivot point - point on the thrust surface from which the voussoir placement begins. It can be defined manually or found as the intersection between a support boundary and an elevated boundary, the previous voussoir's bottom right corner's edge intersection with the thrust surface, or the elevated boundary's intersection with the top transverse face of a voussoir below depending on the situation.
- Stock - dimensionally categorized construction waste. In this thesis, the stock is assumed to consist of quadrilateral elements that are reshaped into hexagonal prisms upon their placement,
- Thrust surface - surface along which forces flow in a compression-only structure,
- Transverse sides - voussoir's sides perpendicular to the force flow as shown in Figure 3.1,
- Vertex search angle - angle formed at the intersection of voussoirs patch and transference faces,
- Voussoir - individual quadrilateral or hexagonal wedge-shaped element from the stock used to tessellate the structure,
- Voussoir frontier - Collection of top transverse faces that face in the direction of the deployment of the most recently placed row of voussoirs.

3.2. Design workflow

To address the highlighted environmental concerns, close the circle on concrete's life cycle, and utilize the benefits of structural geometry, a workflow for using reclaimed concrete in double-curved, compression-only structures is proposed. A high-level overview of it is provided in Figure 3.3. The workflow is initiated by acquiring a stock of reclaimed concrete elements from an existing repository or informing a disassembly process of a building that is scheduled for deconstruction. The acquired stock alongside a form-found shape and its associated force-flow is then used as an input for a stacking algorithm. As the stacking process, which includes steps of trimming voussoirs upon their placement, completes, the retained concrete volume of each voussoir after its trimming is assessed. If the retained volume is not within an acceptable range, the workflow supports several design interventions to increase the volume retained. First, the deployment strategy of the algorithm, which is discussed in the section on User Controls later, can be varied. Second, the input shape can be modified to alter its surface curvature and force flows to better accommodate the existing stock. Third, a different stock can be selected as input from the repository or, if the needed size voussoirs are absent, a disassembly strategy for a building can be informed to reclaim concrete elements of desired dimensions.

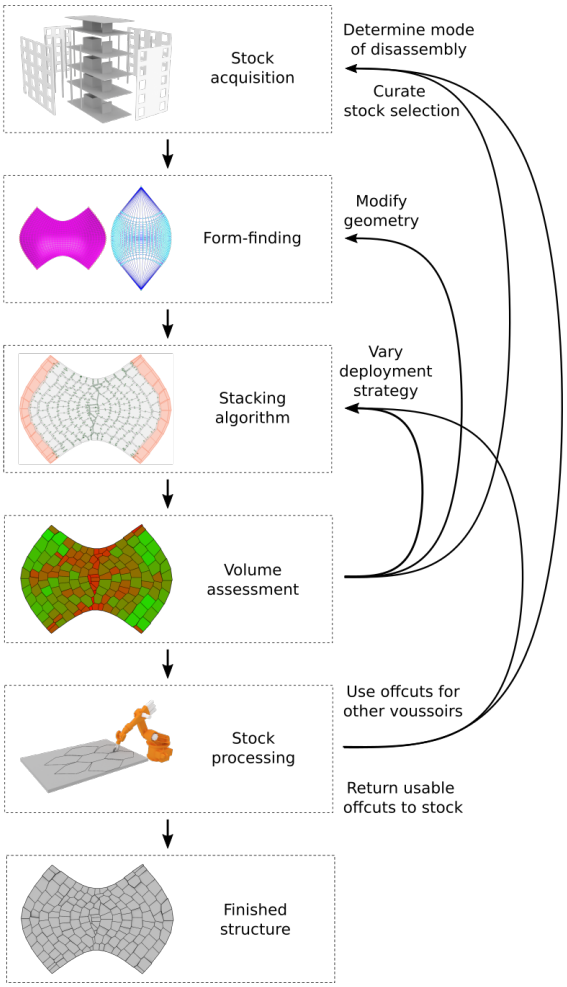

Figure 3.3: Overview of the proposed workflow

The end result is a funicular structure that is created entirely of reclaimed concrete elements and needs no adhesives or mechanical joints. The structure is held up entirely due to its interlocking nature, compression forces, and friction.

The following chapter describes the workflow in greater detail and, primarily, visually demonstrates the stacking algorithm. To clarify commonly used algorithm-specific terminology throughout the chapter, the reader is guided to the section 3.1 List of Terms.

3.3. Stock acquisition

The stock is suggested to consist of planar elements of complete or partial concrete slabs and walls. They could be reclaimed from a building's superstructure or interior construction that constitute up to 52.8% and 13.1% respectively of the concrete consumption in buildings [45]. While extraction details of such stock are beyond the scope of this study, aspects that could expedite the acquisition are highlighted. First, the harvesting process could be facilitated by a centralized database. It could encompass information on when buildings will reach their end-of-service life, when they are scheduled for deconstruction, and what level of concrete recovery can be expected. The latter aspect would be influenced by whether a certain building was prefabricated or cast in-situ as discussed earlier. By using such a database, potential concrete waste flows could be predicted. Even more, not only could waste flows shape the design of new structures, but as suggested in the workflow in Figure 3.3, designers could inform the contractor of the needed size of concrete waste that is desired for the design process. This would influence the methods and level of precision in deconstructing a building. On top of that, the stock should be sourced, stored, processed, and used within a reasonable distance of each location to prevent excessive emissions from transportation. A simplified waste flow is shown in Figure 3.4.

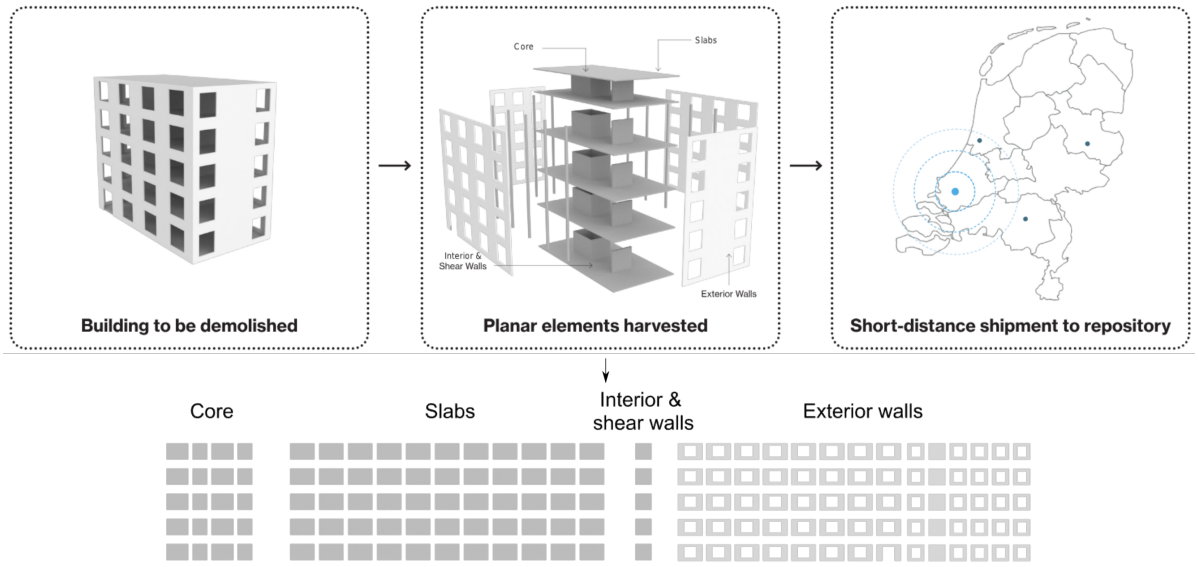

Figure 3.4: A simplified waste flow of reclaimed concrete

The proposed stacking algorithm relies on access to a stock of dimensionally categorized construction waste. For this thesis, stocks were artificially generated by creating randomized quadrilateral prisms of both regular and irregular size voussoirs shown in Figure 3.5. Their length and width range between 50 to 120 cm while their height varies between 20 to 30 cm, which corresponds to a typical slab thickness.

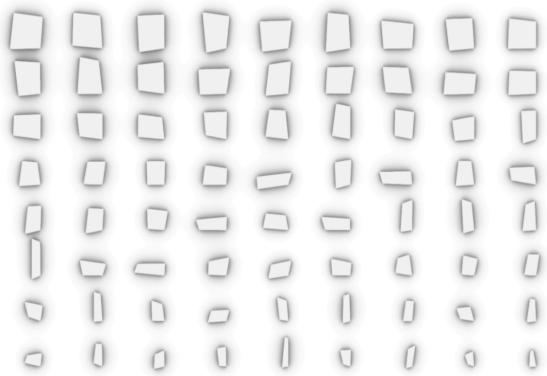

Figure 3.5: Artificially generated stock of various dimensions

3.4. Form-finding & force-flow

The next step of the workflow is creating the desired shape of the structure. The funicular shape can be freely designed as per the desires of the involved stakeholders. For this thesis, a thrust surface representing the shape of a shell in which internal forces are carried in compression is obtained using Rhino Vault 2 (RV2) as shown in Figure 3.6. Such a surface is relevant for the stacking algorithm as maintaining it within the kern of each voussoir is crucial to ensuring that no hinges appear at the interfaces between voussoirs and that no tensile capacity is required.

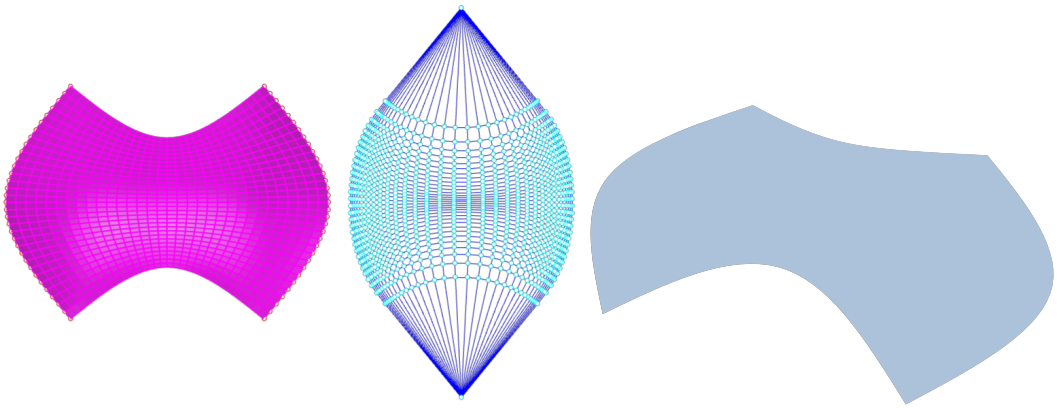

(a) Thrust surface and the horizontal force diagram (b) Perspective view

Figure 3.6: Bowtie thrust surface.

Next, a force flow, represented by an array of vectors, needs to be obtained to establish a force-aware tessellation of the voussoirs, Several options exist for this - extracting the force flow from the Thrust Network Analysis [15], analyzing certain structural heuristics [46], or using the “rain flow analysis”. The latter is a common and simple approach that states that the force flow can be found by following the gradient of the steepest descent for any point on the thrust surface [47]. While simple to implement, this approach fails to account for elevated boundaries, which direct the forces to supporting boundaries as opposed to serving as supports themselves. In this thesis, Grasshopper and Karamba3D were used to identify the force flow as the one shown in Figure 3.7.

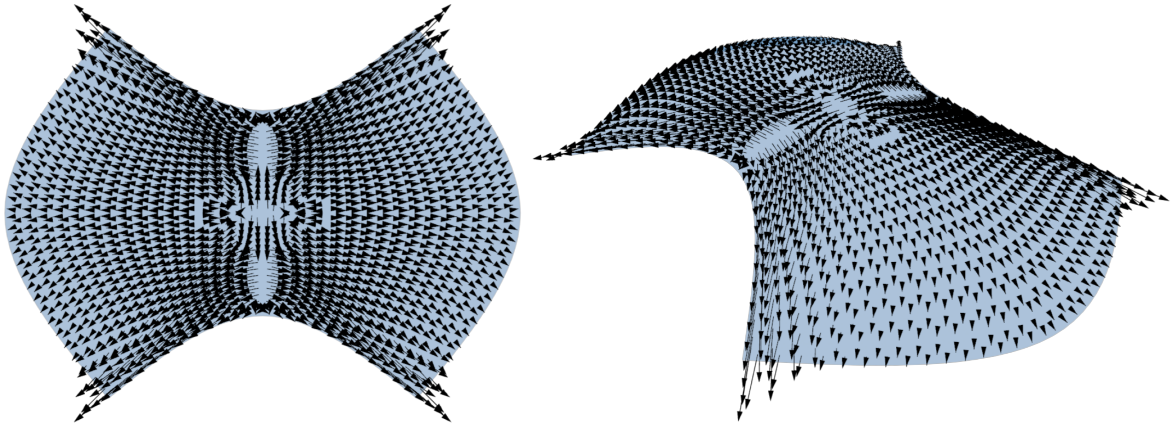

(a) Top view (b) Perspective view

Figure 3.7: Primary direction of the force-flow obtained using Karamba3D

3.5. Stacking Algorithm

With the shape and the force flow ready, the next step of the workflow is to deploy the stacking algorithm. Its goal is to entirely cover a thrust surface with given voussoirs. This entails that this problem is an example of a geometric set cover problem, which is NP-complete. This means that a found solution for the problem can be verified swiftly, however, finding a solution is not guaranteed to be possible in polynomial time. Even though approximation algorithms exist, a new algorithm is designed that:

- takes advantage of the possibility of cutting construction waste into desired shapes, thus modifying the input voussoir and simplifying the problem in comparison to the set cover problem in which shapes could not be cut,
- can be solved quickly,
- allows for various designer inputs

To guarantee the stability and constructability of the final structure, the stacking algorithm is guided by several core design principles:

- Thrust surface must remain within the kern of the voussoir for stability reasons,
- Voussoirs should be arranged in a staggered pattern to ensure stable interlocking,
- Voussoirs' side (patch) faces shown in Figure 3.1 should be as parallel to the local force flow as possible to limit load transfer between them,
- Voussoirs' top and bottom (transverse) faces shown in Figure 3.1, which transfer the load between voussoirs, should be as perpendicular to the force flow as possible to avoid sliding failure

To center the algorithm around the design principles and attend to each voussoir placed in the final structure, the algorithm is designed to stack voussoirs sequentially in a row-by-row manner following the logic shown in Figure 3.8. The logic consists of:

- step: 1.1: Deployment strategy. Allows for customizing the deployment of the algorithm,
- steps 2.1 - 2.5: Initial placement. Positions the voussoir on the thrust surface,
- steps 3.1 - 3.5: Calibration. Adjust placement to the kern, neighboring voussoirs, and force flow,
- steps 4.1 - 4.2: Row clean-up. Cuts voussoirs to smoothen the next support boundary and establish planar non-overlapping interfaces among voussoirs,
- steps 5.1 - 5.3: Post-processing. Merges segmented layers based on the chosen deployment strategy supports manual cleanup, and validates the stability of the structure.

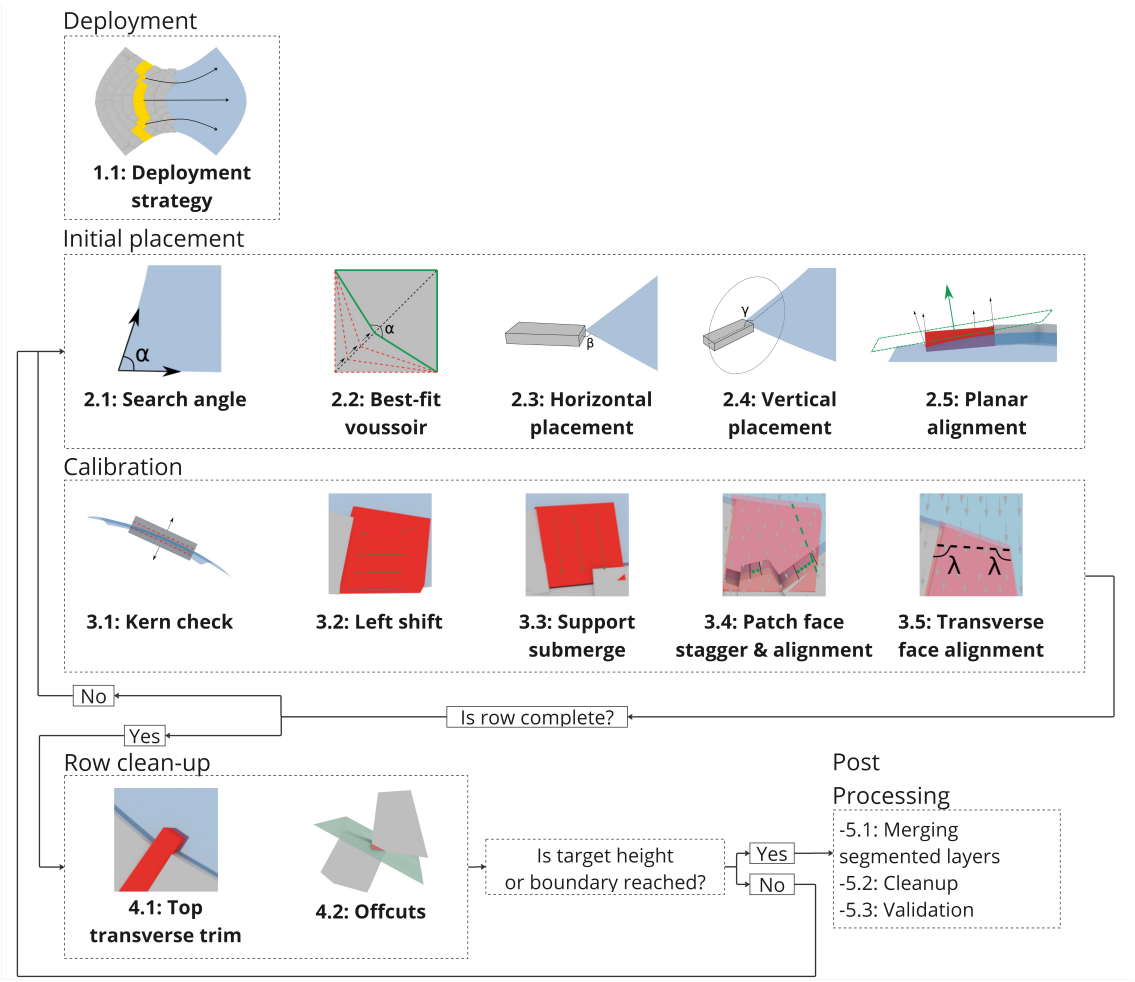

Figure 3.8: Overview of the stacking algorithm

Step 1.1: Deployment strategy
To initialize the algorithm, a designer must select a deployment strategy that defines over what area and in what direction voussoir placement will occur. Several such strategies exist and their benefits are compared in the “User controls”. The present section focuses on the logic of the deployment.

If no voussoirs have been placed and the thrust surface has elevated boundaries, deployment starts at the corner of a support and an elevated boundary as shown in Figure 3.9a. Voussoir deployment will then occur in rows between the two elevated boundaries so that the first row rests on the support boundary and each following row is supported by the previous. If no elevated boundaries exist, as is the case for a dome, the designer must define two interface boundaries parallel to the force flow. Stacking will then take place between them as if they were elevated boundaries as shown in Figure 3.9b.

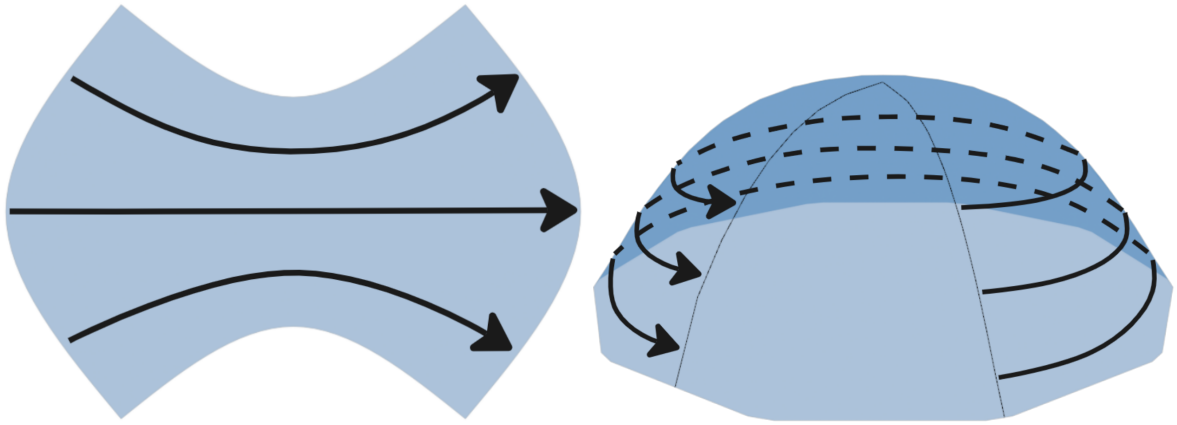

(a) Deployment across a shell (b) Deployment in-between voussoirs

Figure 3.9: Deployment strategies possible for various thrust surfaces

If a set of voussoirs has been placed already, the designer can:

- use the remaining support boundaries to launch a new deployment towards the existing voussoirs as shown in Figure 3.10a,
- stack new rows on top of the existing voussoirs as shown in Figure 3.10b,
- place new rows between the existing ones as shown in Figure 3.10c,
- create a combination of the aforementioned strategies.

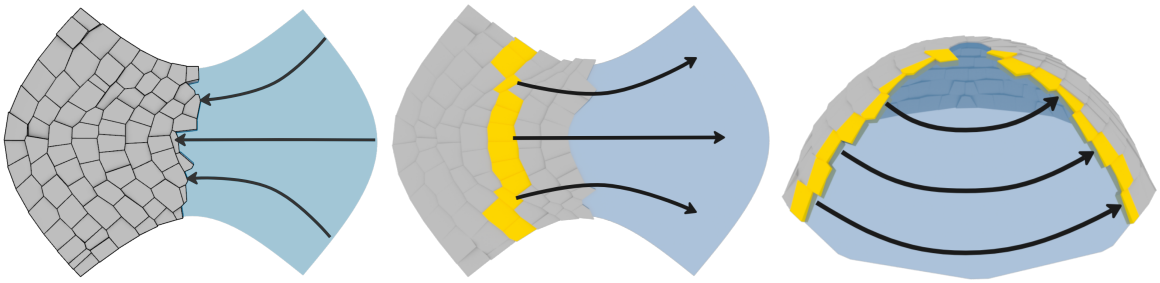

(a) Symmetric deployment (b) Stacked deployment (c) Between deployment

Figure 3.10: Voussoir deployment strategies

When existing voussoirs are selected for the placement of new ones, they are used to delineate the new support boundary in Figure 3.11a or the new interface boundary in Figure 3.11. The curves are defined by first trimming the selected voussoirs to form a voussoir in which only a single face from each voussoir is present and so that the least amount of the offcuts are created as shown in Figure 3.12. Then, the new curve is obtained where the frontier intersects the thrust surface. Note, that voussoirs

used to generate the frontier for the “between” deployment are only cut for the creation of the curve and are not cut in the structure. This is because cutting them would result in a frontier that lacks staggering in the final structure. Instead, an overlap between the frontier voussoirs and the new voussoirs is allowed which is later manually processed by the designer.

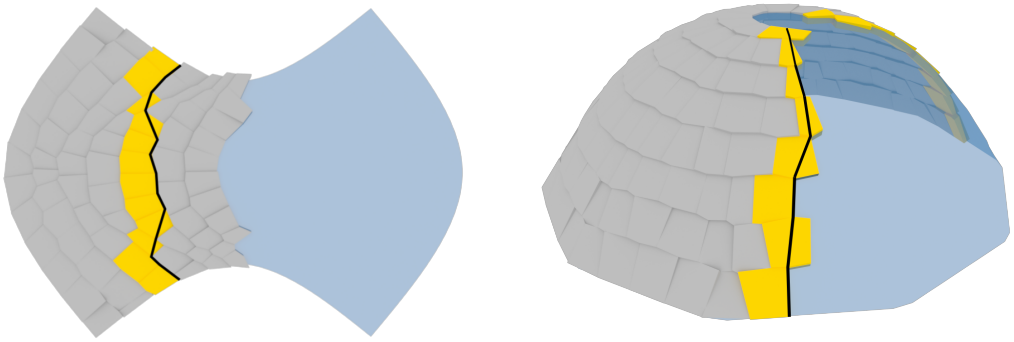

(a) Support boundary (b) Interface boundary

Figure 3.11: Updated boundaries defined based on deployment strategy:

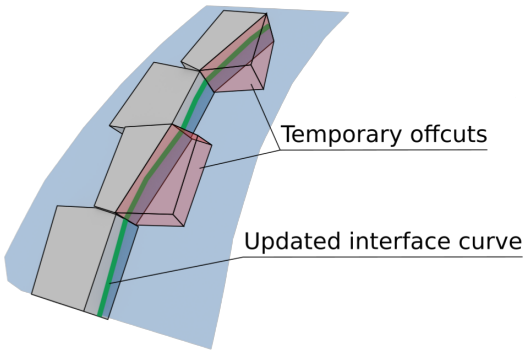

Figure 3.12: Creation of an interface boundary for a “between” deployment

Step 2.1. Initial placement: Search angle
As mentioned, voussoir placement is performed sequentially on a row-by-row basis to confirm that each voussoir is aligned to both the thrust surface and the force flow before moving to the next until a row is completed. The placement is initiated by identifying a pivot point on the thrust surface. A pivot point is found in several ways depending on the level of completion of the stacking:

- for the first voussoir in the first row placed on thrust surfaces with elevated boundaries, the pivot point is at the corner of an elevated boundary and a support boundary as shown in Figure 3.13,

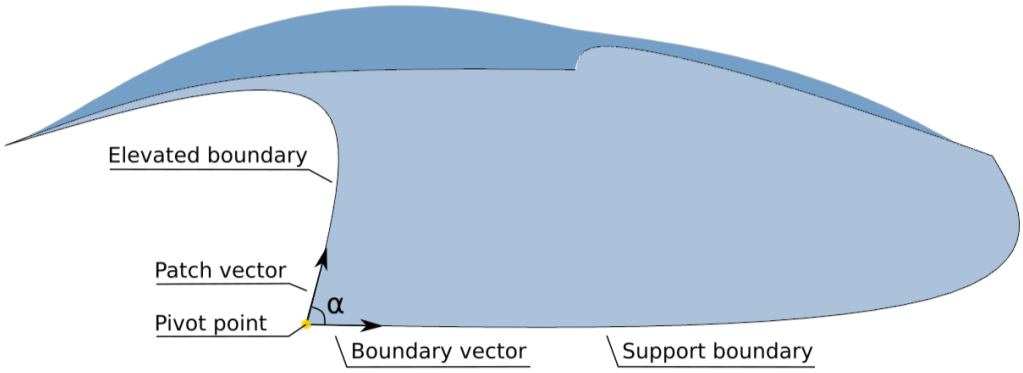

Figure 3.13: Naming conventions for thrust surfaces with elevated boundaries

- for the first voussoir in the first row placed on thrust surfaces with no elevated boundaries, the pivot point is defined where the previously user-defined left interface boundary intersects the support boundary as shown in Figure 3.14,

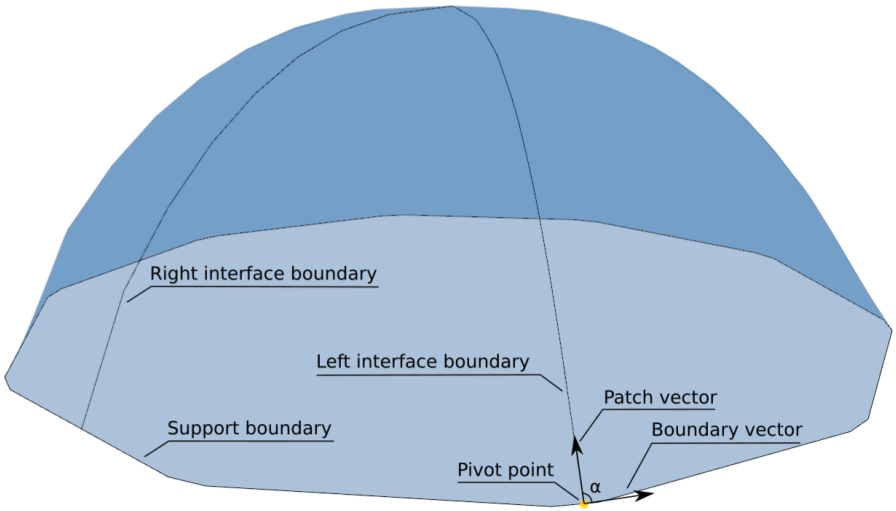

Figure 3.14: Naming convention for thrust surfaces without elevated boundaries

- for the first voussoir in rows two and above, the pivot point is defined as the location where the elevated boundary as shown in Figure 3.15a or interface boundary as shown in Figure 3.15b intersects a voussoir from the row below.

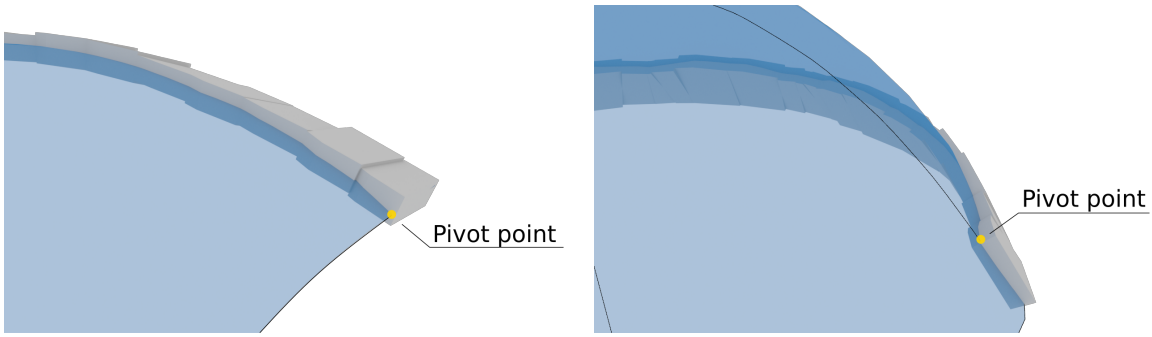

(a) with elevated boundaries (b) without elevated boundaries

Figure 3.15: Pivot point for the first voussoir in rows two and above for a thrust surface:

- for any voussoir that follows the placement of a previous voussoir in the same row, the pivot point is defined where the leading patch face and the bottom transverse face intersect the thrust surface as shown in Figure 3.16.

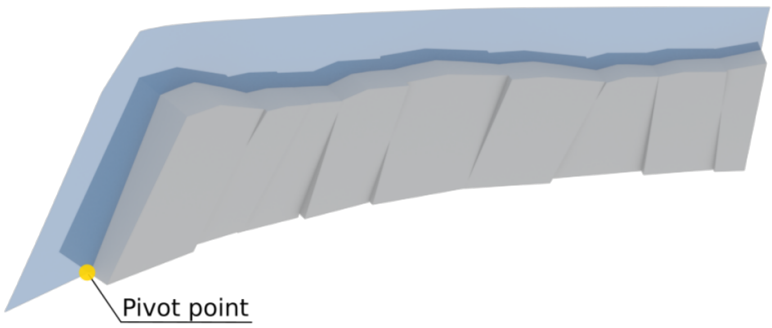

Figure 3.16: Pivot points when preceding voussoirs in the same row exist.

Once a pivot point has been established, two vectors – patch and boundary – are found to form the search angle as shown in Figure 3.13. The patch vector is defined as the reversed average of five force flow vectors closest to the pivot point as shown in Figure 3.2. In this way, the patch vector approximates the force flow around the pivot point instead of finding it exactly. This approximation is performed because the patch side of the voussoir that will be placed will not be limited to the location of the pivot point but rather will extend beyond it. The only exception for this method is made for the first patch vector in each row - that is taken as a tangent to the elevated or interface boundary depending on the deployment strategy as shown in Figure 3.15.

The boundary vector for the first row is the tangent of the support curve as shown in Figure 3.13. For the rows above the boundary vector is chosen from a set of candidate vectors.

The first option is using a vector stretching from the pivot point to the line delimiting the stagger upper limit as shown in Figure 3.17a. As a note, the stagger upper limit is used to position the voussoirs in an interlocking formation and will be explained in a further step in greater detail. However, since during this step of finding the search angle, it is not yet known which voussoir from the stock will be selected, it is, therefore, not known how far it will reach and which voussoir it will use as its right support. Therefore, relying on the suggested boundary vector could result in the new voussoir overreaching its support and forming a cantilever with a void underneath it as shown in Figure 3.17b.

To avoid this, a vector reaching from the pivot point to the upper stagger limit of the following voussoir is considered as shown in Figure 3.17c. However, for the same reasons discussed previously, this approach could also result in a void formation, especially if the to-be-placed voussoir skips a supporting voussoir as shown in Figure 3.17d.

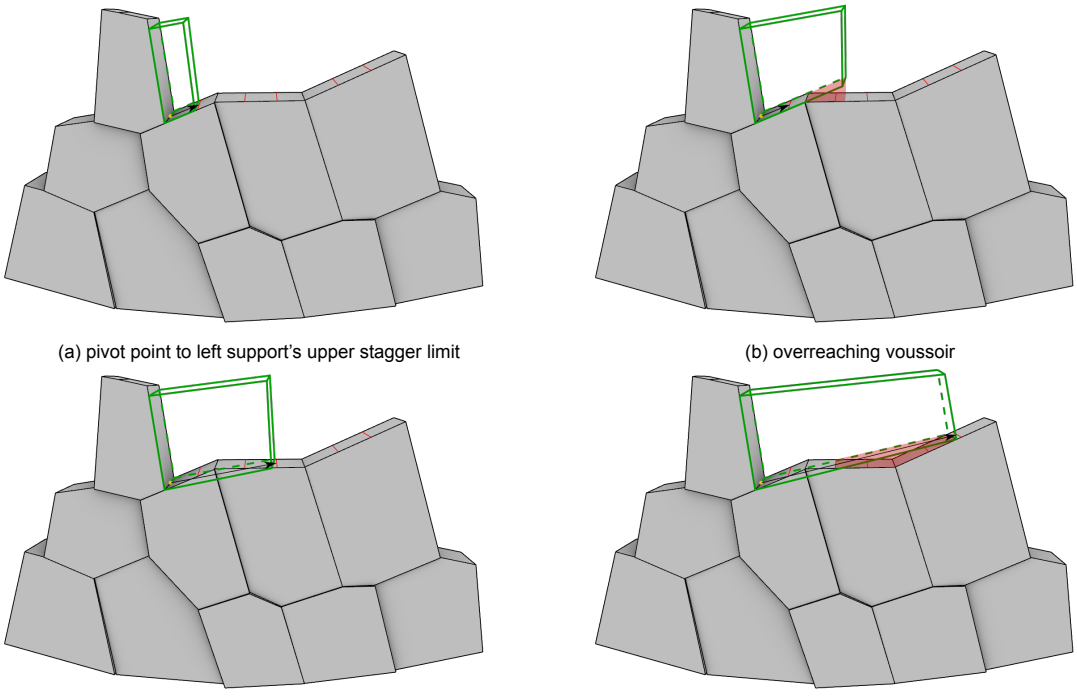

(a) pivot point to left support's upper stagger limit

(b) overreaching voussoir

(c) pivot point to next support's upper stagger limit

(d) void formation

Figure 3.17: Boundary vector search

To guarantee a complete cover of the thrust surface, candidate vectors, including the previously mentioned ones, reach from the pivot point until the upper stagger limits are created. Other candidates include vectors reaching from the pivot point to the top left corner of the next several supporting voussoir. Then, the candidate vector that forms the largest angle alpha with the patch vector is selected to be the boundary vector and alpha is selected as the search angle as shown in Figure 3.18. While such an approach can result in a voussoir placement that is very submerged in the supports, especially when the boundary vector stretches far and the voussoir selected from the stock does not, it guarantees that no voids are formed.

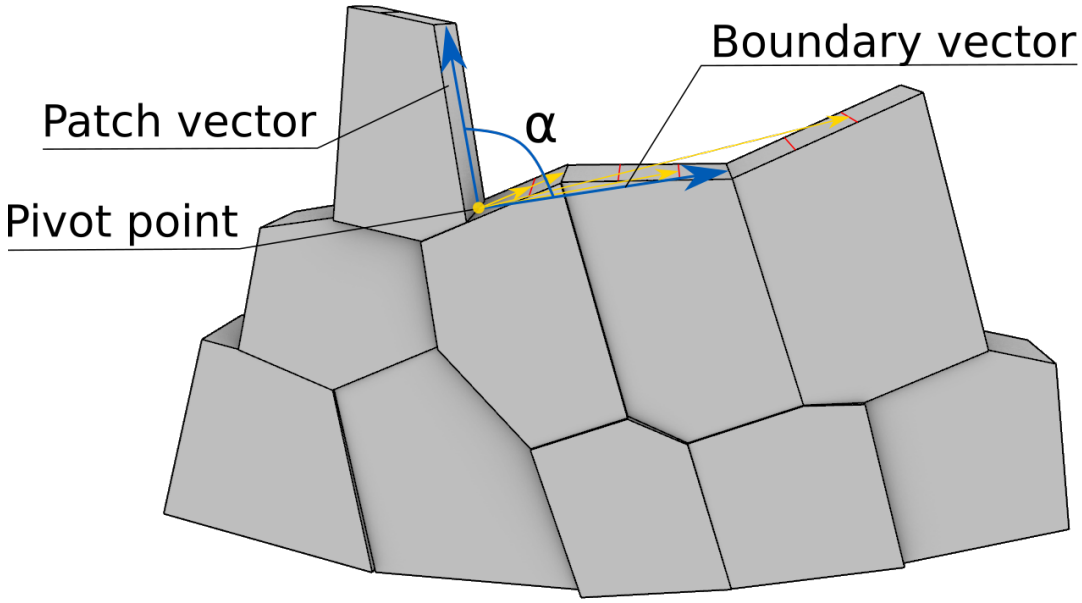

Figure 3.18: Boundary vector and search angle selected among the candidate vectors.

Step 2.2: Initial placement: Best-fit voussoir
Once the search angle is found, the stock is scanned for a voussoir with an angle at one of its corners that is within a user-defined range of the search angle as shown in Figure 3.19. The search happens sequentially and the stock can be sorted in a decreasing, increasing, or random order by voussoir volume.

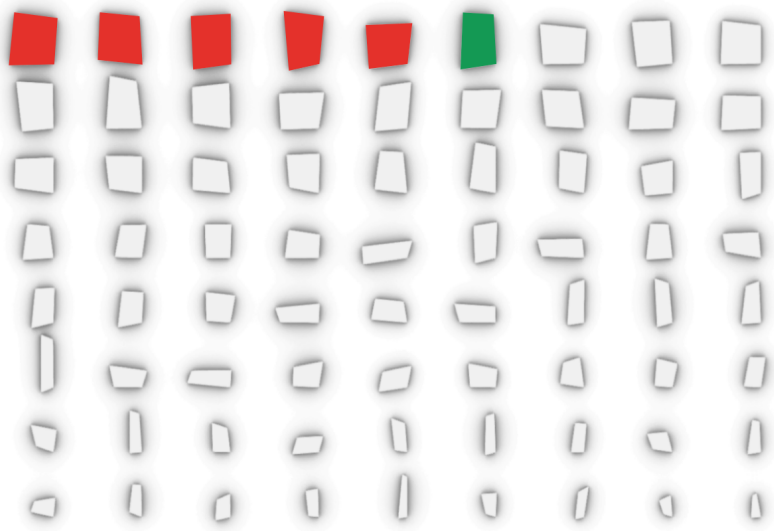

Figure 3.19: Search for a voussoir with the search angle within a sorted stock.

If a voussoir with the search angle alpha is not present in the stock, the voussoir with the closest corner angle is pre-cut. Two possibilities exist:

- If the search angle is larger than the available angles, the vertex corresponding to this angle is moved inwards until the search angle is found as shown in Figure 3.20a.
- If the search angle is smaller than the closest vertex angle, the voussoir is pre-cut by trimming the voussoir sides as shown in Figure 3.20b

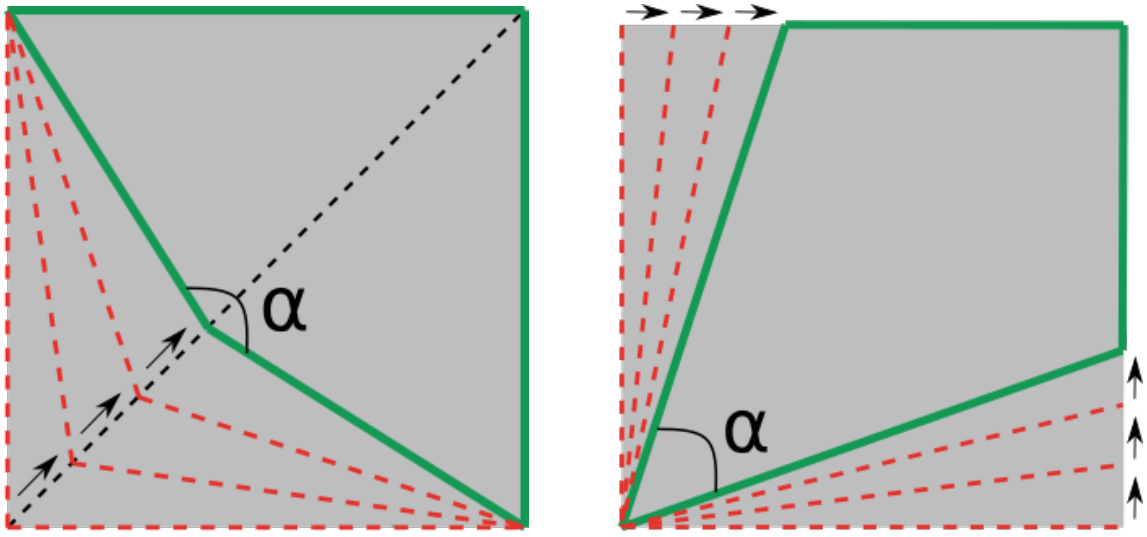

(a) when search angle is larger than corner angles

(b) when search angle is smaller than corner angles

Figure 3.20: Pre-cutting a voussoir

Step 2.3. Initial placement: Horizontal placement

The identified voussoir is moved to the pivot point so that the voussoir's corner that has the found angle coincides with the pivot point on the thrust surface that was previously used to obtain the search angle as shown in Figure 3.21. The voussoir is then horizontally rotated in place around the pivot point. It is done by first measuring the edge length of the voussoir face that will be oriented in the direction of the boundary vector. Next, a search point is moved along the boundary until the distance between the pivot point and the search point exceeds the previously found side length. A rotation angle beta is then formed by the search point, pivot point, and a point belonging to the middle of the voussoirs corner facing the direction of the boundary vector. For voussoirs in rows above, this step is replaced by creating a rotation circle around the pivot point, and angle beta is measured between the original location of the voussoir side and the place where the search circle intersects the shell.

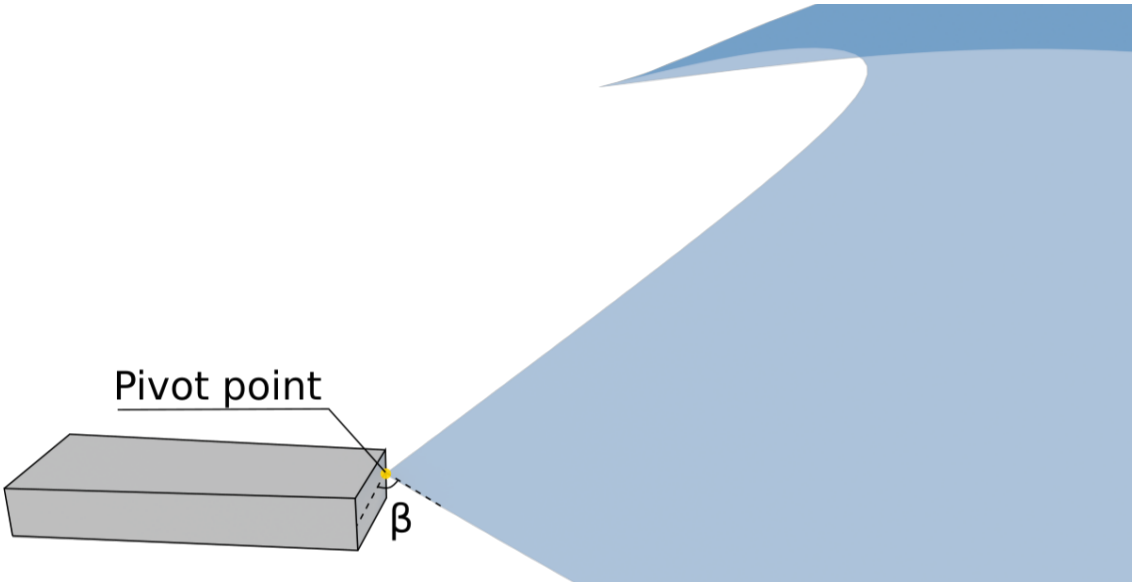

Figure 3.21: Horizontal rotation of a voussoir by angle beta.

Step 2.4. Initial placement: Vertical placement
To align the voussoir vertically, a search circle is formed with a radius equal to the distance between the

pivot point to the midpoint of the top transverse face of the voussoir. The circle is in the plane for which the boundary vector is the normal. This search circle's intersection with the thrust surface is found. A new search angle gamma is found between the pivot point, the thrust surface's intersection point, and a point where the circle intersects the middle curve of the voussoir's top transverse face. This procedure is shown in Figure 3.22. Finally, the voussoir is rotated in place using this angle.

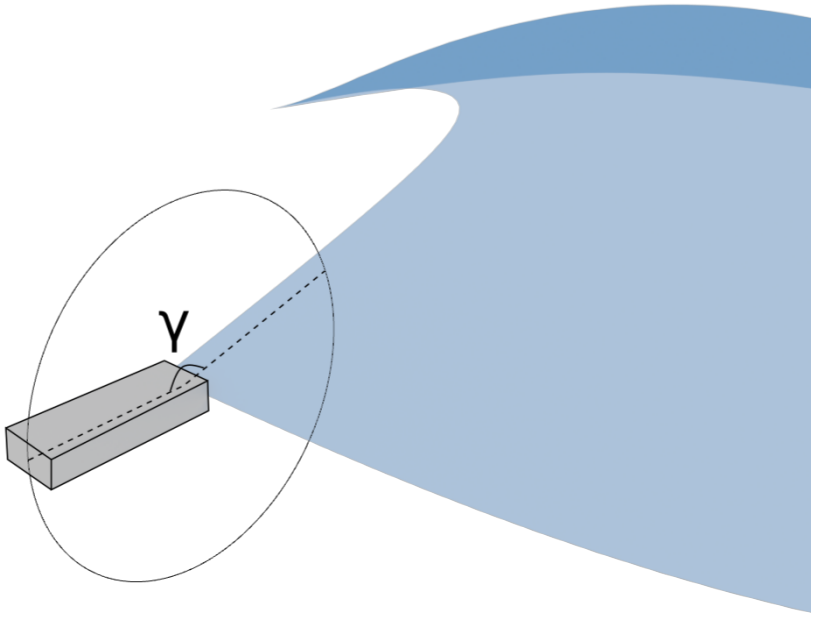

Figure 3.22: Locating the vertical search angle beta.

Step 2.4. Initial placement: Planar alignment
After the vertical alignment, the placement does not yet account for the local curvature of the thrust surface. This can be seen in Figure 3.23 in which the thrust surface at the left corner of the voussoir is noticeably further from the middle of the voussoir than in other places within the voussoir.

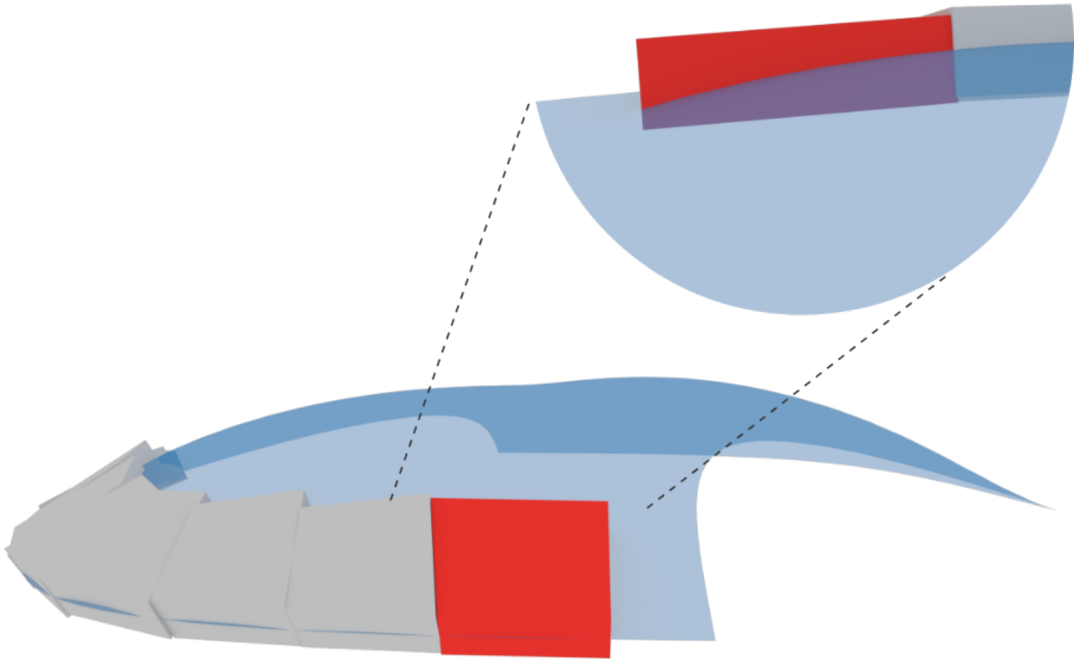

Figure 3.23: Misalignment with the thrust surface.

To align the voussoir with the local curvature, a best-fit plane is created. It is done by obtaining the normal vectors of the thrust surface in locations where the voussoir corner edges cross the thrust surface. These normal vectors are added to obtain a normal vector of the best-fit plane. Such a procedure is chosen because four points resulting from the corner intersection are one too many to construct a plane from just points. Then, using the normal vector of the voussoir's front face, the voussoir is aligned with the best-fit plane by rotating the voussoir around its volume centroid. This procedure is shown in Figure 3.24.

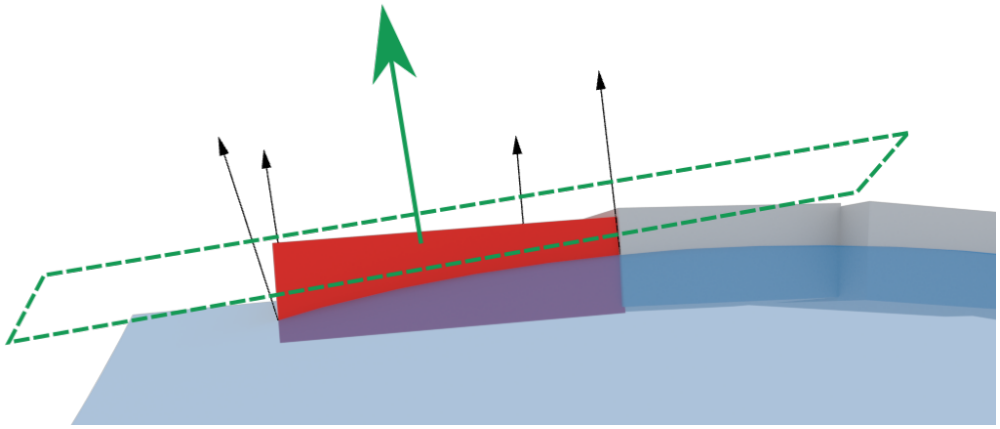

Figure 3.24: Alignment procedure with the thrust surface.

Following this procedure, the voussoir is now aligned with the thrust surface as can be seen in Figure 3.25. This completes the initial placement of a voussoir.

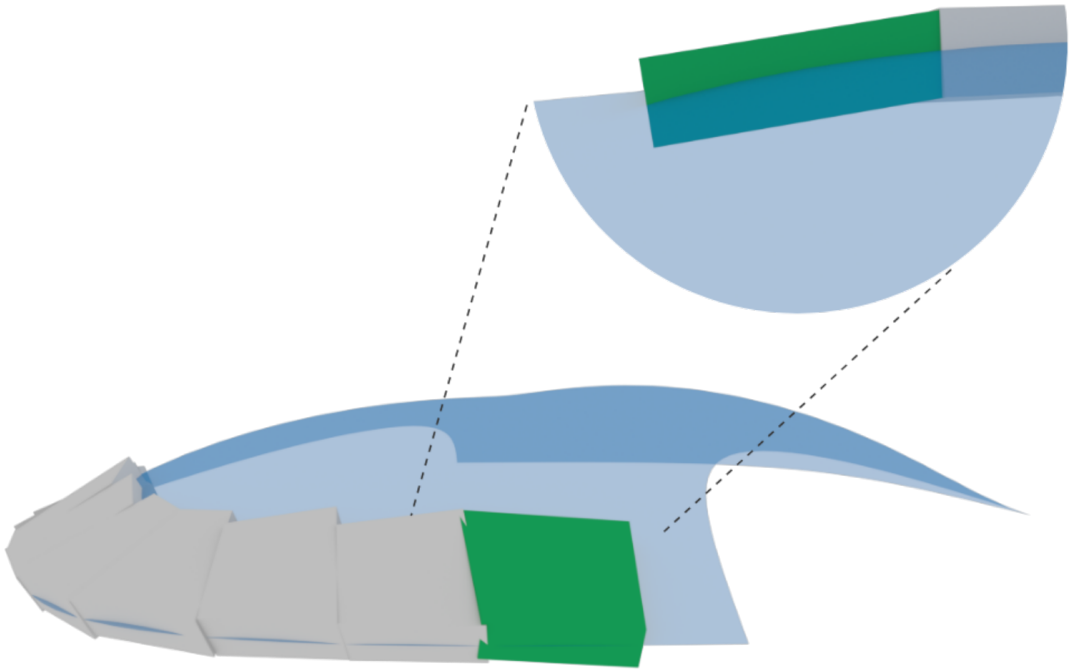

Figure 3.25: Thrust surface-aware placement.

Step 3.1. Calibration: Kern check
Following the voussoir placement, it is checked if the voussoir's kern fits the thrust surface and is adjusted if needed. Then, the voussoir is translated so that its left patch face and bottom transverse face are fully in contact with the neighboring and bottom voussoirs respectively, and the left face is aligned parallel to the force flow.

To ensure that the resulting structure is stable, the thrust surface must remain within the kern as per the middle-third rule visualized in figure 3.26. According to the rule, if the resulting force, which is represented by the thrust surface, is outside the kern, tension forces occur on one side of the cross-section and the effective width is reduced, turning the cross-section closer to a hinge.

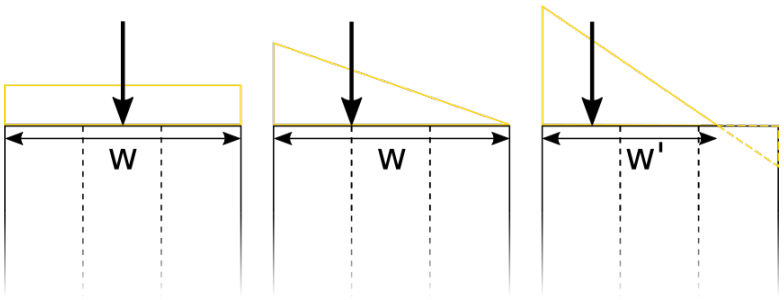

Figure 3.26: Middle third rule for uniform loading, triangular loading, and a loading case where the resultant force is outside the middle third of a cross-section.

Within the algorithm, the middle-third rule is followed by checking if the thrust surface does not intersect faces confining the kern as shown in Figure 3.27. If an intersection exists, the voussoir is incrementally translated along the previously found normal direction until no intersections exist.

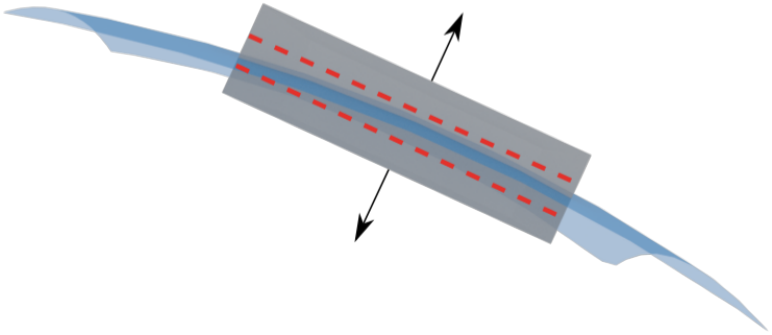

Figure 3.27: Fitting the thrust surface within the kern.

If a fit is not found, a parametrically defined fraction of the voussoir is sliced off as shown in Figure 3.28. This is done to decrease the size of the voussoir to make it less susceptible to the curvature of the thrust surface thus increasing the probability of a successful placement. The new voussoir is then aligned with the thrust surface again and the kern check is repeated until the voussoir fits.

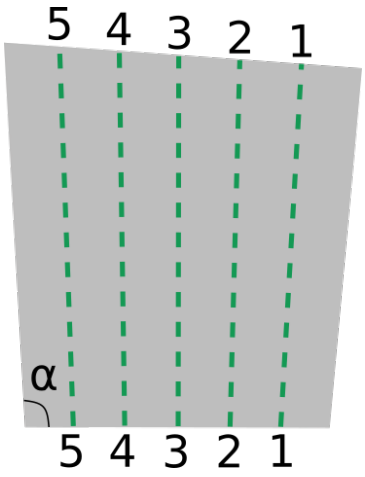

Figure 3.28: Cutting pattern to decrease the voussoir for a better fit.

Step 3.2. Calibration: Left shift
With the kern check completed, it is ensured that a voussoir interface with voussoirs around it can be complete and planar. To elaborate, neighboring voussoirs are linked since pivot points for voussoir placement are taken as the locations where the previous voussoir's bottom corner edge intersects the thrust surface. However, because of the curvature of the thrust surface, the leading voussoir is not in the same plane as the previous voussoir, and therefore a small gap forms between them shown in Figure 3.29.

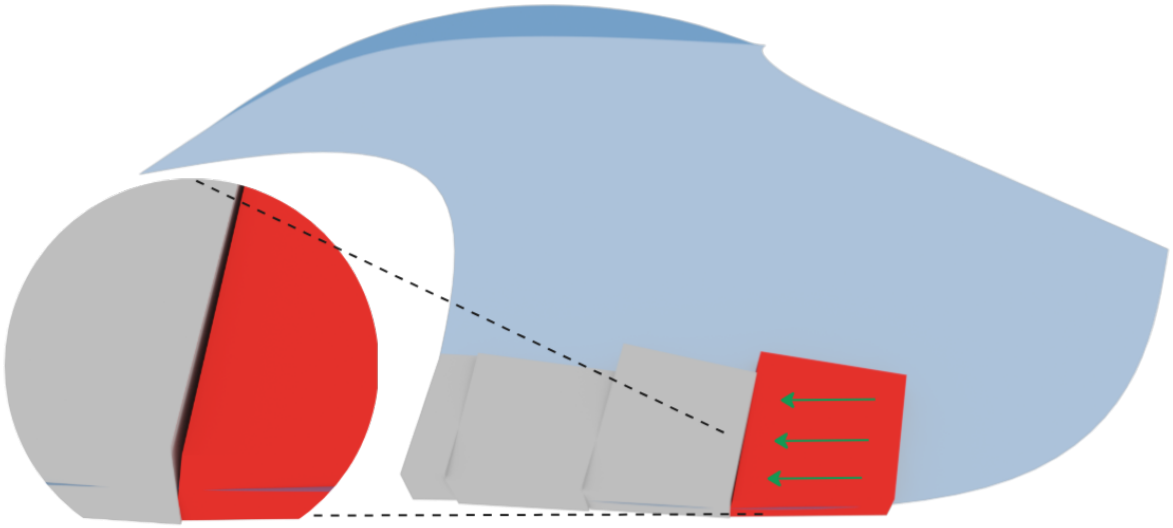

Figure 3.29: Gap between neighboring voussoirs due to thrust surface's curvature.

To solve this error and close the gap, the leading voussoir is pushed back until the gap is sealed like in Figure 3.30. This ensures that neighboring voussoirs are fully in touch, which is relevant for the stability of the structure.

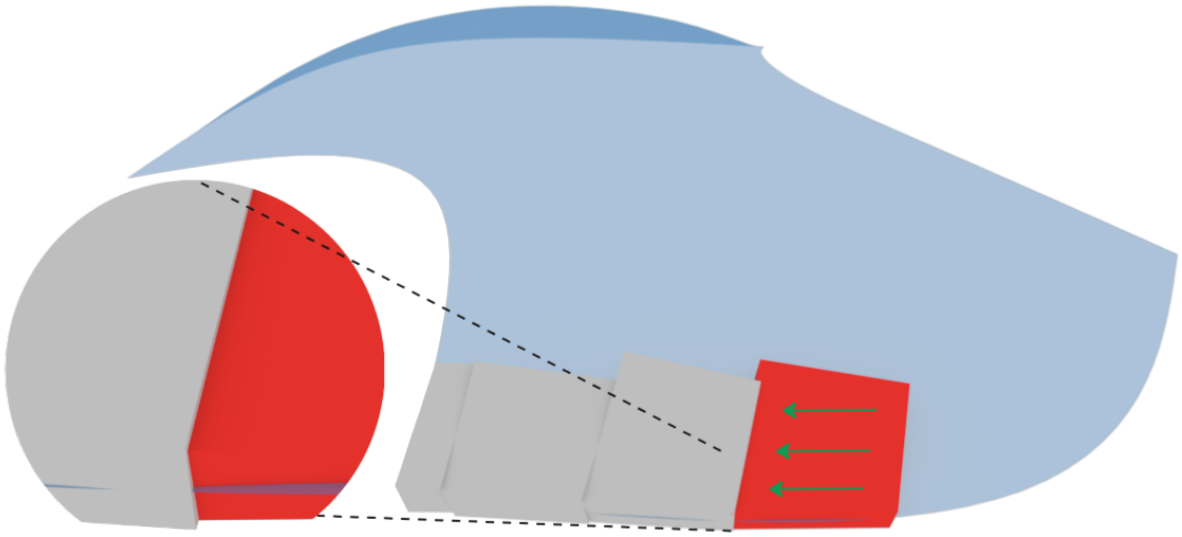

Figure 3.30: Leading voussoir is pushed back to seal the gap.

Step 3.3. Calibration: Support submerge
Similar to step 3.2, the voussoir needs to be pushed downwards to seal the gap that has formed between it and its supports as shown in Figure 3.31. This is done to ensure that planar offcuts and maximum contact surfaces between voussoirs can be created in a later step

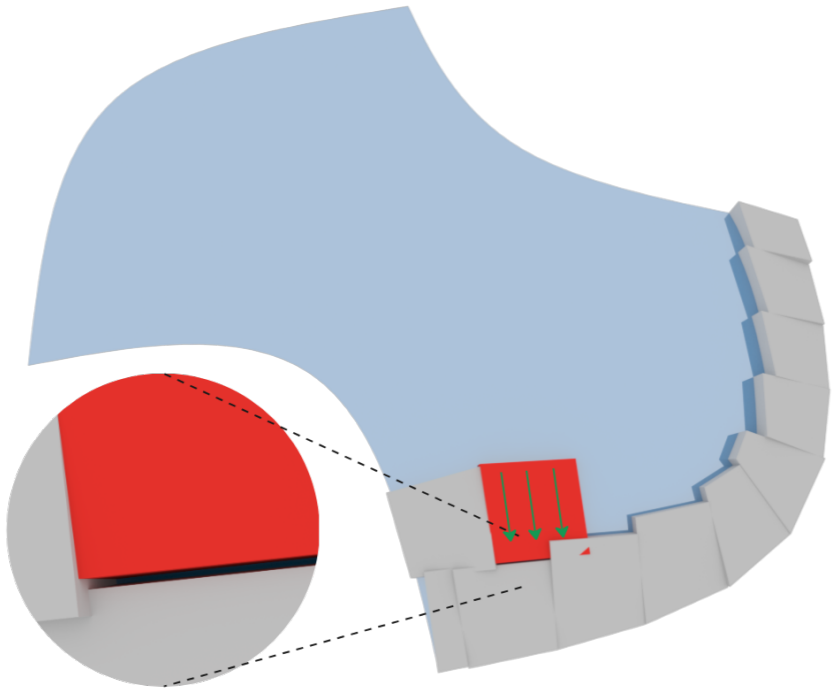

Figure 3.31: Submerging a voussoir in its supports.

Step 3.4. Calibration: Patch face stagger & alignment

Next, voussoir's leading patch side is aligned with the force flow and staggering is ensured as shown in Figure 3.32. The staggering is needed to create an interlocking geometry that prevents the movement of any individual voussoir or a row with respect to other voussoirs. This is done by first identifying the pivot points on the next possible supports, which are points within the middle third of their top transverse faces. It is then checked which potential pivot points are within the placed voussoir. The furthest such point is identified and from it, a cutting plane is found parallel to the force flow. If the cutting plane crosses the voussoir's top patch face, the voussoir is cut along it. If it does not, the next possible pivot point is considered. If none of the pivot points result in a cutting plane that crosses the top patch face of the voussoir, it is allowed to cut the voussoir when the furthest cutting plane crosses either the right or left patch faces.

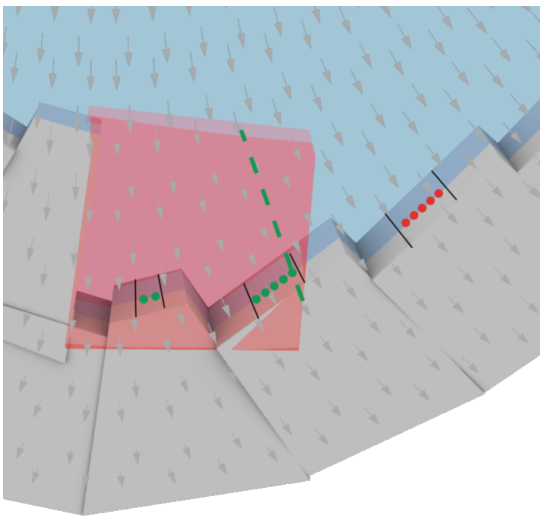

Figure 3.32: Process of aligning and staggering a voussoir.

On top of that, the closest search point to the pivot is used to create a backup voussoir. Its leading patch face is made parallel to the force flow in the same way outlined above. This voussoir is created to future-proof the script and is used without the need for satisfying the following requirements in case an unforeseen error occurs in any of the following steps with the intended voussoir. The closest search point is used to create it to minimize the surface area of the final shell that would be covered by backup voussoirs.

Step 3.5. Calibration: Transverse face alignment

With both of the patch faces aligned, voussoir's top transverse face is aligned perpendicular to the local force flow to prevent sliding as shown in Figure 3.33. Since both patch faces have been aligned parallel to the force flow, but are not necessarily parallel to each other due to the shifting force flow, the top is cut so that it forms equal angles lambda with both patch sides. This approximates a face that is most perpendicular to both patch faces.

With the previous step complete, the voussoir has been positioned and the steps are repeated for the next voussoir. Before that, the voussoir is placed in a COMPAS network data structure to maintain the connectivity relationships between voussoirs to identify neighbors and supports. A network is a geometric implementation of an edge graph and can be seen in Figure 3.34. Each vertex represents a voussoir whereas each edge represents that the voussoirs are connected.

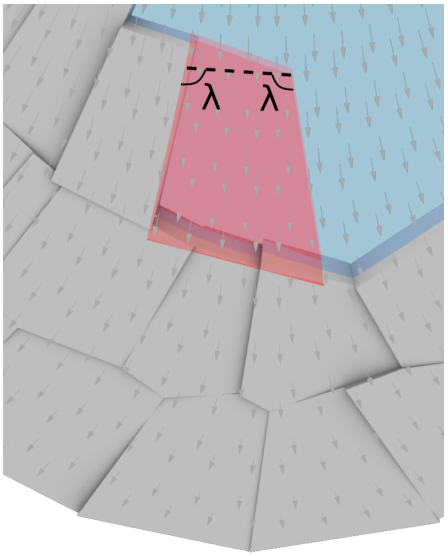

Figure 3.33: Process of aligning the top transverse face perpendicular to the local force flow.

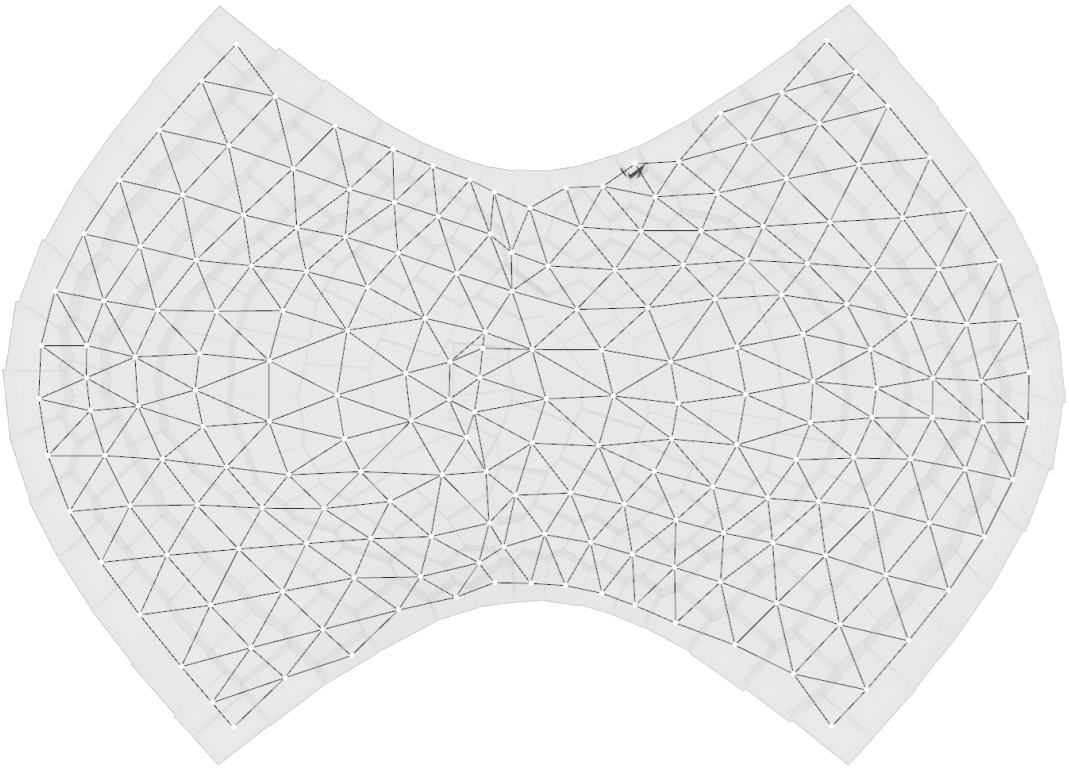

Figure 3.34: Geometric representation of a network data structure.

Step 4.1. Row clean-up: Top transverse trim

Once a voussoir crosses the right elevated boundary or an interface boundary, a row of voussoirs is completed. Then the clean-up process of preventing uneven top transverse curve alignments, removing overlaps between voussoirs, and establishing planar interfaces is performed. This stage also serves the purpose of planarizing faces for fabrication and build purposes. More specifically, all offcuts are made planar to allow for simpler machining without the need for a mill, saw, water jet, or other tools that have more degrees of freedom than their simpler counterparts. On top of that, offcuts are always complete. That is, a cut never stops in the middle of a voussoir.

First, the entire row is checked for voussoirs with top transverse faces that tower over at least one of their neighboring voussoirs. They need to be trimmed so that voussoirs in the row that will be placed above can be supported evenly, without individual voussoirs needing to overcompensate for elevation differences in supports. Otherwise, transverse interfaces that vastly differ from the force flow would be created which could create sliding of the voussoirs.

To solve this, voussoirs that are towering over their neighbor by more than a parametrically defined tolerance are cut. The cutting plane for this is defined using points from the neighbor's top transverse face over which the central voussoir towers and a vertex from the other side of the central voussoir's top transverse face. An example of voussoirs that need trimming are identified in Figure 3.35a and the results are shown in Figure 3.35b.

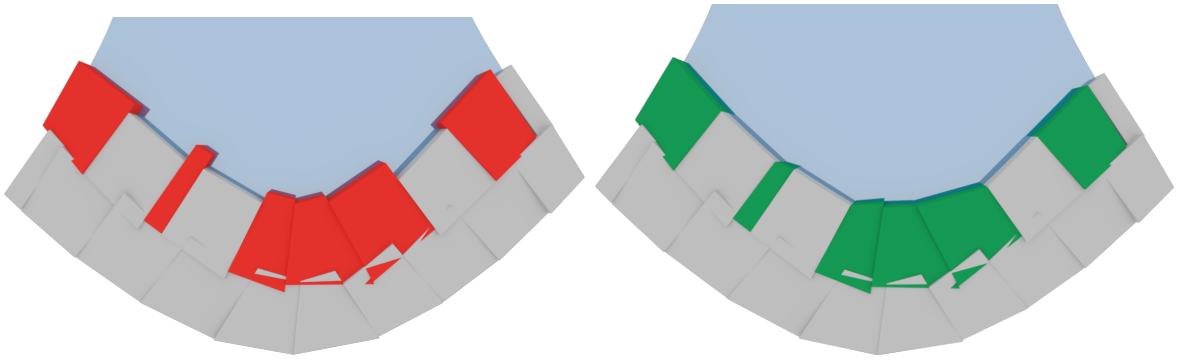

(a) Identified voussoirs (b) Cut voussoirs

Figure 3.35: Top transverse face alignment to the local force flow

However, such cutting improperly aligns the transverse curves which had been aligned before. Therefore, they are aligned again followed by a repeated leveling of the top interfaces.

Step 4.2. Row clean-up: Offcuts

As the final step of the automated stacking algorithm, the overlapping parts of voussoirs are cut to create planar interfaces. It is also at this step that the quadrilateral voussoirs are turned into hexagonal prisms, which inherently enhance the interlocking of the voussoir network. First, an offcut with the neighboring voussoir on the left side is performed by using the left neighbor's right patch face to create a trimming plane as shown in Figure 3.36a. A planar offcut is ensured because input stock was assumed to have planar side faces and the central voussoir was shifted left in step 3.2: Left shift to have a complete overlap with the neighboring voussoir. Next, the bottom offcuts for the supporting voussoirs are performed. Importantly, for bottom offcuts the trimming planes are created by using two vertices that belong to a face that has already been offcut and a third vertex which results in a complete planar offcut. Otherwise, the offcuts can be misaligned or non-planar, which would demand more complicated processing techniques. The process is shown in Figure 3.36b and Figure 3.36c. All offcuts are shown in Figure 3.37.

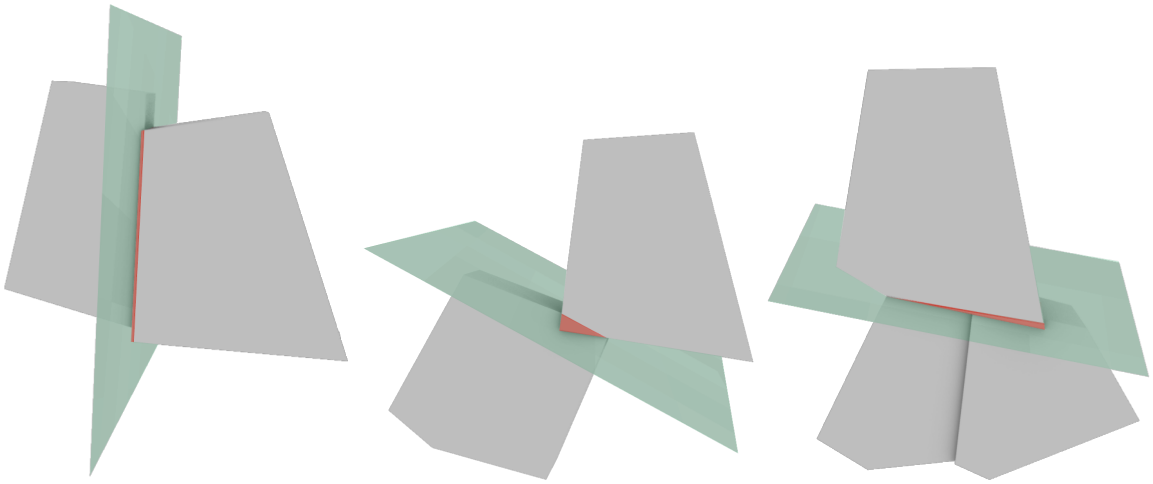

(a) cutting using left neighbor (b) cutting using left support (c) cutting using right support

Figure 3.36: Cutting process with the left and supporting voussoirs

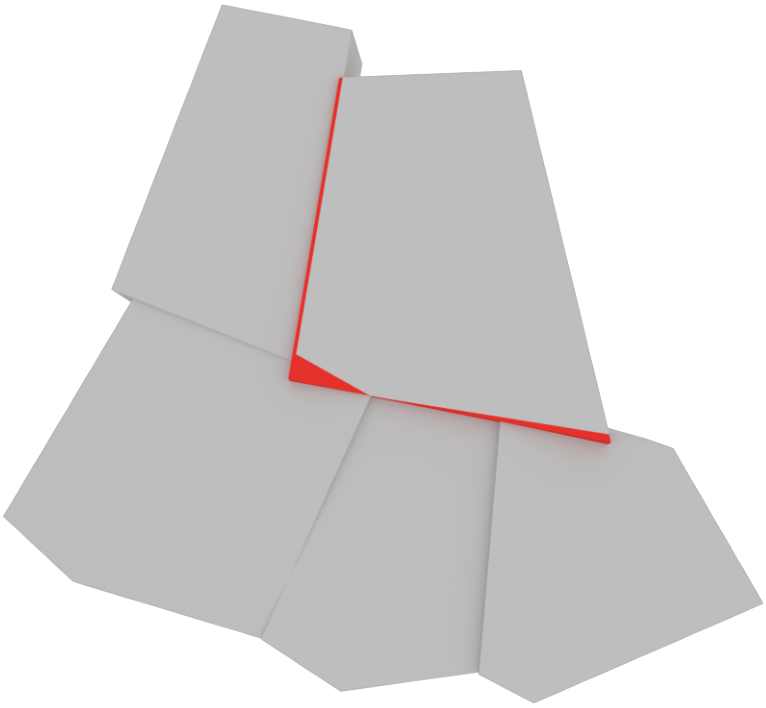

Figure 3.37: Complete offcuts for a voussoir.

Step 5.1. Post-Processing: Merging segmented layers
Due to the various deployment options, the created voussoirs from different deployments are combined after the completion of each so that the next deployment can use all of the previously placed voussoirs as input geometric and stock-related constraints. This is done by serializing the voussoirs as a .json file that stores information on meshes, connectivity, and attributes assigned to the voussoirs during their placement.

Step 5.2. Post-Processing: Cleanup
Depending on the deployment strategy, certain interfaces between voussoirs obtained during different runs of the algorithm must be manually cut to ensure proper staggering and grip between voussoirs. On top of that, the algorithm has built-in safety features that prevent, for instance, certain offcuts from being created if the cutting plane does not cut the voussoir as intended. Therefore, the final step is to manually examine the result and cut any voussoirs as needed.

Step 5.3. Post-Processing: Validation
Structural models of historical masonry structures demonstrate that stability governs the design of vaulted structures not stresses [15]. Therefore, in the final steps, the results and the method are validated to ensure the stability of the structure. This is done using the Rigid Block Equilibrium method available via COMPAS. It uses a COMPAS assembly data structure and indicates if contact forces that would result in a compression-only structure can be found as shown in Figure 3.38. An alternative approach that could be examined as a more preliminary check is finding the angle of deviation from the force flow for the side surfaces of a voussoir as well as the angle of deviation for the top sides being perpendicular to the force flow. This latter approach is not explicitly demonstrated in this thesis.

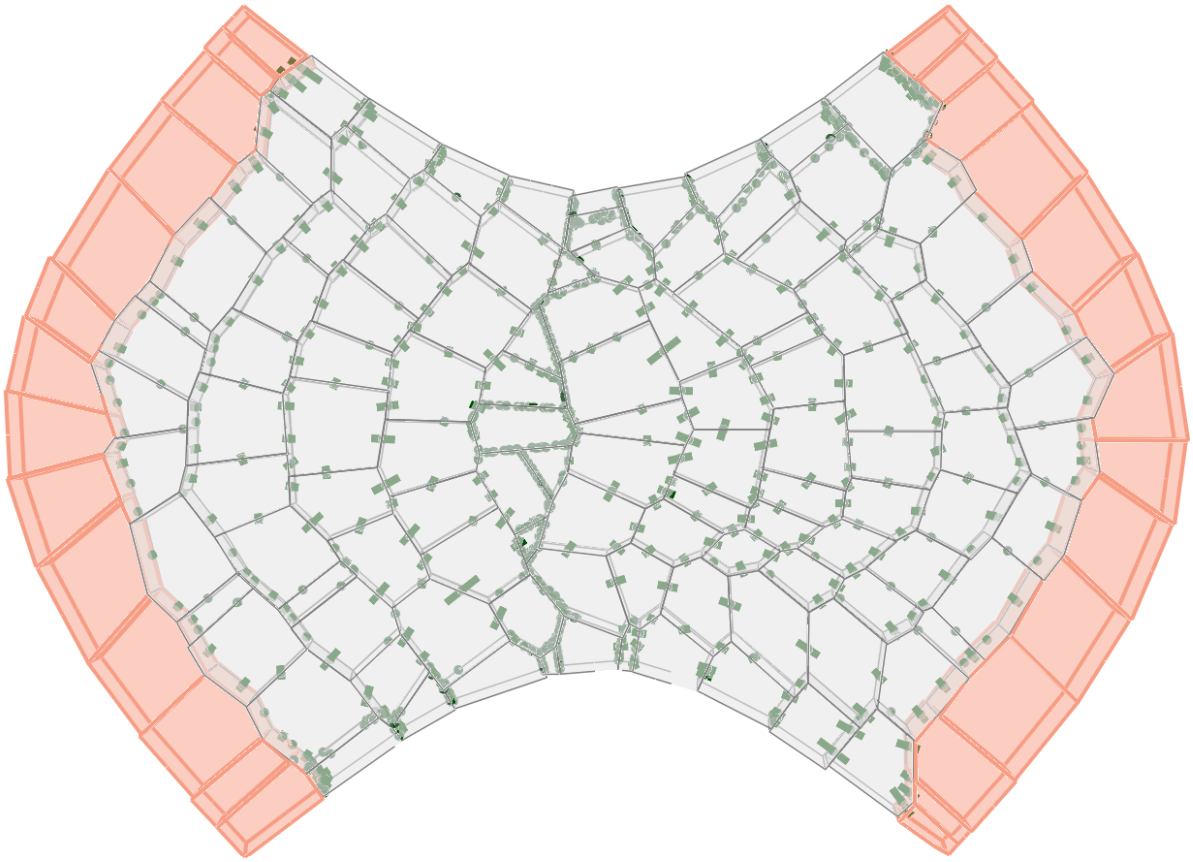

Figure 3.38: Validated results. A force equilibrium resulting in a stable structure is found.

3.6. User Controls

Throughout the placement process, the user has the option to determine the retained volume of each voussoir after it has been cut and placed. If such results, aesthetics of the structure, stability, or any other user-relevant criteria do not satisfy the prioritized requirements, a user has the option to adapt or even iteratively change the design. As was discussed in the workflow and shown in Figure 3.3, a designer can change how the algorithm is deployed, modify the input shape, vary what stock is used, and inform the deconstruction process. These options are outlined in the following sections.

Deployment strategy variation

As outlined in step 1.1: Deployment, by defining different deployment strategies, the designer can apply the algorithm to segmented parts of the thrust surface that are catered to the force-flow, geometry, presence of elevated boundaries, existing voussoirs, desired voussoir pattern, desired stock, etc. For instance, a designer might decide to split the thrust surface into parts so that the voussoir placement symmetrically tends toward the center of the structure as shown in Figure 3.39. By doing this, the user can achieve aesthetical symmetry and simplify the placement process as the placement does not cross the center, which is where the force flow rapidly changes directions.

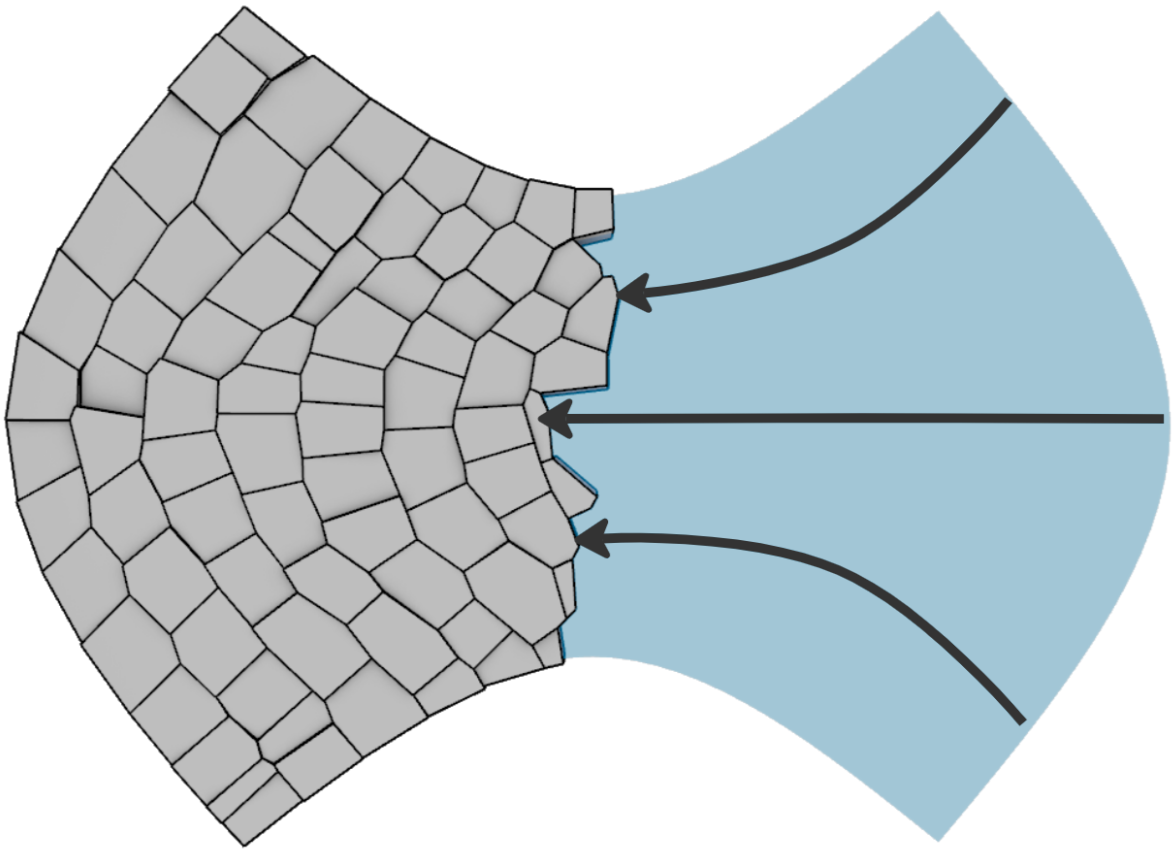

Figure 3.39: Symmetric voussoir deployment.

An alternative option is to base the next section on the existing voussoirs as shown in Figure 3.40a. This can prove useful if rows in the previously placed rows converge upwards at an uneven pace. This is because “step 4.1: Top transverse trim” attempts to align the top transverse face perpendicular to the force flow as well as trim voussoirs that are leaning over its neighbors. If the voussoir frontier is not progressing upwards uniformly, voussoirs are excessively cut in step 4.1 to align and smoothen the frontier. To avoid these offcuts, the voussoir frontier can be selected manually from voussoirs across various rows, which is currently not supported by the sequential nature of the stacking algorithm. In this way, half and partial rows can be created to even out the advancement of the rows towards the center which in return minimizes the excessive offcuts on the side of the advancing rows as can be seen in Figure 3.40.

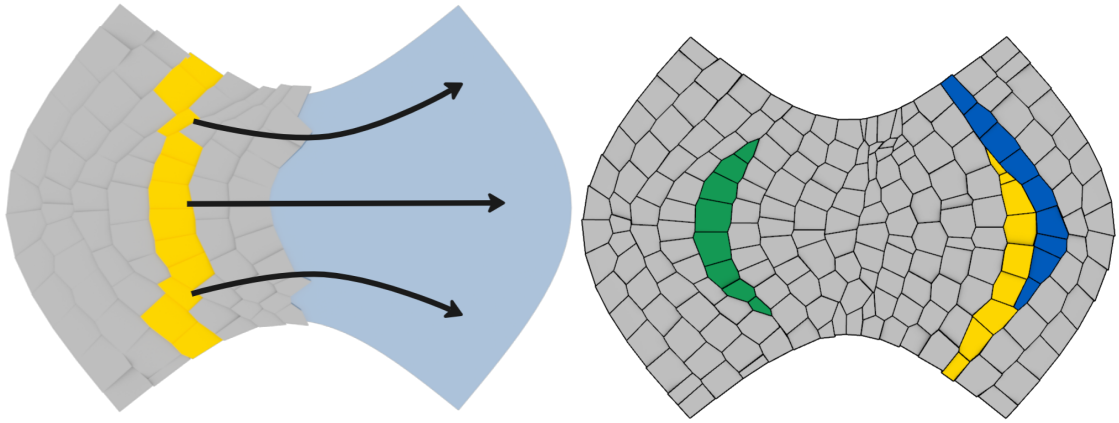

(a) Deployment direction (b) Creation of half rows (green) and partial rows (yellow & blue)

Figure 3.40: Shell created using stacked deployment

Next, the user can segment any complicated geometry into simpler surfaces, which are tessellated separately and stitched together in post-processing. For instance, as seen for the shell in Figure 3.41a and 3.41c, the force flow in the shell rapidly changes directions in locations shown in Figures 3.41b and 3.41d thus complicating the voussoir placement there. Even more, in the middle, forces not only flow towards the edges in a radial direction but also shift towards the middle of the edges thus the middle can also be separated into four symmetric sections to simplify tessellation.

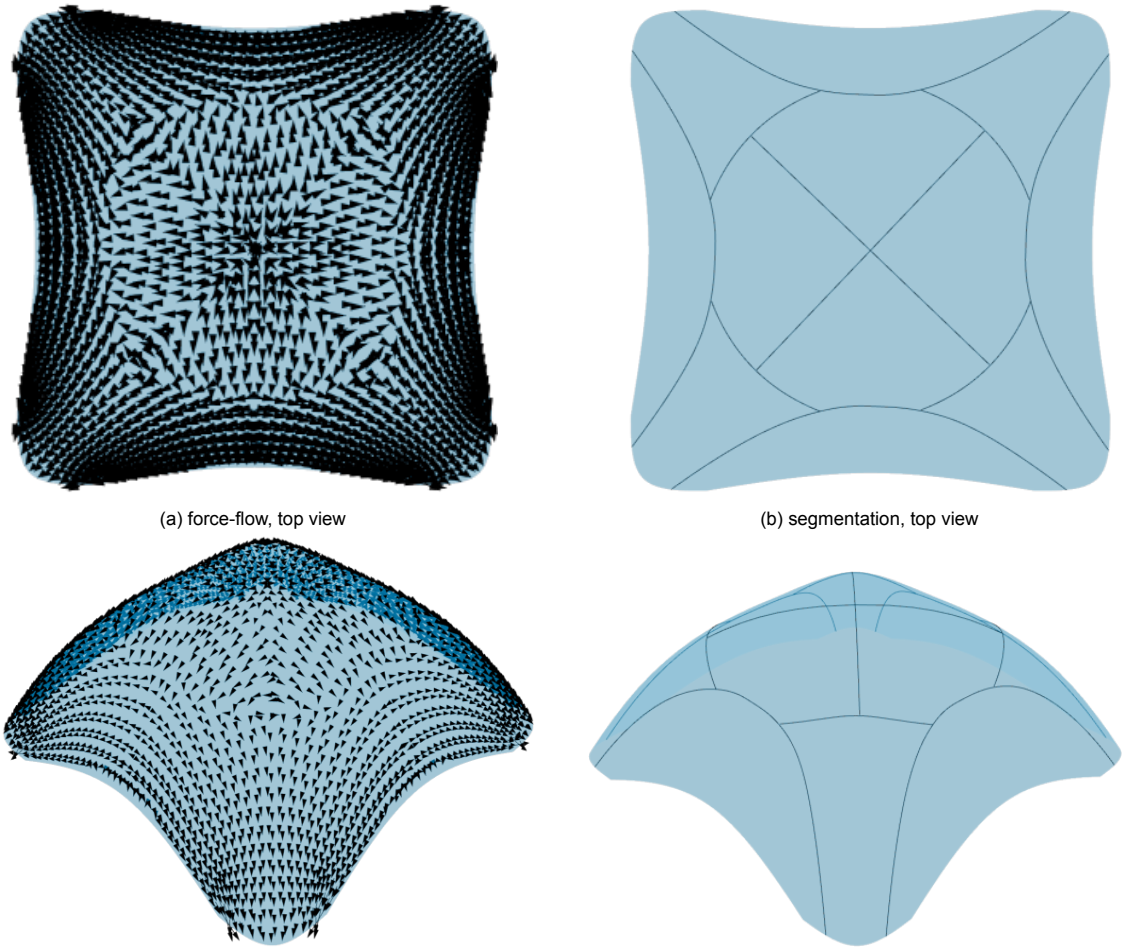

(a) force-flow, top view (b) segmentation, top view

(c) force-flow, perspective view (d) segmentation, perspective view

Figure 3.41: Segmentation of shell based on its local force-flow

Once the segmentation boundaries are delineated, each section is separately tessellated as shown in Figure 3.42. Once each segment is completed, they are manually post-processed and stitched together to form the final structure. This is done by not cutting the voussoirs which intersect the boundaries of the segments in locations. Thus, they hang over the segment and will overlap voussoirs of the neighboring segment. These overlaps provide sufficient space where a user can manually cut the voussoirs to still ensure a staggered boundary and a complete cover of the thrust surface.

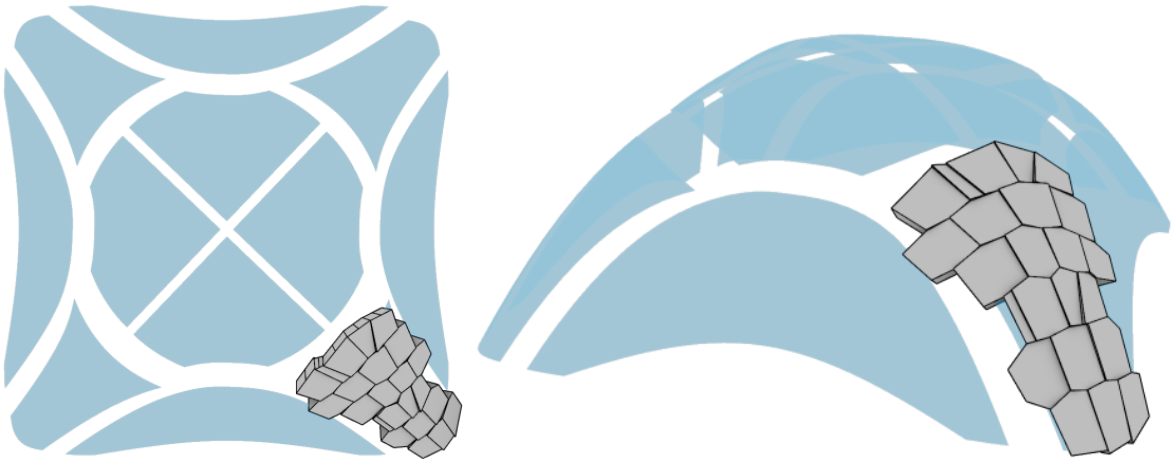

(a) top view (b) perspective view

Figure 3.42: Separately segmented sections of a shell

It is important to note that for such a structure as this, the capability of deploying the algorithm across segmented parts is not merely used to optimize volume as it was for the pedestrian bridge. Rather, segmentation is an important design decision that future-proofs the creation of any shape and without it, this structure is impossible to tessellate in a single launch with the currently proposed algorithm.

Input shape modification
An alternative approach to dealing with the rapid changes in the force flow is to smoothen them by modifying the input geometry. This can be done by transforming elevated boundaries into supports, varying the dimensions of the shape, and assigning additional supports, among other strategies. While the algorithm is tested for various shapes, targeted shape modification strategies are not explicitly examined in this thesis.

Stock curation
Because the algorithm supports voussoirs placement over segmented sections of the thrust surface, the user can vary what stock is used per segment. This can be desired for placing thicker voussoirs at the bottom of the structure or in places where dynamic loads are expected. This is because thicker voussoirs would have a wider kern that could accommodate changes in the thrust surface, thus increasing the load-bearing capacity of a structure before it requires tensile capacity for stability. This thesis will examine the impact of selecting voussoirs of various dimensions as well as geometrical regularity.

Informed mode of deconstruction
Finally, if desired voussoirs are absent in any repository, a designer could inform the contractor to adapt their mode of deconstruction to produce a desired stock. This could entail specifying quantities and dimensions of a desired stock which would alter the technologies and level of carefulness that the contractor would follow. Details of how such a deconstruction could occur are beyond the scope of this thesis.

3.7. Waste Minimization

Once a structure has been created, the final voussoirs are compared to their initial states to assess the amount of retained volume and offcuts. However, depending on their size and geometry, certain offcuts

can be returned to the stock rather than disregarded as waste. Furthermore, depending on what order the cuts are performed, different size offcuts can be created as visible in Figure 3.43a and Figure 3.43b. This can impact if the offcuts should be discarded or returned to the stock for further placement and thus the total concrete volume retained. On top of that, the order of cuts impacts the total cut length, which corresponds to the processing required. The preference, of course, is for selecting a cutting pattern that minimizes the cutting.

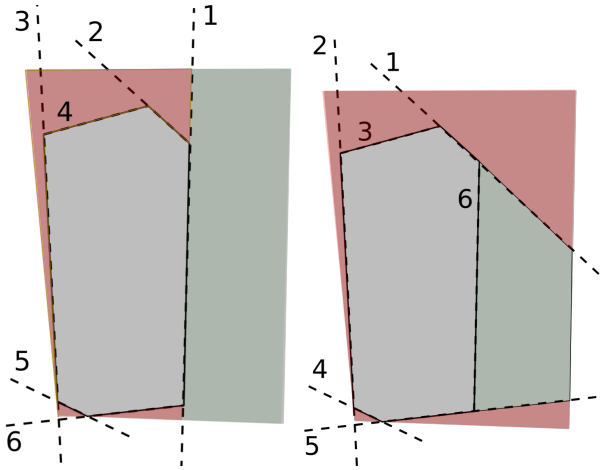

(a) resulting in smaller retained volume

(b) resulting in larger retained volume

Figure 3.43: Different voussoir cutting patterns

Nevertheless, analyzing cutting patterns to maximize useful offcuts and minimizing the cutting length is beyond the scope of this thesis. Rather a fudge factor that accounts for the waste generated is used. It is multiplied by the volume of the extracted voussoir to obtain the total volume used for creating a voussoir. The remaining volume is either discarded, used for creating a different voussoir in the same structure, or retained in the stock for future placements. This process is depicted in the following pseudo-code:

Algorithm 1 Waste minimization

$Volume_{min}$ = minimum useful offcut volume defined by designer
Sort voussoirs by volume in a decreasing order
for $voussoir_1 = 1, 2, \dots, N$ **do**
    $Volume_{waste}$ = $Volume_{final}$ * fudge factor
    $Volume_{remaining}$ = $Volume_{initial}$ - $Volume_{final}$ - $Volume_{waste}$
    if $Volume_{remaining}$ > 0 **then**
        for $voussoir_2 = 1, 2, \dots, N$ **do**
            if Volume voussoir$_2$ < Volume$_{remaining}$ **then**
                Cut $voussoir_2$ from waste of $voussoir_1$
            end if
            if Volume voussoir$_2$ > Volume$_{remaining}$ **then**
                if $Volume_{remaining}$ > $Volume_{min}$ **then**
                    Retain offcut in stock for future structures
                end if
                if $Volume_{remaining}$ < $Volume_{min}$ **then**
                    Discard offcut as waste
                end if
            end if
        end for
    end if
end for

4

Results

“The foremost [design] task lies [...] in leaving off everything that is not necessary. A well-shaped shell is such a dominant structure, that it needs no addition of other dominant elements. On the contrary, it forbids them. The shell is the supporting structure and the space enclosure at the same time. So it cannot be but honest.”

- Heinz Isler, 1980

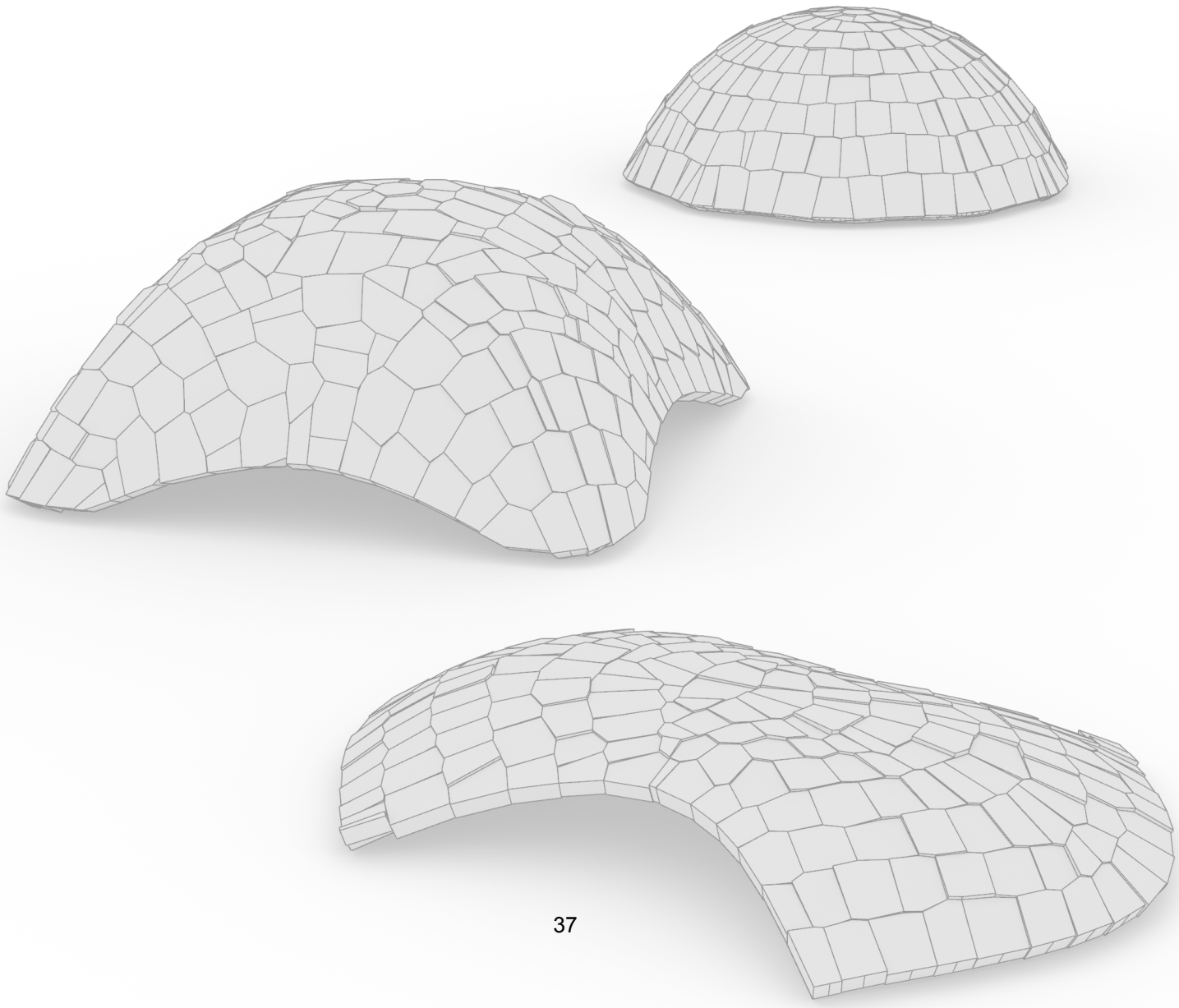

The following chapter tests the stacking algorithm proposed. In particular, it examines how the structure and the volume retained by each voussoir depend on:

- stock dimensions,
- regularity of the voussoir shapes,
- deployment strategy,
- shape of the thrust surface

Three different thrust surfaces were tessellated in this thesis:

- a pedestrian bridge referred to as the “Bowtie”,
- a dome with a decagonal polygon with rounded corners as its base,
- shell structure referred to as the “Pillow”

Two different randomly created input stocks with 600 elements in each are used for generating the results: 0p7-1p0-0p0 and 0p7-1p0-0p2. Their characteristics can be found in Table 4.1. The naming convention refers to the dimensions in meters of the voussoirs present in the stock where “p” can be read as “point”. The first number refers to the lower bound of the voussoir length and width while the second number refers to their upper bound. The final number refers to the maximum deviation from the bounds that the voussoirs can have. Therefore, the stock 0p7-1p0-0p0, for which the deviation number is 0, consists of regular elements whereas the stock 0p7-1p0-0p2 is of irregular voussoirs for which the length and width can vary by 0.4 meters at most. The height for all elements is between 20 to 30 cm.

On top of that, each stock is sorted differently by volume to access voussoirs in a different order since the stacking algorithm searches for the search angle in a sequential manner as was shown in step 2.2 of the stacking algorithm. This is done to study the impact of stock sorting on the results and see how voussoir size influences the retained volume. When a stock is sorted in decreasing order, a suffix “decr” is attached to the name. When sorting is done in increasing order the suffix is “incr”. When no sorting is performed, the suffix is “rand”.

Table 4.1: Characteristics of the stocks used in this thesis

Stock name	Element count	Voussoir type	Dimensions (m)			Stock assortment
			Length	Width	Height	
0p7_1p0_0p0_decr	600	Regular	0.7 - 1.0	0.7 - 1.0	0.2 - 0.3	Decreasing
0p7_1p0_0p0_incr						Increasing
0p7_1p0_0p0_rand						Random
0p7_1p0_0p2_decr		Irregular	0.5 - 1.2	0.5 - 1.2		Decreasing
0p7_1p0_0p2_incr						Increasing
0p7_1p0_0p2_rand						Random

4.1. Pedestrian bridge “Bowtie”

The primary thrust surface studied in this thesis and shown in Figure 4.1 is a shallow pedestrian bridge referred to as the “Bowtie” due to their resemblance. As was discussed, it was form-found using Rhino Vault 2, it is 7.1 meters wide, 9.9 meters long, and 1.2 meters high and is shown next to the 1.9 meter tall author to scale. Thus, in its span and height, it resembles the Re:Crete bridge mentioned in the Theoretical Framework. Simultaneously, the span could potentially be elongated as, for instance, stone arches that use post-tensioning have reached up to 45 meters in span [46].

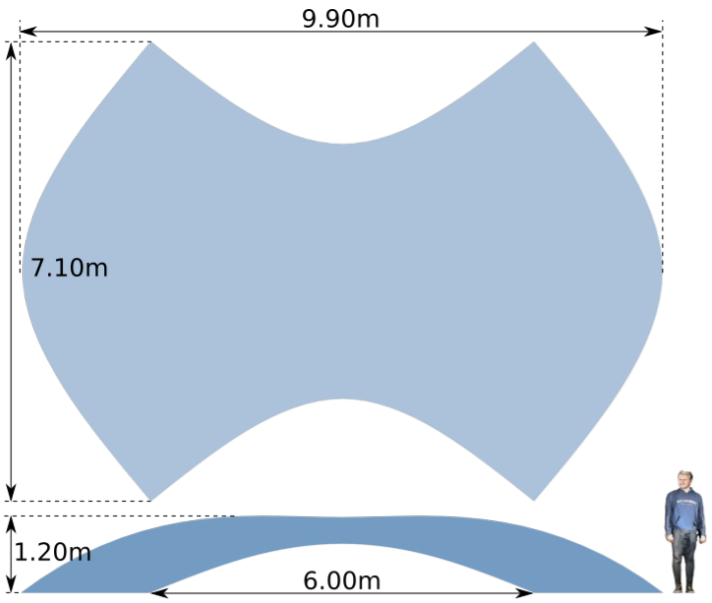

Figure 4.1: Dimensions of the primarily studied thrust-surface “Bowtie”

Symmetric deployment
The Bowtie was tessellated using all six stocks in symmetric deployment and the results are displayed in Figure 4.2. As discussed in step 1.1, symmetric deployment entails that all shells were created by first deploying the algorithm across half of the shell towards the center followed by a second deployment from the other support boundary towards the center.

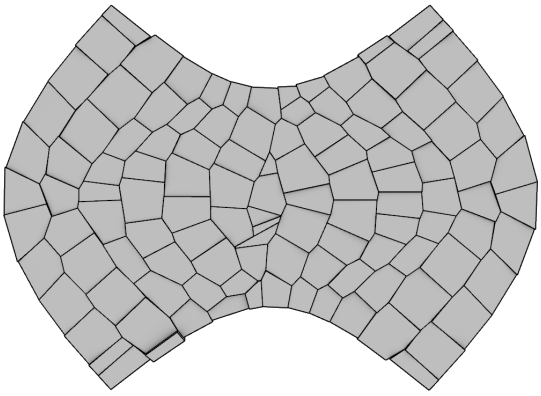

(a) 0p7-1p0-0p0-decr

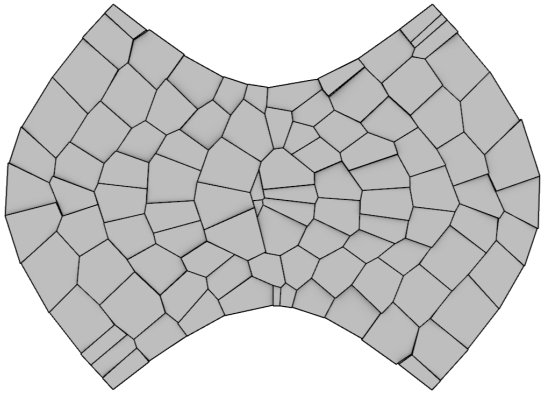

(b) 0p7-1p0-0p2-decr

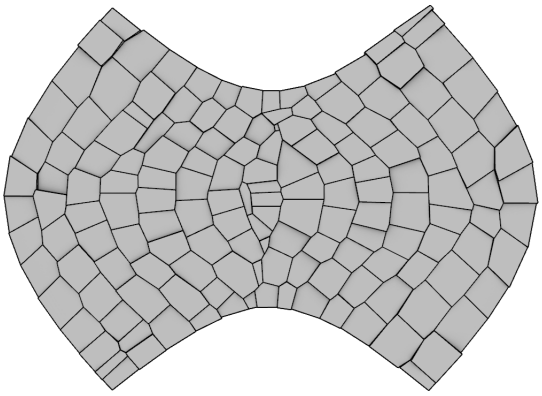

(c) 0p7-1p0-0p0-rand

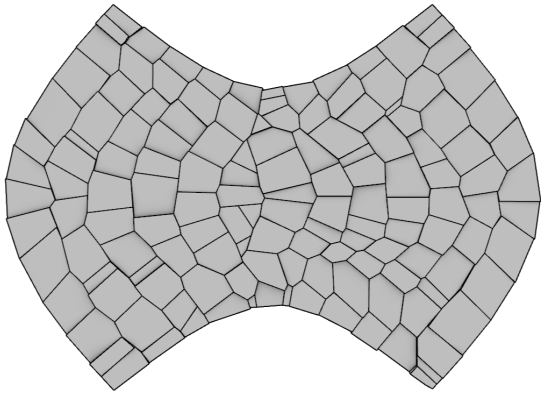

(d) 0p7-1p0-0p2-rand

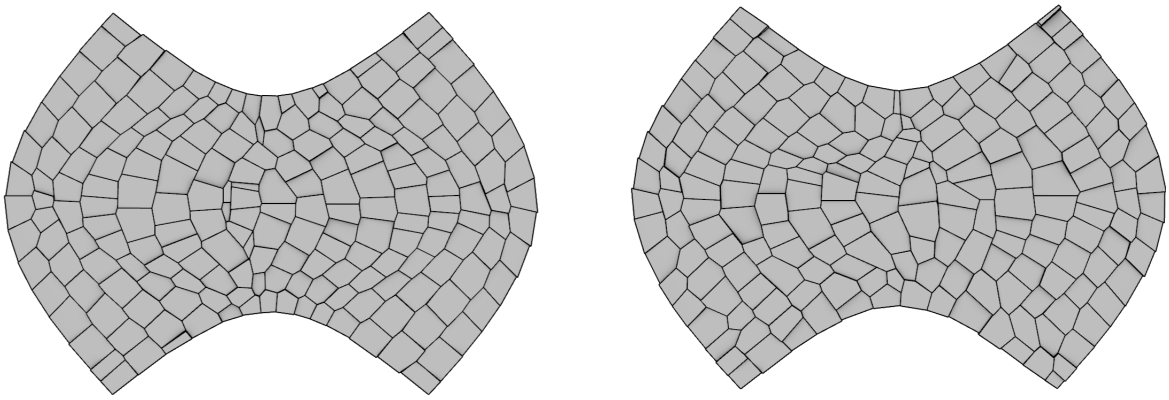

(e) 0p7-1p0-0p0-incr (f) 0p7-1p0-0p2-incr

Figure 4.2: Tessellated Bowtie structure using various stocks

All results were assessed after completion. First the retained volume of each voussoir before waste minimization was calculated and plotted. Figure 4.3 shows this for the Bowtie tessellated with 0p7-1p0-0p2-decr stock. Results show consistency and the volume retained in all attempts averaged between 43.3% and 48.5%. Plots for all other stocks can be found in the Appendix. Results for all stocks are summarized in Table 4.2.

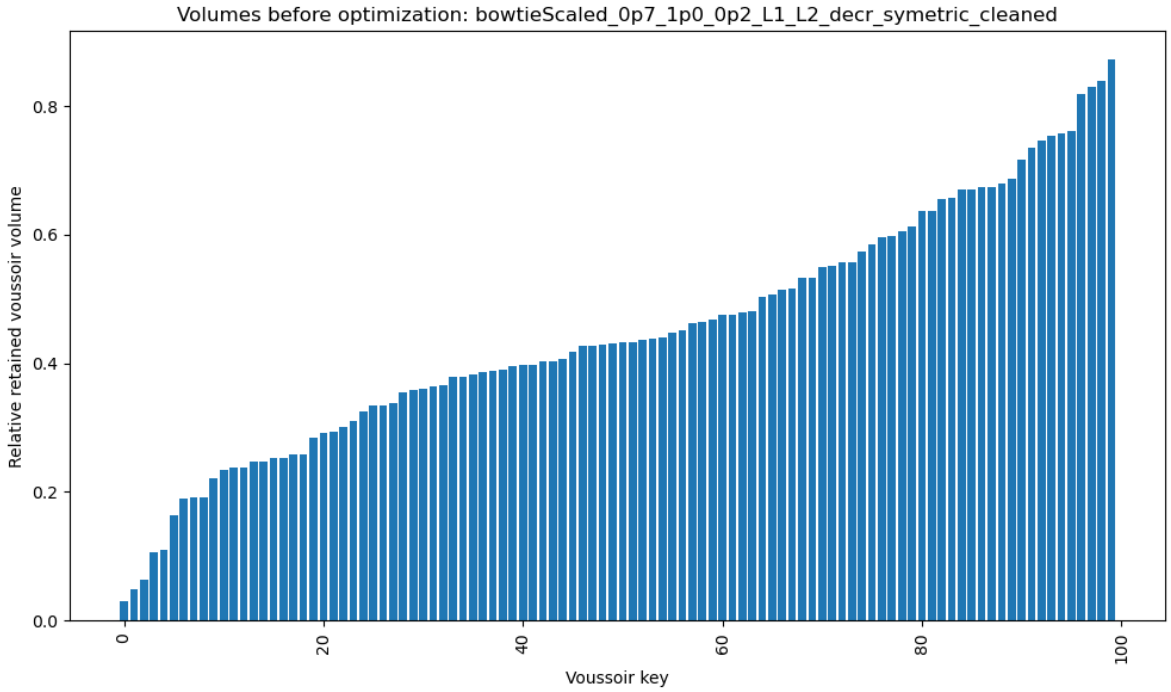

Figure 4.3: Relative retained volume of each voussoir placed in a Bowtie from the 0p7-1p0-0p2-decr stock

Table 4.2: Voussoir volume retained in the structure before waste

Stock name	Voussoir count	Tot volume (m^3)	Vol retained (%)	Vol discarded (%)
0p7_1p0_0p0_decr	116	14.8	48.3	51.7
0p7_1p0_0p0_rand	154	12.8	47.6	52.4
0p7_1p0_0p0_incr	200	12.0	48.5	51.5
0p7_1p0_0p2_decr	100	14.7	44.7	55.3
0p7_1p0_0p2_rand	141	13.2	43.3	56.7
0p7_1p0_0p2_incr	193	12.0	44.1	55.9

These results were also visually represented to study the patterns of where offcuts are created. They are shown in Figure 4.4 in which green means that voussoirs have not been cut much while red entails a great amount of offcuts. It can be noticed that voussoirs at the elevated boundary as well as the interface between voussoirs from different deployment runs are cut more. This is likely because the algorithm does not take into account the dimensions of the space within which a voussoir will be placed on the thrust surface. Rather it selects the voussoirs based on a search angle and the assortment defined by the user.

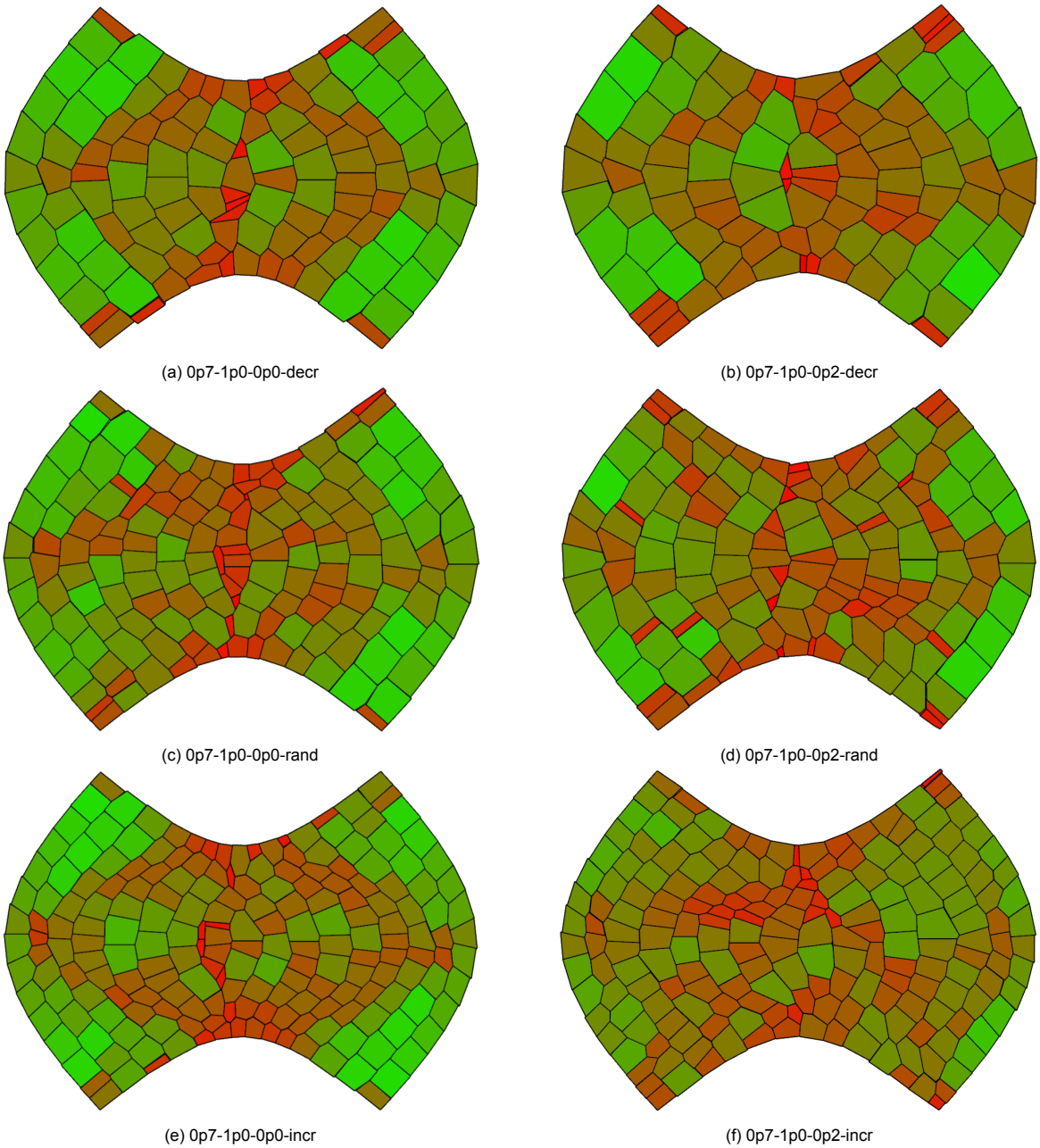

(a) 0p7-1p0-0p0-decr

(b) 0p7-1p0-0p2-decr

(c) 0p7-1p0-0p0-rand

(d) 0p7-1p0-0p2-rand

(e) 0p7-1p0-0p0-incr

(f) 0p7-1p0-0p2-incr

Figure 4.4: Relative volume change of each voussoir. Green indicates no change

On top of that, some side voussoirs are cut more because the voussoir frontier is not advancing toward the center at a relatively even pace. This is because due to the geometry, the voussoirs at the elevated boundary are closer to the center by default. In other words, if the segment is split using transverse curves that are perpendicular to the force flow, it can be seen that their spacing at the ends is smaller than their spacing in the middle as shown in Figure 4.5. This is merely because the length

of the side boundary is 3.55 meters whereas a curve along the middle of the segment is 5.22 meters. Therefore, voussoirs placed in those ends should be smaller than the voussoirs placed in the middle. However, the current approach of searching the voussoir of best-fit does not account for this. Rather, to maintain the transverse faces perpendicular to the force flow, the voussoirs by the elevated boundary are excessively cut.

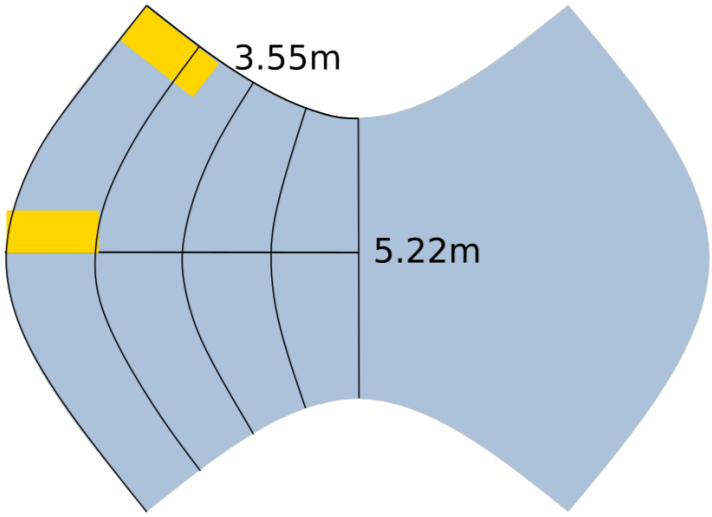

Figure 4.5: Transverse curves demonstrating uneven spacing between them

Next, it was checked if the waste volumes can be minimized as per the “Waste minimization” section. Two different fudge factors (FF) were considered: 0.2 (optimistic scenario) and 0.5 (pessimistic scenario). They describe a fraction of the voussoir volume that is discarded as unrecoverable waste volume when cutting a voussoir. For instance, if the fudge factor equals 0.2 and a voussoir with a volume of 0.1 m^3 is cut, the unrecoverable waste generated is 0.02 m^3. The remaining offcut volume is compared with the other voussoirs in the structure as well as the minimum salvageable volume that can be returned to the stock for future placement in other structures. It was assumed that this volume is 0.027 m^3 (0.3 x 0.3 x 0.3). The updated retained volumes for the Bowtie stacked using 0p7-1p0-0p2-decr stock are shown in Figure 4.6 for the pessimistic scenario and Figure 4.7 for the optimistic scenario. Plots for the other stocks can be found in the appendix. Results are summarized in Table 4.3 and Table 4.4.

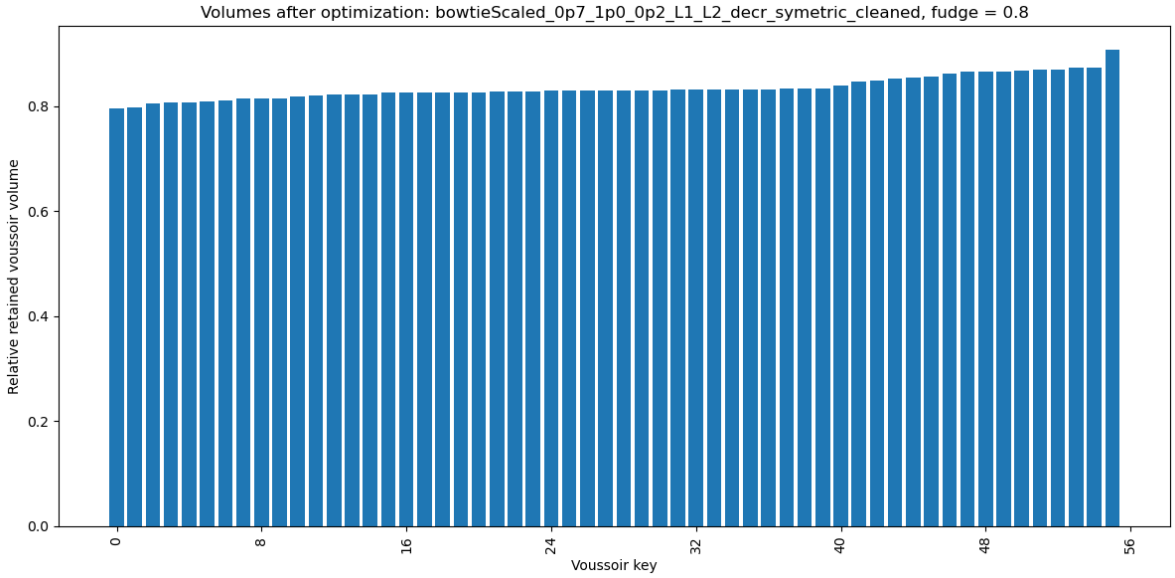

Figure 4.6: Relative retained volume of each voussoir placed in a Bowtie from the 0p7-1p0-0p2-decr stock after waste minimization, FF = 0.2

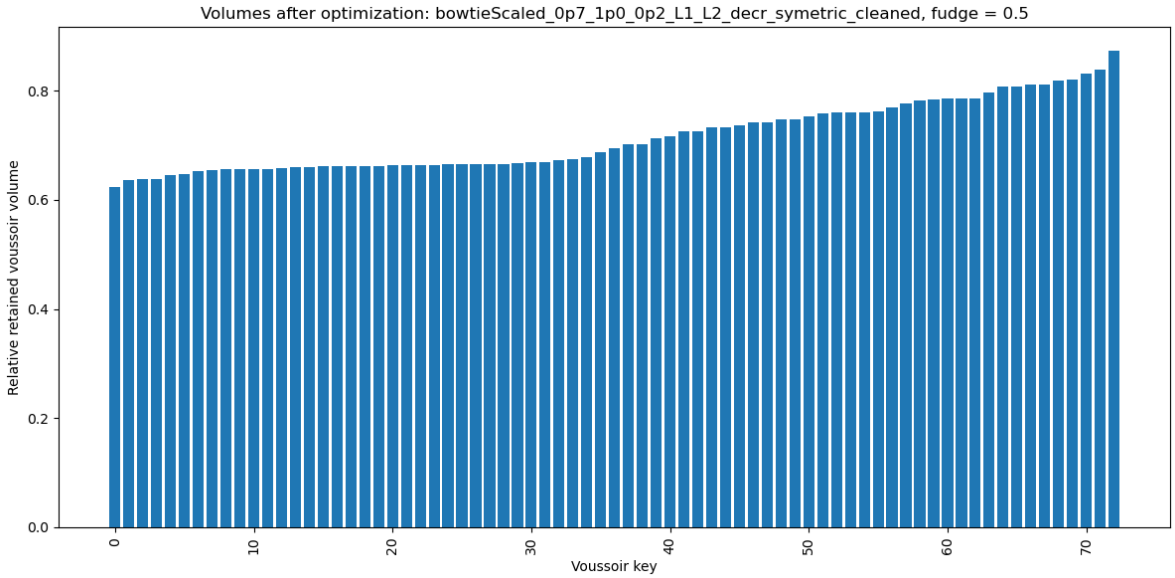

Figure 4.7: Relative retained volume of each voussoir placed in a Bowtie from the 0p7-1p0-0p2-decr stock after waste minimization, FF = 0.5

Table 4.3: Voussoir volume retained in the optimistic waste minimization scenario

Fudge factor = 0.2 Stock name	Voussoir count	Elements used	Tot volume (m^3)	Vol retained (%) In structure	In stock	Total	Vol discarded (%)
0p7_1p0_0p0_decr	116	73	14.8	76.5	6.5	83.0	17.0
0p7_1p0_0p0_rand	154	88	12.8	77.7	4.3	82.0	18.0
0p7_1p0_0p0_incr	200	130	12.0	74.5	6.2	80.7	19.3
0p7_1p0_0p2_decr	100	56	14.7	79.0	4.4	83.4	16.6
0p7_1p0_0p2_rand	141	68	13.2	81.4	0.4	81.8	18.2
0p7_1p0_0p2_incr	193	114	12.0	74.5	8.1	82.6	17.4

Table 4.4: Voussoir volume retained in the pessimistic waste minimization scenario

Fudge factor = 0.5 Stock name	Voussoir count	Elements used	Tot volume (m^3)	Vol retained (%) In structure	In stock	Total	Vol discarded (%)
0p7_1p0_0p0_decr	116	94	14.8	59.9	12.8	72.7	27.3
0p7_1p0_0p0_rand	154	109	12.8	64.8	3.2	68.0	32.0
0p7_1p0_0p0_incr	200	163	12.0	59.0	11.7	70.7	29.3
0p7_1p0_0p2_decr	100	73	14.7	61.4	10.0	71.4	28.6
0p7_1p0_0p2_rand	141	88	13.2	64.8	3.2	68.0	32.0
0p7_1p0_0p2_incr	193	147	12.0	57.5	9.8	67.3	32.7

Stacked deployment

To assess if various deployment strategies can result in different results, the Bowtie was tessellated in a stacked manner discussed in step 1.1. In this deployment, several rows were first tessellated. Then the stacking algorithm was relaunched by stacking the new voussoirs on top of manually selected voussoirs from the existing rows. This enabled a smoothening of the voussoir frontier and the creation of a half-row which allowed the new voussoirs in the second launch of the stacking algorithm to proceed forward in a more even manner. The retained volume was in a similar range as before ranging from 42.6% to 48.7%. The results are shown in Figure 4.8 and Table 4.5.

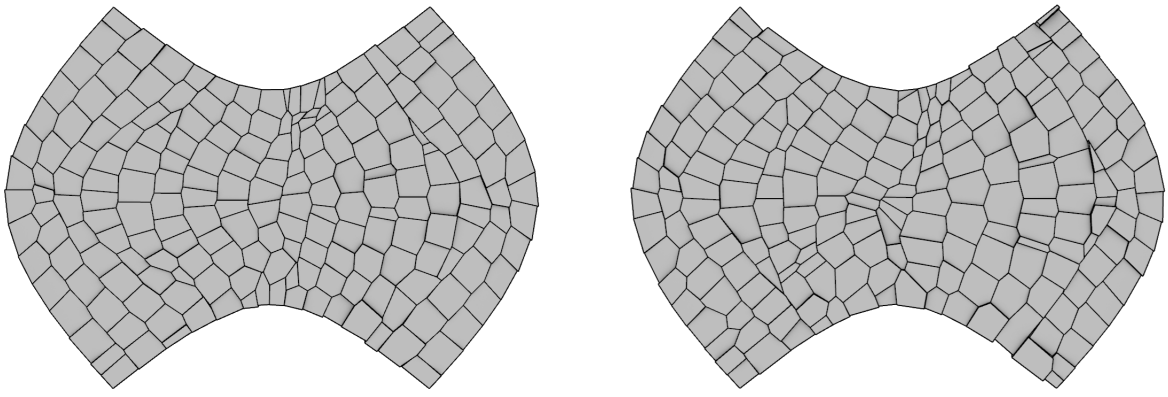

(a) 0p7-1p0-0p0-incr (b) 0p7-1p0-0p2-incr

Figure 4.8: Tessellated bowtie structure using various stocks with a stacked deployment

Table 4.5: Voussoir volume retained in the structure before waste minimization

Stock name	Voussoir count	Tot volume (m^3)	Vol retained (%)	Vol discarded (%)
0p7_1p0_0p0_incr	201	11.9	48.7	51.3
0p7_1p0_0p2_incr	204	12.1	42.6	57.4

Similar to the symmetric deployment, it is assessed visually where on the thrust surface voussoir volumes are retained at what rates. For this deployment, the greatest offcuts occur in the middle as seen in Figure 4.9. This is because in the stacked deployment voussoir placement crosses the middle of the shell which is where the force flow changes directions from left to right as was shown in figure 3.41c. To be more specific, due to the vector field of the force-flow being dense, the flip in consecutive vectors does not occur at 180 degrees instantly and several in-between vectors exist that direct the force to the elevated boundary. These vectors influence the direction in which the voussoirs are cut, resulting in several excessively cut voussoirs. Thus, the vector field should either be cleaned or deployment over locations where the force flow rapidly changes directions should be avoided.

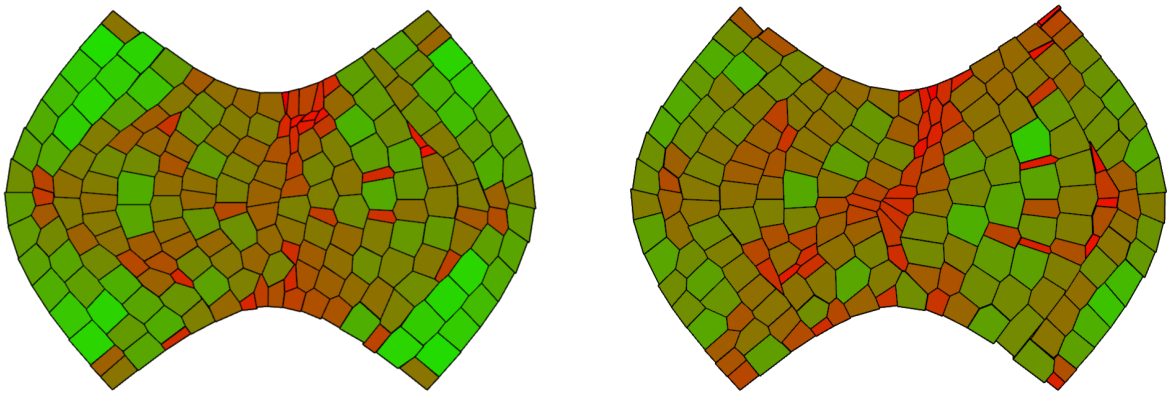

(a) 0p7-1p0-0p0-incr (b) 0p7-1p0-0p2-incr

Figure 4.9: Relative volume change of each voussoir. Green indicates no change

Furthermore, Table 4.6 summarizes the retained volume after waste minimization with fudge factors 0.2 and 0.5. It can be seen that both stocks perform similarly and the retained volume is up to 82.5% in the optimistic scenario and 67% is the pessimistic scenario.

Table 4.6: Voussoir volume retained after waste minimization

Stock name	Fudge factor	Vous count	Elements used	Tot vol (m^3)	Vol retained (%)			Vol discarded (%)
					In structure	In stock	Tot	
0p7_1p0_0p0_incr	0.2	201	133	11.9	73.3	9.1	82.4	17.6
	0.5		163	11.9	59.9	10	69.9	31.1
0p7_1p0_0p2_incr	0.2	204	110	12.1	77.5	5	82.5	17.5
	0.5		145	12.1	59.6	7.4	67	33

Mixed deployment

To test if the previously discussed deployment methods can improve each other’s shortcomings, they are combined in a mixed deployment to create the structure shown in Figure 4.10. The voussoir count, total volume, volume retained, and volume discarded are shown in Table 4.7. The regular stock was chosen as it showed slightly better volume retention rates in the previous deployments.

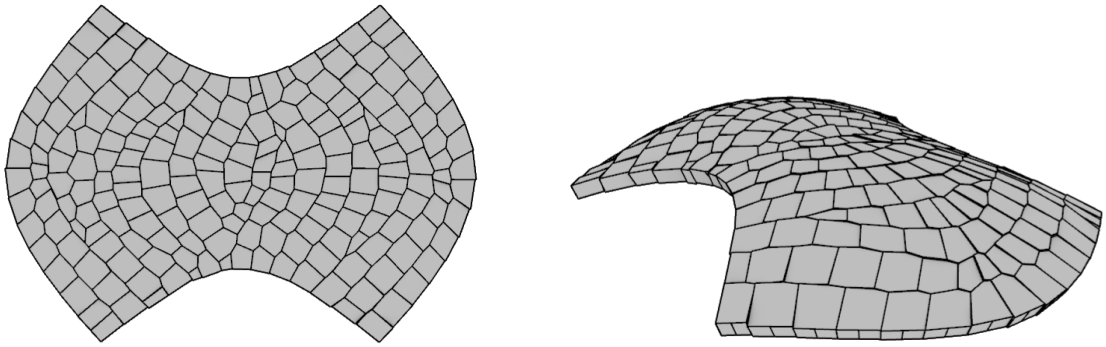

(a) Top view (b) Perspectve

Figure 4.10: Bowtie tessellation using a mixed combination of symmetric and stacked deployment

Table 4.7: Voussoir volume retained in the structure before waste minimization

Stock name	Voussoir count	Tot volume (m^3)	Vol retained (%)	Vol discarded (%)
0p7_1p0_0p0_incr	201	12.8	51.2	48.8

To elaborate further on the deployment strategy, the algorithm was launched six times in directions and sections shown in figure 4.11. In this way, the symmetric sides which were previously created in one go are now created in a stacked manner. This allowed for the creation of several half-rows, which smoothened the leading voussoir frontier and therefore limited the excessive offcuts from aligning edge voussoir transverse faces perpendicular to the force flow. On top of that, this deployment did not have to cross the middle of the shell where the force flow changes directions rapidly like it was for the stacked deployment. Therefore, no excessively offcut voussoirs were created from due to it.

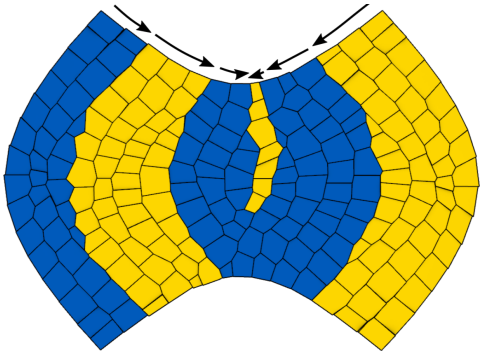

Figure 4.11: Tessellation strategy of the mixed deployment

However, new instances of where voussoirs are cut excessively emerge. For instance, as seen in Figure 4.12, despite the half rows smoothening the voussoir frontier, they themselves are excessively cut, thus offsetting their benefits. Even though the retained volume across the entire structure was 51.2% which is the largest retained volume rate among all of the deployment strategies, more structures should be examined to quantify the benefits of mixing deployment strategies for the benefit of volume retention. For the same stock, the symmetric deployment retained 48.5% while the stacked deployment retained 48.7%. Simultaneously, these results highlight a need for the algorithm to implement a dimension constraint when searching for a viable best-fit voussoir.

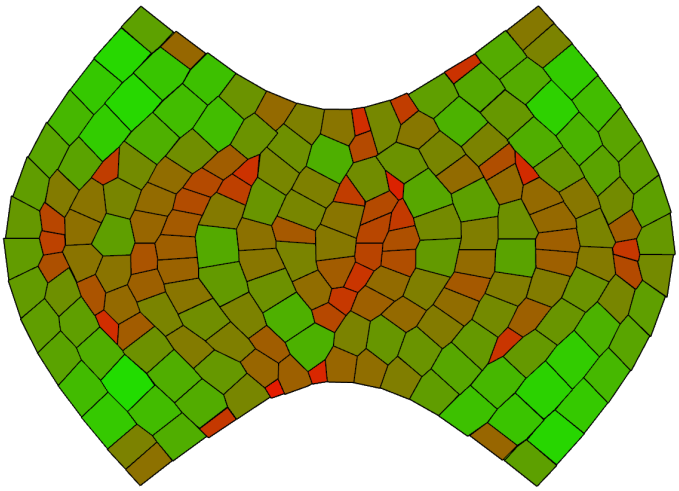

Figure 4.12: Retained volume of Bowtie tessellated with mixed deployment

Finally, waste is minimized as before. In the optimistic scenario 83.3% of the volume can be retained within the structure or the stock while in the pessimistic scenario 69.1% is retained as seen in Table 4.8.

Table 4.8: Voussoir volume retained after waste minimization

Stock name	Fudge factor	Vous count	Elements used	Tot vol (m^3)	Vol retained (%)			Vol discarded (%)
					In structure	In stock	Tot	
0p7_1p0_0p0_incr	0.2	201	149	12.8	70.2	13.1	83.3	16.7
	0.5		163		60.7	8.4	69.1	30.1

4.2. Dome

To assess if the algorithm provides similar results for other thrust surfaces, a dome with a decagonal base with a diameter of 9.7 meters and a height of 3.6 meters shown in Figure 4.13 was tessellated. The force-flow of this structure is shown in Figure 4.14.

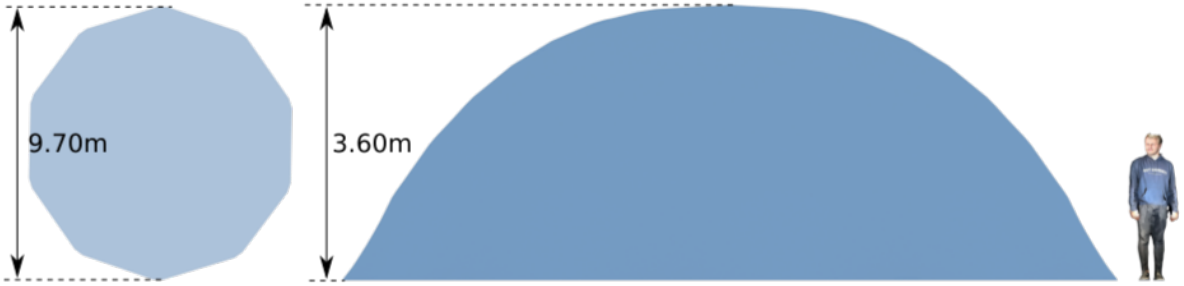

Figure 4.13: Thrust surface of the dome

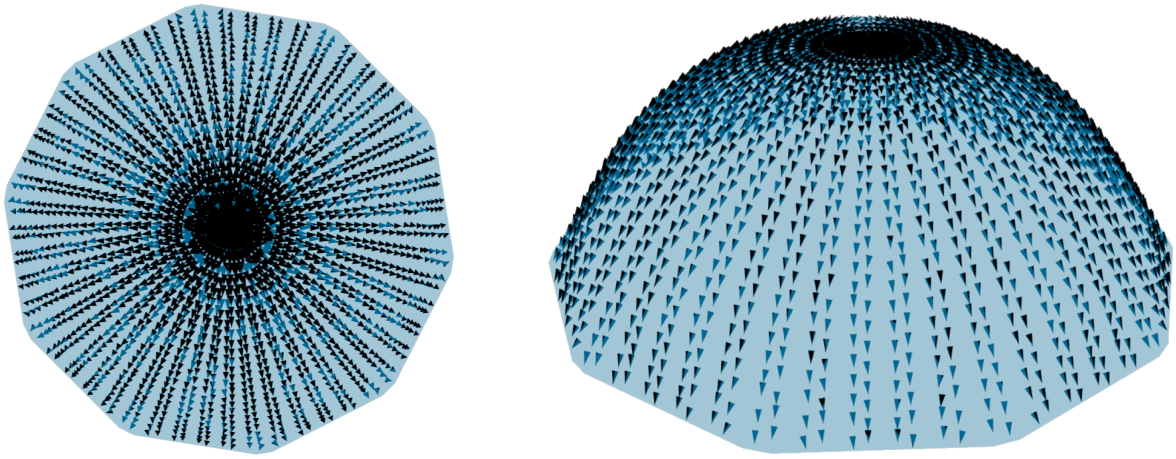

(a) Top view (b) Perspective

Figure 4.14: Force flow of the dome

Two stocks were used to create the structure. As before, the 0p7-1p0-0p0-decr stock of regular voussoirs was used. As for the second stock, a 0p7-0p8-0p2-decr stock was created. It is a subset of the previously used 0p7-1p0-0p2 stock and was chosen because the curvature of the shell was too great to support the placement of the larger voussoirs from the original stock without excessive offcuts stemming from step 4.2. The stocks are summarized in Table 4.9.

Table 4.9: Characteristics of the stocks used for tessellating the dome thrust surface

Stock name	Element count	Voussoir type	Dimensions (m)			Stock assortment
			Length	Width	Height	
0p7_1p0_0p0_decr	600	Regular	0.7 - 1.0	0.7 - 1.0	0.2-0.3	Decreasing
0p7_0p8_0p2_decr	302	Irregular	0.5 - 1.0	0.5 - 1.0		

The stacking algorithm was performed in two runs using the “between” deployment described in the step 1.1 and the results are shown in Figure 4.15. The interfaces of voussoirs from different runs were manually processed. Similarly, the top voussoir, referred to as the singularity, was manually designed. Because of this, the singularity is not taken into account in assessing the volume retained as this piece could either come from the stock or be custom made from new materials.

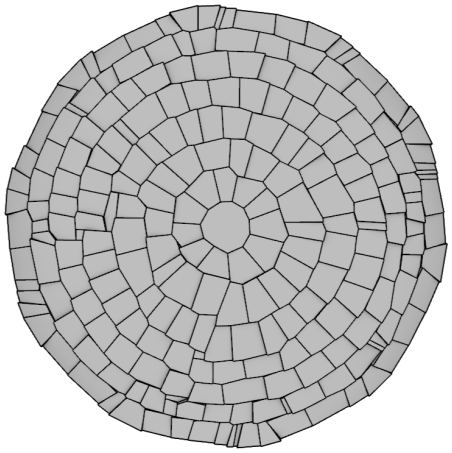

(a) 0p7-0p8-0p2-decr, top view

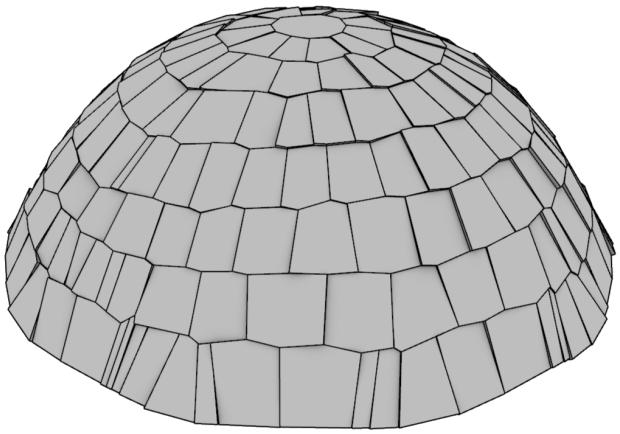

(b) 0p7-0p8-0p2-decr, perspective view

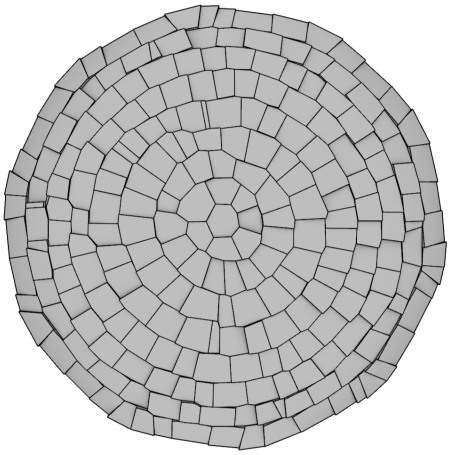

(c) 0p7-0p8-0p2-decr, top view

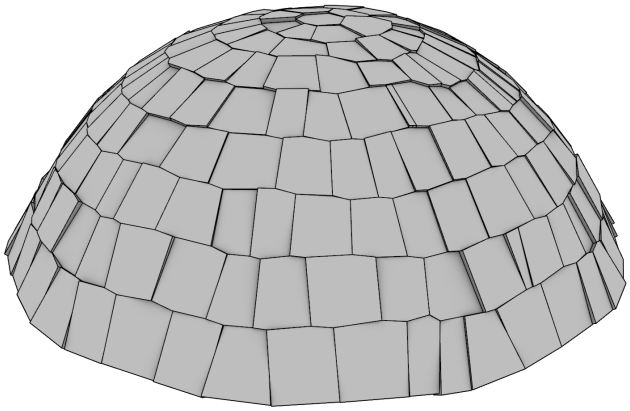

(d) 0p7-0p8-0p2-decr, perspective

Figure 4.15: Tessellated dome structure

As seen in Table 4.10, the volume retained is 53.8% for the regular stock and 44.2% for the irregular stock. Such a discrepancy could arise due to the radial symmetry of the shape and the fact that both the bottom and top transverse faces have to be aligned with the force flow which as seen in figure 4.14 does not significantly change directions from bottom to top transference face. Therefore, the irregular stock has to be trimmed more as their bottom and transverse faces are not aligned before offcuts. This can also be seen visually in Figure 4.16a and Figure 4.16b when compared to Figure 4.16c and Figure 4.16d with voussoirs losing volume at a slower pace. On top of that, it can be noticed that at the corners of the decagonal base indicated in Figure 4.16a and 4.16c for both stocks voussoirs are cut more. This aligns with expectations because in those locations the local curvature increases, which means that smaller voussoirs need to be used to maintain the thrust surface within the kern. Even more, it appears that for some of these corners the pattern of excessively cutting voussoirs propagates upwards despite the local curvature becoming more similar to the rest of the dome. This might be because voussoirs need to stagger and since the bottom voussoirs are excessively cut, the voussoirs on top have fewer locations where they could end to establish sufficient staggering. This results in them being cut more, too.

Table 4.10: Voussoir volume retained in the dome structure before waste minimization

Stock name	Voussoir count	Tot volume (m^3)	Vol retained (%)	Vol discarded (%)
0p7_1p0_0p0_decr	238	30.9	53.8	46.2
0p7_0p8_0p2_decr	231	32.5	44.2	55.8

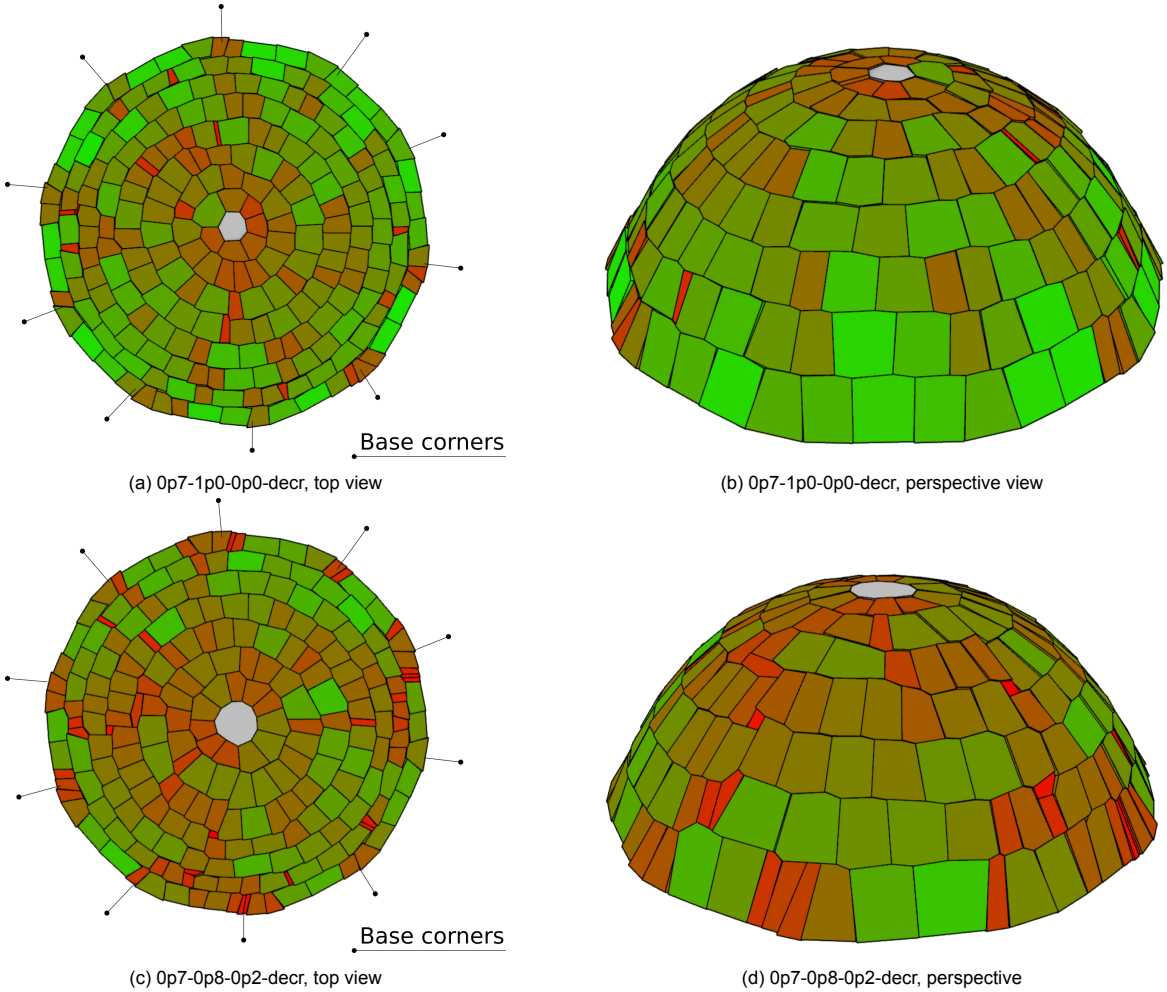

(a) 0p7-1p0-0p0-decr, top view

(b) 0p7-1p0-0p0-decr, perspective view

(c) 0p7-0p8-0p2-decr, top view

(d) 0p7-0p8-0p2-decr, perspective

Figure 4.16: Relative volume change of each voussoir. Green indicates no change

Finally, it is checked what fraction of the volume can be retained after waste minimization. The results for that are shown in Table 4.11. For both stocks, the total retained volume in the optimistic scenario is approximately 85% and 70% in the pessimistic scenario.

Table 4.11: Voussoir volume retained after waste minimization

Stock name	Fudge factor	Vous count	Elements used	Tot vol (m^3)	Vol retained (%)			Vol discarded (%)
					In structure	In stock	Tot	
0p7_1p0_0p0_decr	0.2	238	177	30.9	71.8	13.2	85.0	15.0
	0.5		208		61.7	9.8	71.5	28.5
0p7_0p8_0p2_decr	0.2	231	136	32.5	74.2	10.2	84.4	15.6
	0.5		173		59.0	11.3	70.3	29.7

4.3. ”Pillow” shell

The last shape studied is a shell structure shown in Figure 4.17. It has four elevated boundaries, four supporting boundaries, side sections in which forces act as if the local structure is an arch, and a top section in which forces flow almost as they would in a dome. Thus, this shape captures the complexities of the previous shapes and demonstrates the capabilities of the algorithm to tessellate complicated structures.

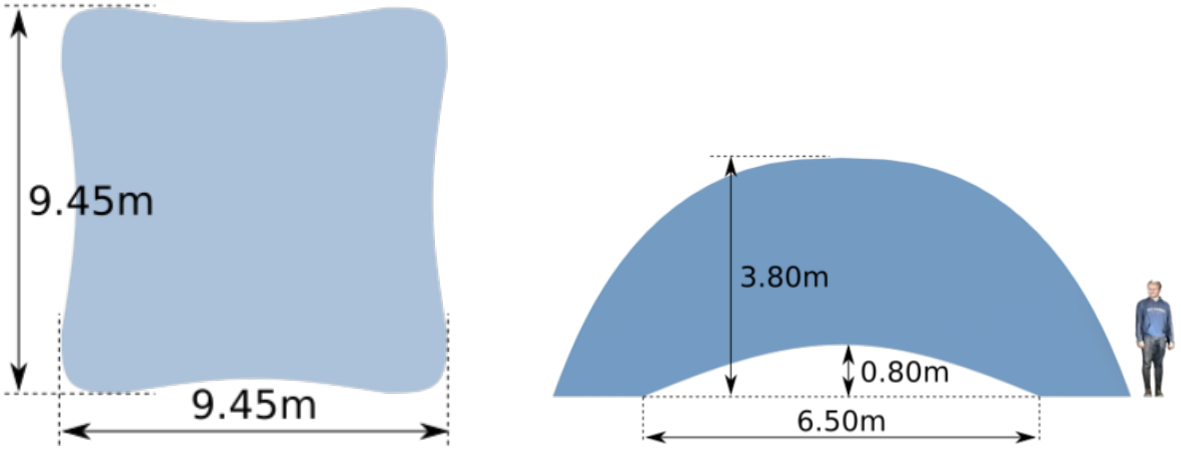

(a) Top view (b) Side view

Figure 4.17: Thrust surface of the pillow shell

As was discussed in the chapter on “User Controls”, the pillow shell has a complex force flow that rapidly changes directions in various locations and was shown in Figure 3.41c. For that reason, the shell was split into a total of 12 segments that were tessellated separately in 16 rounds of algorithm deployment. The four segments above the elevated boundaries that structurally behave as an arch were tessellated using the symmetric deployment while others were tessellated in one go. A total of 292 voussoirs were used and the results can be seen in Figure 4.18 and Table 4.12

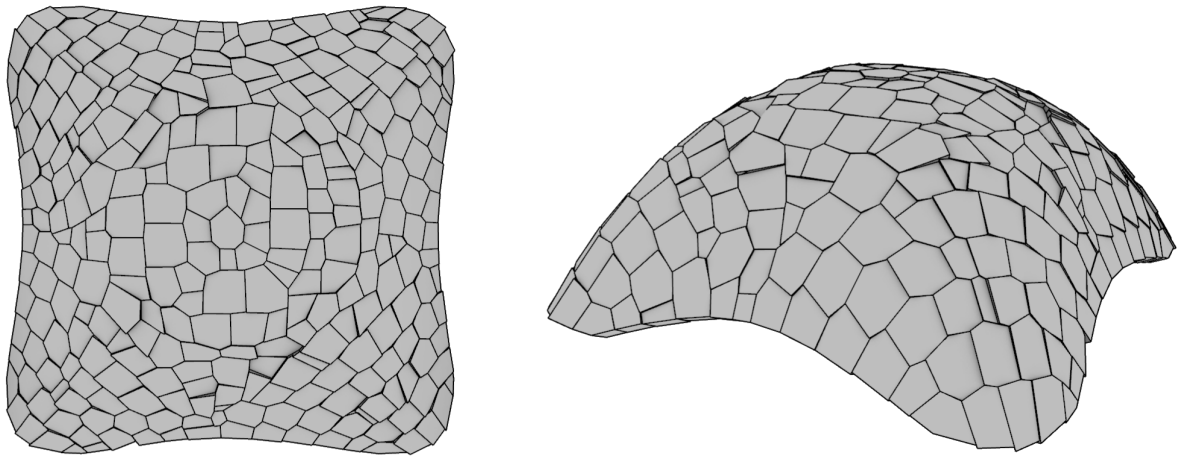

(a) Top view (b) Perspective

Figure 4.18: Tessellated pillow shell structure

Table 4.12: Voussoir volume retained after waste minimization

Stock name	**Voussoir count**	**Tot volume (m^3)**	**Vol retained (%)**	**Vol discarded (%)**
0p7_1p0_0p0_incr	292	47.5	43.4	56.6

The retained volume in the structure is 43.4%, which is similar to the retained volume amount for the previous structures. Particular attention is paid to the boundaries where different segments were stitched together to see if this step results in excessive offcuts. Visually examining Figure 4.19 it can be seen that for the boundaries in the center of the structure indeed offcuts are greater than elsewhere. Nevertheless, for the boundaries of the side segments this trend seems to diminish. A more quantified approach should be taken to assess this.

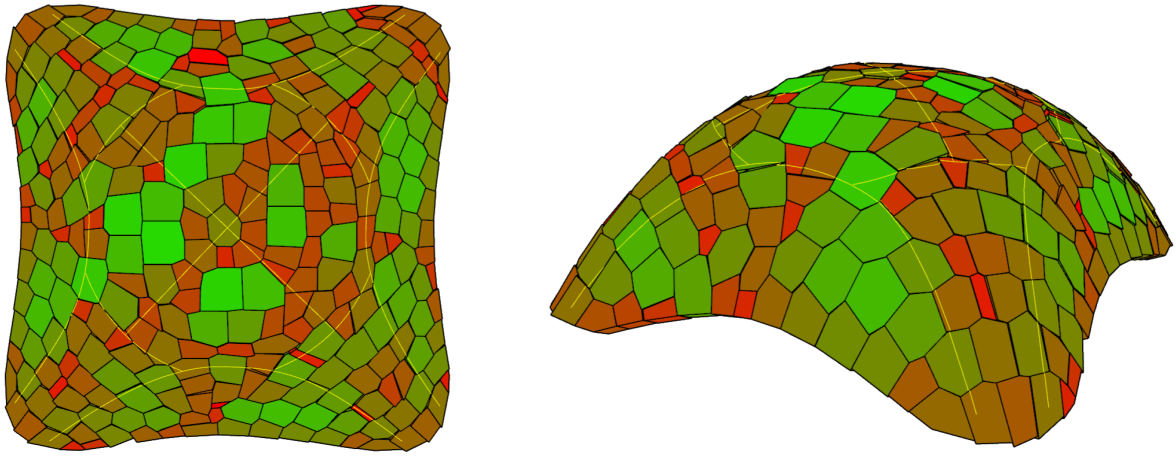

(a) Top view (b) Perspective

Figure 4.19: Retained volume of each voussoir in the pillow shell structure vs. segmentation boundaries

As with the previous structures, it is checked what level of volume could be retained if voussoir cutting was optimized. As seen in Table 4.13, in the optimistic scenario 83% were retained, while in the pessimistic it is 70%.

Table 4.13: Voussoir volume retained after waste minimization

Stock name	Fudge factor	Vous count	Elements used	Tot vol (m^3)	Vol retained (%)			Vol discarded (%)
					In structure	In stock	Tot	
0p7_1p0_0p0_incr	0.2	292	158	47.5	80.4	2.6	83.0	16.7
	0.5		206		61.5	8.5	70.0	30.1

4.4. Validation

To ensure that the structure remains stable, several relevant steps were taken throughout the algorithm. More specifically, as seen in Figure 4.20, patch faces were aligned parallel to the force flow, transverse faces were aligned perpendicular to the force flow, voussoirs were arranged in a staggered pattern, voussoirs were cut to be hexagonal to enhance the interlocking, and the thrust surface was kept within the kern of each voussoir.

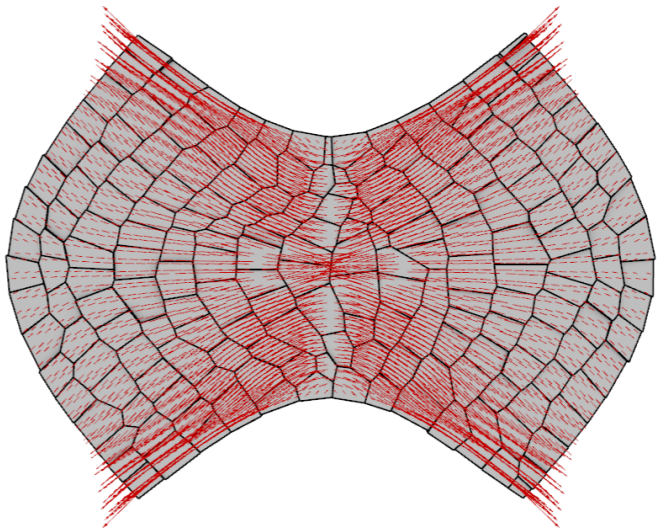

Figure 4.20: Force flow interaction with the voussoirs

To further guarantee that the structures are stable, all presented structures have been validated using the Rigid-Block Equilibrium method available in COMPAS. It determines if a static equilibrium in which only compression forces are required to maintain the stability of the structure exists under self-weight. A study of structures' response under dynamic loads is beyond the scope of this study. The equilibrium forces are shown with the green bars in all of the figures to follow. Voussoirs in pink entail that they are fixed supports. Equilibrium for the Bowtie shell using the 0p7-1p0-0p0 regular stock in decreasing, random, and increasing order can be seen in Figure 4.21a, Figure 4.21b, and Figure 4.21c respectively. Similarly, equilibrium for the Bowtie shell using the 0p7-1p0-0p2 irregular stock in decreasing, random, and increasing order can be seen in Figure 4.22a, Figure 4.22b, and Figure 4.22c respectively. Next, equilibrium of the dome structure with stocks 0p7-1p0-0p0 and 0p7-0p8-0p2 are shown in Figure 4.23. Finally, the stability results are shown for the pillow shell in Figure 4.24.

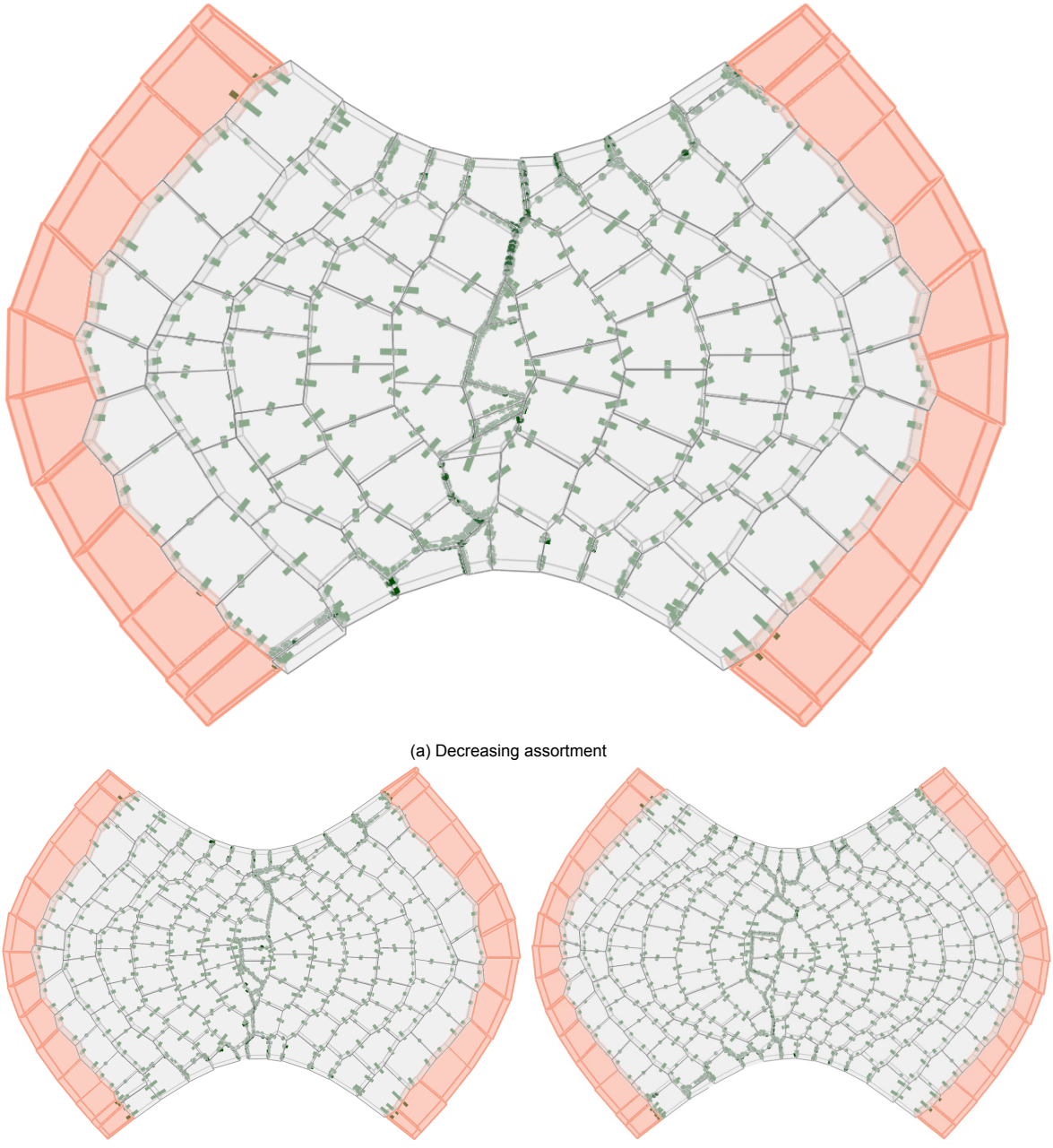

(a) Decreasing assortment

(b) Random assortment

(c) Increasing assortment

Figure 4.21: Validation of the Bowtie shell stacked using a symmetric deployment and 0p7-1p0-0p0 regular stock with various assortments

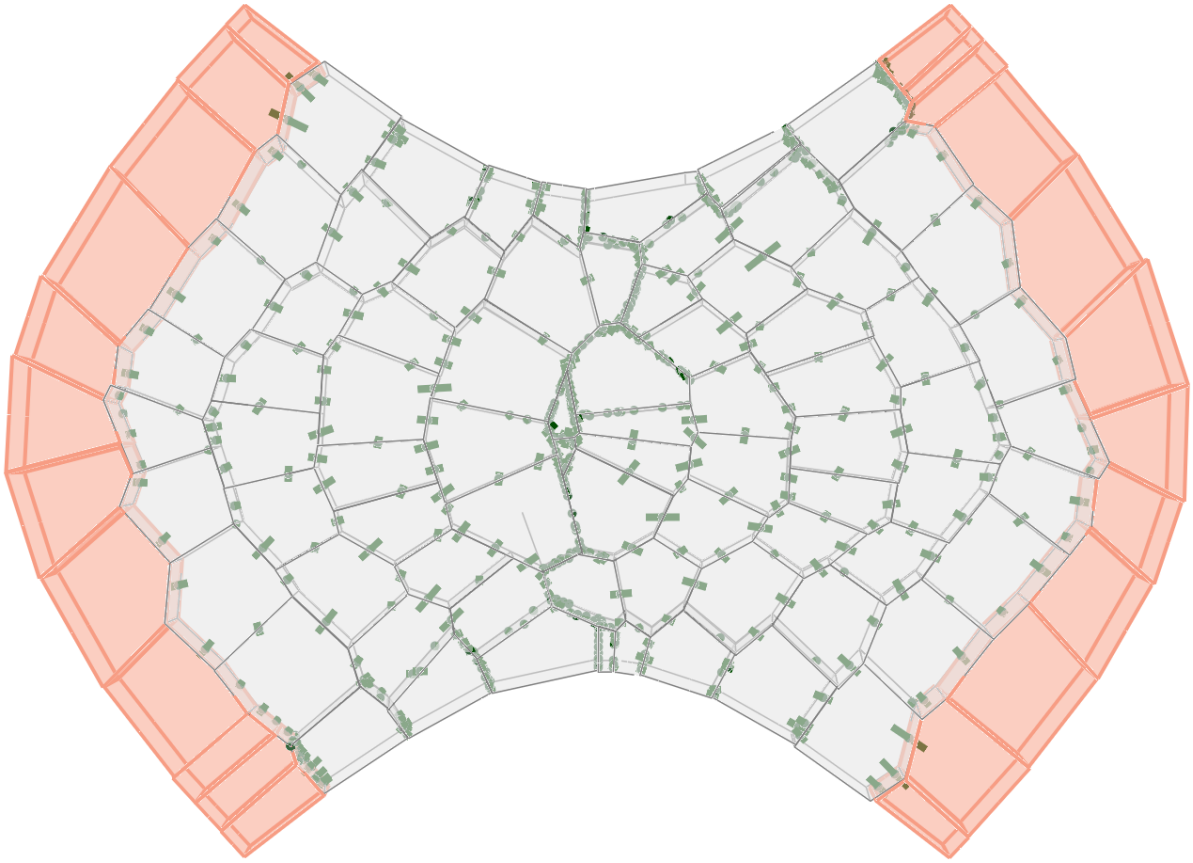

(a) Decreasing assortment

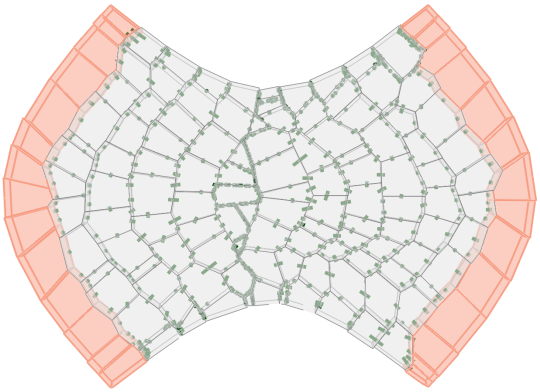

(b) Random assortment

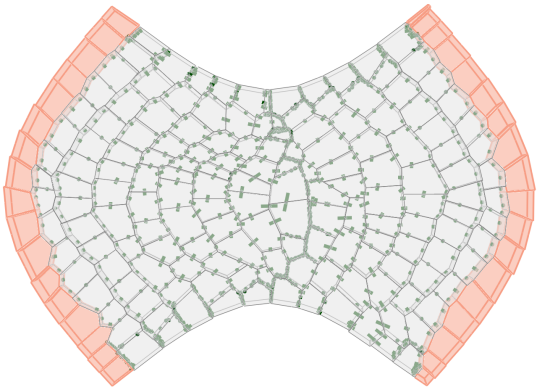

(c) Increasing assortment

Figure 4.22: Validation of the Bowtie shell stacked using a symmetric deployment and 0p7-1p0-0p2 irregular stock with various assortments

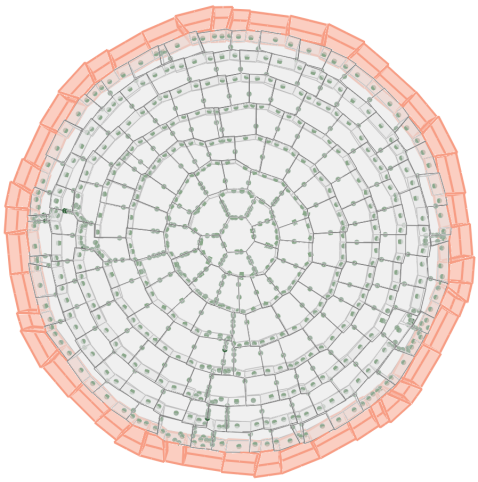

(a) 0p7-1p0-0p0, top view

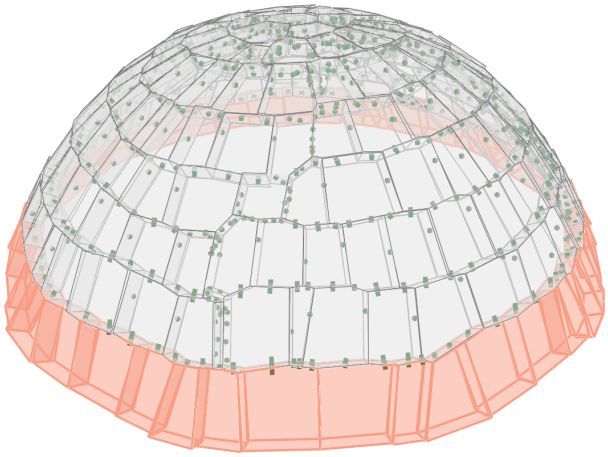

(b) 0p7-1p0-0p0, perspective

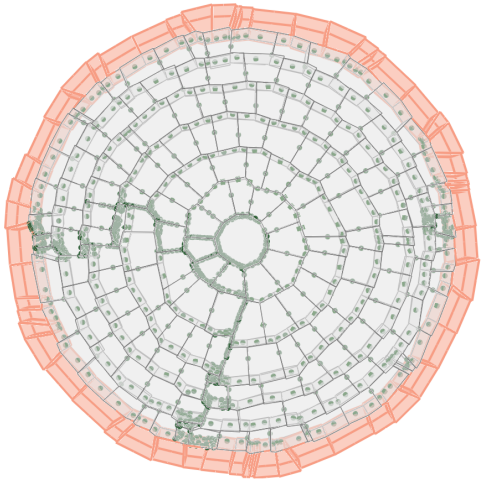

(c) 0p7-0p8-0p2, top view

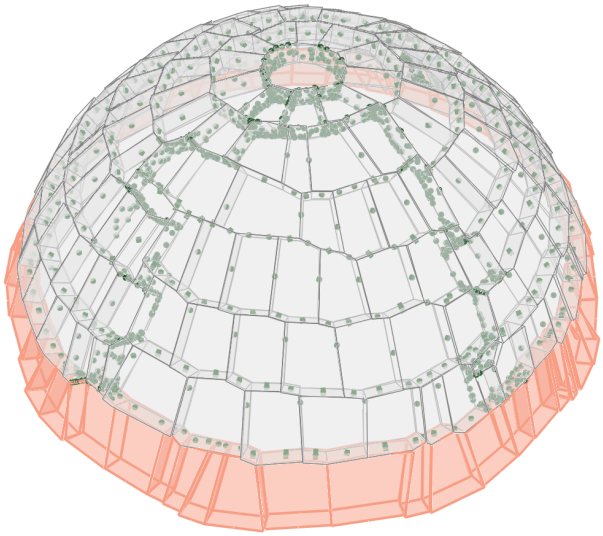

(d) 0p7-0p8-0p2, top view

Figure 4.23: Validation of the decagonal dome shell

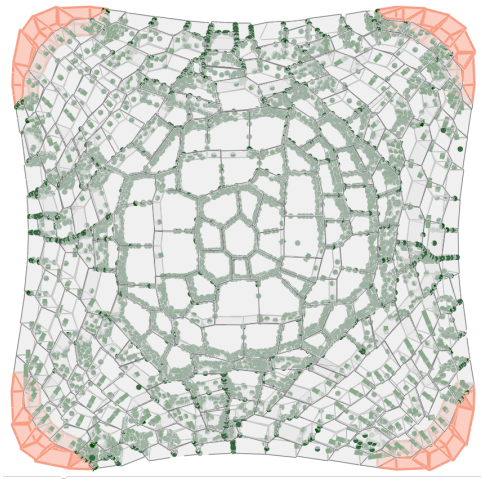

(a) top view

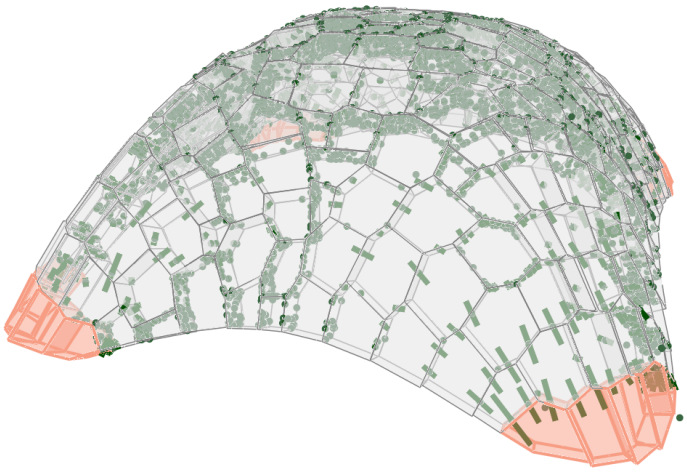

(b) perspective

Figure 4.24: Validation of the Pillow shell

5

Discussion

“Anyone can build a bridge, but it takes an engineer to build a bridge that barely stands”

- Author unknown

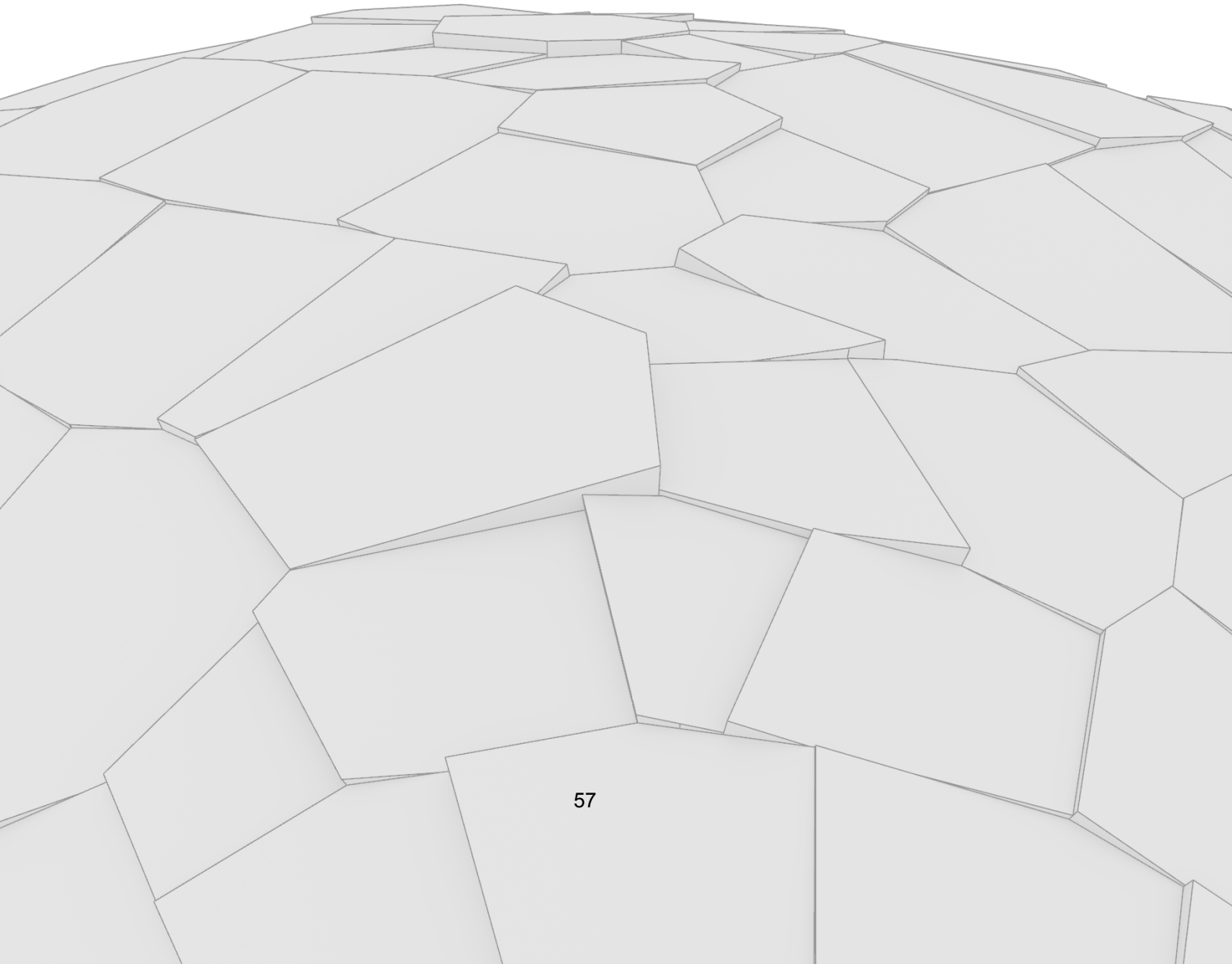

Twelve tessellated structures have been presented in this thesis. The following chapter discusses these results with respect to different stocks, deployment strategies, thrust surface shapes, and waste minimization. Since not a statistically significant number of results have been generated, these results serve a supplementary role in discussing the logic of the stacking algorithm. On top of that, waste minimization and stability errors are discussed. Finally, the limitations of the stacking algorithm are listed and recommendations for future improvements are discussed. These discussions have resulted in specific suggestions for the presented workflow, which are shown in Figure 5.1 and discussed in the following chapter.

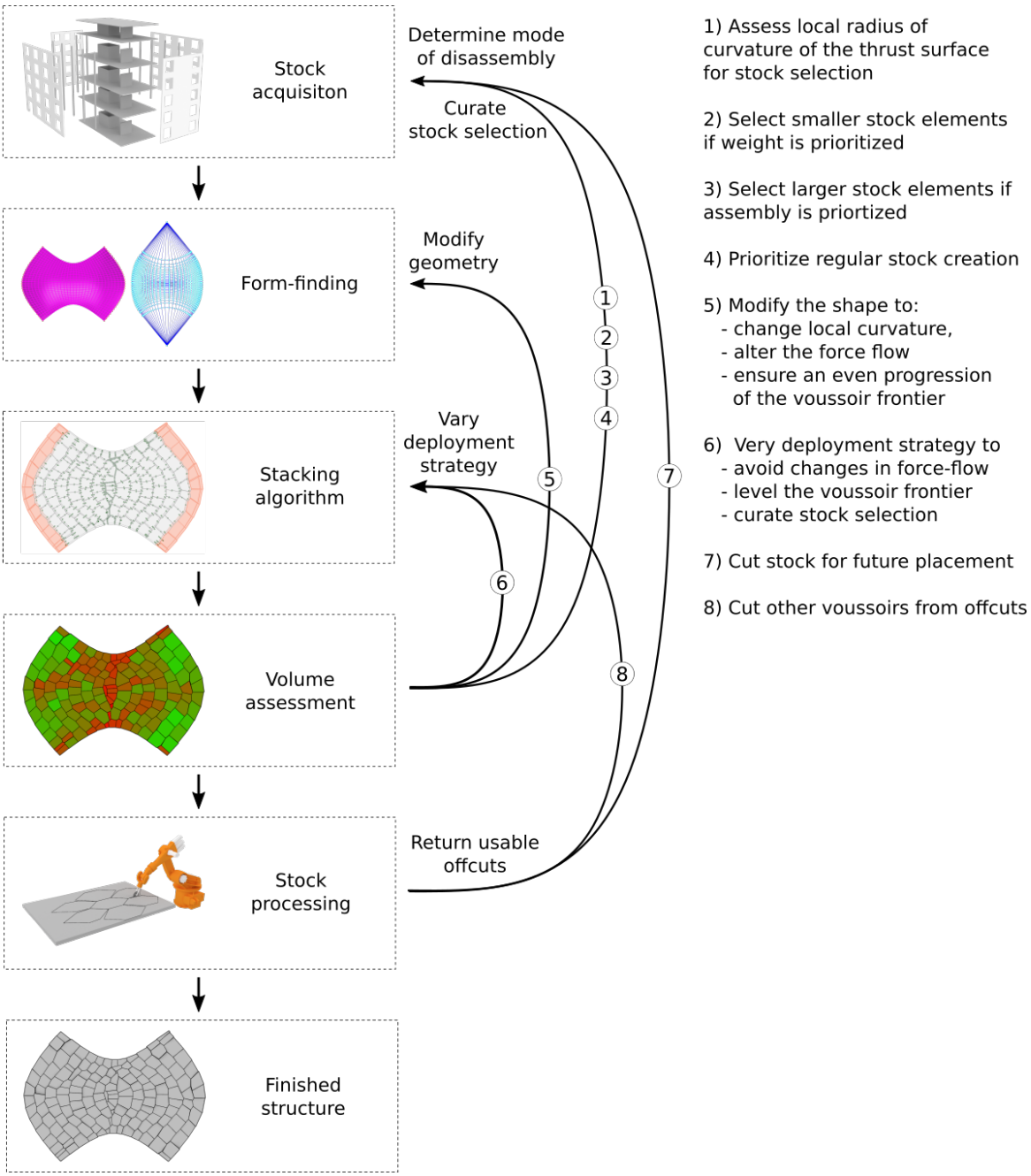

Figure 5.1: Workflow with highlighted methods for user interaction

5.1. Result assessment

Regular versus irregular stock
As shown in the Results chapter, the irregular stock was cut more than the regular stock. In fact, when considering the results before waste minimization, the regular voussoirs retained on average 48.8% of their initial volume while the irregular voussoir retained 43.8%. These results are summarized in Table 5.1. Nevertheless, the Pillow shell was only tessellated with a regular stock. Since it was the most difficult shape to tessellate due to the many changes in force flow and the consequently required high degree of segmentation it showed a lower retention rate of 43.4%. Therefore, the Pillow should also be tessellated with an irregular stock for a more apt comparison.

Table 5.1: Relative retained volume based on the dimensional regularity of the stock

Stock type	Results checked	Vol retained (%)	Vol discarded (%)
Regular	7	48.79	51.21
Irregular	5	43.78	56.22

A further investigation should be conducted to isolate and quantify the cutting stages in which the offcuts are mainly produced to crystallize the reasons for the discrepancy and devise an informed update to the stacking algorithm. Nevertheless, potential reasons can be suggested based on the knowledge of the algorithm. More specifically, regular shapes most probably perform better in the steps:

- 3.4: Patch face stagger & alignment in which the leading patch face is staggered and aligned parallel to the force flow,
- 3.5: Transverse face alignment in which the top transverse face is aligned perpendicular to the force flow.

These steps are highlighted because it is more likely that for an irregular stock, the leading patch face and the top transverse faces are misaligned to the force flow and, thus, require cutting. This is because when placing a voussoir using the search angle discusses in step 2.1, the bottom transverse face as well as the patch face coinciding with the previous voussoir are automatically aligned with the force flow. Then, since the force flow in the considered thrust surfaces or the segmented sections used for deployment does not abruptly change directions, it is probable that the force flow at the leading patch face and top transverse face will be in the same general direction as for their already positioned opposite side faces. Therefore, for regular voussoirs, for which the opposite faces are parallel, their geometry is more likely to follow the necessary direction guided by the force flow and not require additional cutting.

This suggests several strategies for the workflow presented in figure 3.3. First, the deconstruction of a building should be performed to maximize regular-size voussoirs obtained. This means that methods using any form of crushing, even if they result in large elements, should be abandoned. Second, any post-processing of the stock when voussoirs are cut out of larger elements should follow cutting patterns that create regular-size offcuts in situations when these offcuts are voluminous enough to be returned to the stock for future placement.

Stock selection
Next, it is discussed how the manner in which the stock is sorted - and therefore in what order a best-fit voussoir is sought as explained in step 2.2 - influences the results. To study this, the strategy for selecting voussoirs from both the regular and irregular stocks was varied. Namely, three strategies were considered:

- sorting the stock in decreasing order by volume (decr),
- random order (rand),
- increasing order (incr).

To standardize the comparison shown in Table 5.2, only the Bowtie with symmetric deployment is considered as it was the only thrust surface and deployment strategy with which all three stock selection strategies were implemented.

Table 5.2: Relative retained volume versus stock assortment for a Bowtie with symmetric deployment

Stock sorting strategy	Results checked	Voussoirs used	Voussoir volume (m^3)	Vol retained (%)	Vol discarded (%)
Decreasing	2	108	14.75	46.5	53.5
Random	2	147.5	13	45.45	54.5
Increasing	2	196.5	12	46.3	53.7

As can be seen, the volume retained varies by a maximum of 1% entailing no significant difference. However, the number of voussoirs used in the structure was 1.8 times larger as 108 voussoirs were used for the decreasing sort and 196.5 for the increasing sort. This difference is intuitive since smaller voussoirs are taken from the same stock in the increasing sort. Simultaneously, they can approximate the thrust surface better and therefore result in an 18.6%, or 2.75 m^3, reduction in volume when compared to the decreasing sort. With an average density of concrete of 2400 kg/m^3 this is a reduction of 6600 kg. The random sort falls in between these results.

With this in mind, a decreasing sort would result in less processing needed because fewer voussoirs would have to be cut and likely simplify the assembly process since fewer voussoirs have to be placed. On top of that, simpler formwork could potentially be used as it would have to support fewer voussoirs during the assembly process. However, the increasing sort would result in a more refined and lighter structure, which could be especially important if the structure is placed on top of other structures that need to carry its load.

At the same time, the thrust surface curvature, which has not been explicitly studied in this thesis, also contributes to these results. To see how, it can be imagined that if the surface was flat, larger voussoirs would approximate the thrust surface as well as smaller voussoirs. This would make the final volume used more comparable among the assortment strategies while the decreasing assortment would still require fewer voussoirs and, thus, less processing. For this reason, surface curvature should be studied as an important contributor to the way the stock is sorted and how the best-fit voussoir is selected.

Using the current algorithm and having analyzed the results, random assortment represents a middle-ground among the three options. However, ultimately, the assortment choice depends on the priorities of the specific project.

Deployment strategy
Next, it was examined if the deployment strategy has an impact on the volume retained in the structure. Note, that this is different than using deployment strategies to enable the tessellation in the first place like it is for the Pillow shell which could not be tessellated without segmenting its thrust surface.

For this comparison, the Bowtie was tessellated using three different deployment strategies - symmetric, stacked, and mixed - that have been discussed in the section “User controls”. All strategies resulted in similar voussoir volume retained - symmetric deployment retained 46.1%, stacked deployment retained 45.7%, and mixed deployment retained 51.2% as shown in Table 5.3.

Table 5.3: Relative retained volume based on the deployment strategy

Deployment strategy	Results checked	Vol retained (%)	Vol discarded (%)
Symmetric	6	46.1	53.9
Stacked	2	45.6	54.4
Mixed	1	51.2	48.8

While symmetric and stacked results indicate no significant difference, this could be attributed to an ill-informed launch of the stacked deployment. This is because by examining Figure 4.4, which visualizes each voussoir's relatively retained volume, it can be seen that voussoirs already in the second row (stacking occurs from left to right), experience a high degree of cuts. This is due to the shape of the thrust surface because of which the voussoir frontier moves towards the middle, thus, engulfing the middle voussoirs which get excessively cut. To potentially solve this a half row should be created already in the second row, rather than in the fifth like it was done, to even out the frontier and allow for a more even progression of the rows. This highlights the importance of using volume analysis in the midst of the design process.

Simultaneously, by observing the volume difference of each voussoir, it can be noticed that the stacked deployment struggles with placing voussoirs in the middle of the Bowtie. This could be because there the force flow flips and from flowing to the left support boundary briefly flows to the elevated boundaries and then to the right support boundary. This results in the alignment of the voussoir patch faces that are aligned with the local force flow around the pivot point but are significantly varying from the relevant force flow directions identified for the previous voussoirs. In this regard, the symmetric deployment avoided the problem by never crossing the boundary where the force flow changes directions.

To solve the shortcomings of each of the methods, a mixed deployment strategy was examined. By using it, 51.2% of the voussoir volume could be retained, which is 5-6% more than for the other strategies. In this deployment, the structure was tessellated symmetrically from both sides like it was for the symmetric deployment. However, each of the symmetric segments was tessellated in a stacked manner. In this way, the mixed deployment introduced half-rows, the lack of which was a shortcoming for the symmetric deployment and did not cross the boundary where the force flow flips directions, which was a shortcoming of the stacked deployment.

However, the introduction of half-rows presents a new challenge as voussoirs in it are excessively cut to align the leading voussoir frontier perpendicular to the force flow. This highlights that while deployment strategies can improve the tessellation, further functionality must be introduced into the algorithm that checks what volume of the voussoir will be cut off upon placement and feeds this into the search for the voussoir of best-fit. Such functionality improvement aligns with what was discussed previously in analyzing the dimensional regularity of the stock.

Shape

Finally, it was checked if the results are consistent for different form-found geometries. To do this, three thrust surfaces were considered - a Bowtie with two supports and two elevated boundaries, a dome with a single decagonal support boundary, and a Pillow shell with four supports and four elevated boundaries. As can be seen in Table 5.4, the tessellation of the dome was marginally more efficient with an average of 49% of volume retained in comparison to 46% for the Bowtie and 43.4% for the Pillow.

Table 5.4: Relative retained volume based on the shape of the thrust surface

Thrust surface	Results checked	Vol retained (%)	Vol discarded (%)
Bowtie	8	46.0	54.0
Dome	2	49.0	51.00
Pillow	1	43.4	56.60

While the results appear similar, it has been observed that the tessellation of each shell presents both similar as well as unique challenges. They are summarized in Table 5.5 and are discussed in the following paragraphs.

Table 5.5: Challenges associated with tessellating each shell due to its shape

Shape	Challenges	
	Unique	**Common**
Bowtie	- uneven progression of the voussoir frontier	- cutting to ensure staggering
Dome	- high local curvature at the corners of the decagonal base curve	- fitting the thrust surface within the kern - size-blind placement of the final voussoir in each row
Pillow	- high degree of the required segmentation	- cutting of half-row voussoirs

First, the tessellation of the Bowtie is made more complicated due to the uneven advancement of the voussoir frontier towards the middle of the shell as was shown in Figure 4.4. This stems from the fact that voussoirs advancing upwards in the center have to cover a greater distance to reach the middle than the voussoirs advancing on the sides. This is true since the placement happens in rows and, therefore, the same number of voussoirs are present in the middle and the side. Thus, the side voussoirs must be smaller.

Second, tessellating the dome was challenging due to the high local curvature at the corners of the decagonal base as was shown in Figure 4.16. This resulted in voussoirs not being able to fit the thrust surface within the kern and, therefore, voussoirs were cut smaller to fit as per step 3.1. Even more, such cutting resulted in a voussoir frontier with several short top transverse faces, which complicated the staggering of the voussoirs in rows above. This resulted in a propagating column of voussoirs on top of each other that needed more offcuts than their neighbors which were stacked on top of voussoirs with longer top transverse faces and thus more easily to find staggering solutions.

Third, the pillow shell had to be segmented into twelve different segments for tessellation due to the varying force flow. Then these segments were patched together manually in post-processing. While doing this is time-consuming it also introduces a level of human errors that not only might result in excessive offcuts but also could lead to issues with stability.

Lastly, several challenges are common to all shapes, such as cutting off a voluminous amount to ensure staggering, fitting the thrust surface within the kern, placing the final voussoir in each row beyond the delineating boundary, and cutting half-row voussoirs in the stacked deployment. They all point to a shortcoming of the algorithm, which is made when the best-fit voussoir is found by only identifying the search angle and not by looking at the local curvature of the shell, where staggering could occur, force flow at the faces that need aligning and the local curvature of the thrust shape.

Overall, tessellating various shapes has highlighted unique and shared challenges that stem from the geometry of the thrust surface. Later, in the section on recommendations, several suggestions will be made to correct these challenges. Nevertheless, it has also been shown that the challenges do not prevent the creation of a structure, and several methods were suggested for how a designer can use the workflow to mitigate the challenges.

Waste minimization

Since the previously discussed results show that approximately 50% of the original voussoir volume does not end up in the structure, waste minimization is crucial to improve the environmental sustainability of the proposed stacking algorithm. The minimization method discussed in the section “Waste minimization” checks if voussoirs in the structure can be created from the offcuts of other voussoirs by first determining the usable offcut volume. It is determined using a fudge factor (FF) that finds how much unrecoverable waste volume is generated when cutting a voussoir as a proportion of its final volume. On top of that, it is checked if the offcut volume can be returned to the stock even if none of the other voussoirs can be created from the offcut as long as the offcut is larger by volume than a predefined volume of 0.027 m^3 (0.3x0.3x0.3). Two scenarios - an optimistic (FF = 0.2) and a pessimistic (FF = 0.5) - are considered and the results are shown in Table 5.6 and Table 5.7.

Table 5.6: Relative retained volume in the optimistic scenario

Thrust surface shape	Deployment	Stock	Sorting	Vol retained (%)			Vol discarded (%)
				In structure	In stock	Total	
			Decreasing	76.5	6.5	83.0	17.0
		0p7_1p0_0p0	Random	77.7	4.3	82.0	18.0
	Symmetric		Increasing	74.5	6.2	80.7	19.3
			Decreasing	79.0	4.4	83.4	16.6
Bowtie		0p7_1p0_0p2	Random	81.4	0.4	81.8	18.2
				74.5	8.1	82.6	17.4
	On top	0p7_1p0_0p0		73.3	9.1	82.4	17.6
		0p7_1p0_0p2		77.5	5.0	82.5	17.5
	Mixed	0p7_1p0_0p0	Increasing	70.2	13.1	83.3	16.7
Dome	Between	0p7_1p0_0p0		71.8	13.2	85.0	15.0
		0p7_0p8_0p2		74.2	10.2	84.4	15.6
Pillow	Mixed	0p7_1p0_0p0		80.4	2.6	83	16.7
			Average:	**75.9**	**6.9**	**82.8**	**17.1**

Table 5.7: Relative retained volume in the pessimistic scenario

Thrust surface shape	Deployment	Stock	Sorting	Vol retained (%)			Vol discarded (%)
				In structure	In stock	Total	
			Decreasing	59.9	12.8	72.7	27.3
		0p7_1p0_0p0	Random	64.8	3.2	68.0	32.0
	Symetric		Increasing	59.0	11.7	70.7	29.3
			Decreasing	61.4	10.0	71.4	28.6
Bowtie		0p7_1p0_0p2	Random	64.8	3.2	68.0	32.0
				57.5	9.8	67.3	32.7
	Stacked	0p7_1p0_0p0		59.9	10.0	69.9	31.1
		0p7_1p0_0p2		59.6	7.4	67	33
	Mixed	0p7_1p0_0p0	Increasing	60.7	8.4	69.1	30.1
Dome	Between	0p7_1p0_0p0		61.7	9.8	71.5	28.5
		0p7_0p8_0p2		59.0	11.3	70.3	29.7
Pillow	Mixed	0p7_1p0_0p0		61.5	8.5	70	30.1
			Average:	**60.8**	**8.8**	**69.7**	**30.4**

In the optimistic scenario, approximately 82.8% of the voussoir volume could be retained while in the pessimistic scenario, the fraction is 69.7%. To improve the accuracy of such minimization, the algorithm should account for the dimensions of the offcuts and not only the stereometry. On top of that, the offcut volumes might not always be a single block due to the cutting pattern chosen which could split up usable offcut into two or more unusable volumes. Therefore it is more probable that the actual retention rate would be closer to the pessimistic scenario. Additionally, a further iteration of the waste minimization step could be to analyze if the voussoir could be created more efficiently from a different otherwise unused voussoir from the stock. The specifics of such optimization are beyond the scope of this thesis.

Stability errors

During the validation of the results for the Bowtie shell that was stacked using the regular stock with decreasing voussoir assortment, the initial configuration failed. This can be seen in Figure 5.2a as tension forces in red were needed to maintain equilibrium in the structure. Upon closer inspection, it can be noticed that the reason for this is a geometric failure in cutting the voussoir as its face is not aligned with the face of the support and, thus, a void is formed. Because of this, no interface between the voussoir and its support was detected, which would otherwise serve as a transverse face that channels the loads to the supports. To address this issue the voussoir was manually re-cut to align the interfaces and upon a repeated validation step an equilibrium was reached.

Similarly, the initial tessellation of the pillow shell failed due to a single interface not being cut perpendicular to the force flow. Because of this, compression forces, which act perpendicular to the interface, were no longer acting along the thrust surface and the voussoir would pop out unless tensile forces were introduced. This can be seen in Figure 5.2b and was manually fixed.

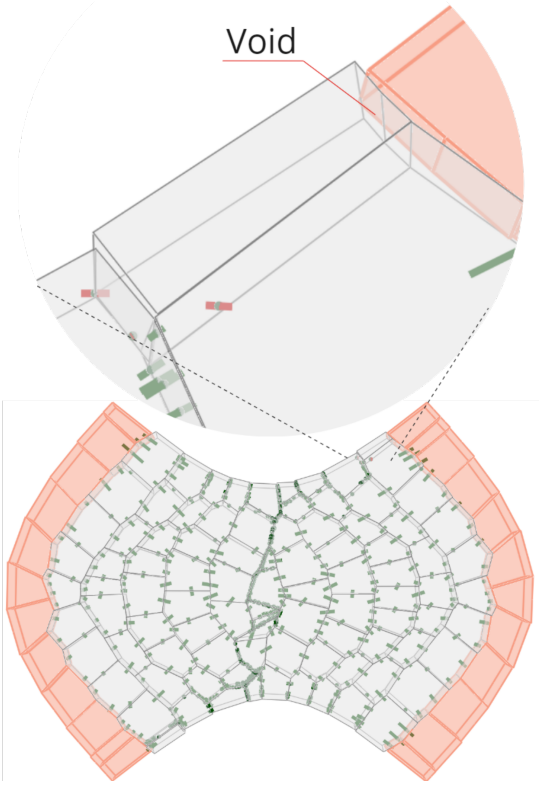

(a) tension forces required in the structure due to an improperly cut interface

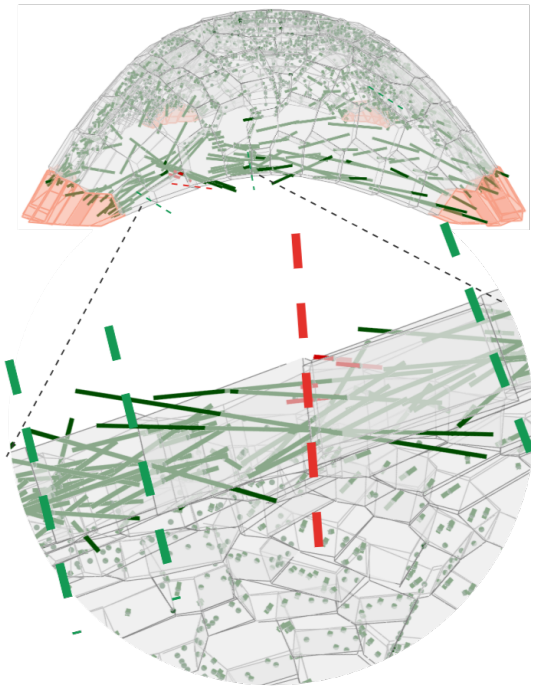

(b) Tensile forces present in the stacking

Figure 5.2: Cases when a compression-only equilibrium failed initially

5.2. Limitations and Recommendations

The following section outlines the limitations of the stacking algorithm and provides recommendations for improvements. First, the underlying assumptions and design principles that guided the development of the stacking algorithm are discussed. Next, improvements for specific steps of the algorithm are suggested. These improvements are based on the identified challenges in the discussion section, some of which were previously addressed by how a designer can interact with the stacking algorithm as a part of the algorithm. Here, the recommendations will focus on additional functionality that is currently absent.

Addressing assumptions

The stacking algorithm uses a stock of quadrilateral prisms as an input. Quadrilaterals were chosen due to the necessity to align the two patch faces parallel to the force flow, the bottom, and top faces perpendicular to the force flow, and the ability to easily turn quadrilaterals into hexagonal prisms, which enhances the interlocking nature of the tessellation. This means that the algorithm at its current state does not support the placement of any voussoirs that are not initially quadrilaterals. This is especially relevant since many of the offcuts created are triangular and, therefore, could not be retained in the stock without additional processing which creates an additional hurdle for the waste minimization discussed previously. On top of that, construction waste comes in many sizes. To use those, additional functionality would have to be introduced. For instance, a function could determine a range of possible quadrilaterals that could be carved and use this range as an input to the algorithm. Otherwise, the algorithm could be expanded to support those that are not quadrilaterals. However, this would create additional challenges with interlocking, staggering, and voussoir alignment with respect to the force flow.

The next assumption was to stack the voussoirs in a sequential manner in rows. While this was done to ensure valid placement of each voussoir, such an approach could miss more optimal placements for a certain voussoir as well as how it impacts the placement of future voussoirs. Therefore, a different algorithmic approach could be explored that assesses the placement of several voussoirs at the same time in various configurations and determines which of the configurations is more optimal. Such an approach could also solve the necessity of creating half-rows to smoothen the voussoir frontier which was described previously, by recognizing that a half-row is needed automatically.

Finally, an underlying assumption of the algorithm is that all voussoir faces need to be cut because construction waste would have jagged faces. Partially because of this assumption step 3.2 and step 3.3 exist to level the face as well as close the gap that has formed with the previous voussoir. However, since it is suggested that offcuts can be returned to the stock and that none-quadrilateral shapes could be used for stacking by extracting a range of possible quadrilateral voussoirs from them, this assumption should be revisited. More specifically, the alignment of voussoirs could be based not just on a search angle, but on how faces would line up so that no offcuts would have to be performed on one of the voussoirs faces that is being placed. This would decrease the number of required cuts during the processing of the stock.

Recommendations

Aside from addressing assumptions integrated into the stacking algorithm, certain functionality of the currently proposed algorithm can be improved.

Most importantly, the best-fit voussoirs must be found by using more than the search angle and additional search parameters are shown in Figure 5.3. First, it should be checked how far a potential voussoir would reach by checking how to place it so that it automatically staggers. Second, the distance to the boundary that delineates the end of a row should be used to find voussoirs that do not overshoot the thrust surface. Third, it should be checked how tall is the previous voussoir so that the new voussoir's top transverse face is as aligned with the previous top transverse face as possible. Fourth, the vector flow be checked in the locations where the leading patch face and the top transverse face will be placed to see if a voussoir can be found that automatically aligns with the force flow. Fifth, the local radius of curvature for a shell should be found to see if the thrust surface can fit within the kern without additional cuts.

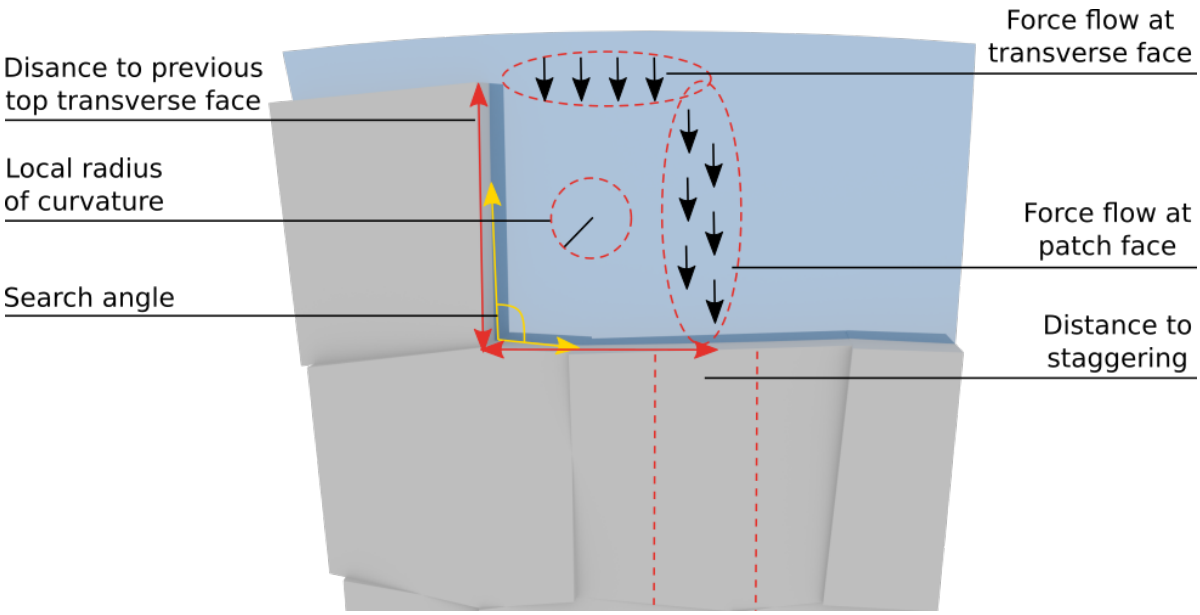

Figure 5.3: Suggested criteria for searching the voussoir of best-fit

Next, the patch vector, which governs the alignment of the patch faces parallel to the force flow, stems from a locally averaged force flow. However, it is averaged around a pivot point and neglects the possibility of vectors changing direction further up the voussoir. Thus, such averaging could result in a voussoir face that is locally aligned with the force flow at the bottom but might not always be aligned at the top, especially for larger voussoirs. To minimize this, the direction of the side should be taken as the average vector direction alongside the entire length of the voussoir side.

With an improved patch vector, next the placing of the voussoirs can be enhanced. Currently, once a search angle is found in the stock which is formed by two of the voussoir faces, the face that will become that patch face and the face that will become the transverse face is chosen at random among the two. While not an issue for regular voussoirs for which these faces are identical, this can result in two very different placements for irregular voussoirs. Therefore, the orientation of the voussoir should be chosen so that it best aligns with the top transverse face of the previous voussoir as well as results in staggering without excessive offcuts. As it is currently not done, the algorithm has a greater chance of resulting in stacking solutions in which certain voussoirs experience a dip with respect to their neighbors as shown in Figure 5.4. Such a dip is smoothened, but could still negatively influence the positioning of the next rows.

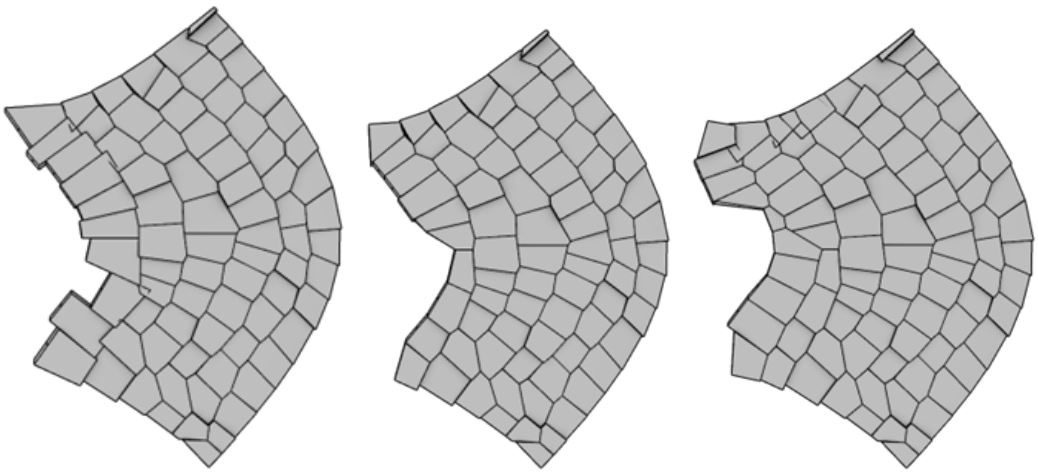

(a) Initial dip in the frontier (b) Smoothened frontier (c) Next row placements

Figure 5.4: Issue with a dip in a voussoir row

To address the steps in which offcuts are created, currently, voussoirs are only cut in a single direction in step 3.1. This is done to decrease their size to allow the thrust surface to fit within the kern if it does not after the initial alignment. However, if a voussoir is large in both length and width, cutting it in a single direction might not result in a smaller voussoir that fits the thrust surface within the kern. In fact, it was impossible to create the dome with the 0p7-1p0-0p2-decr stock without needing to offcut most of the voussoir. Therefore, the stock had to be limited to 0p7-0p8-0p2. For this reason, the voussoir should be shrunken in the other direction, too.

To further improve which voussoirs are selected from the stock, the idea of assortment must be revisited. Currently, if, for instance, the “increasing” sort is selected, the smallest voussoirs will be placed first followed by larger ones. While the difference might be negligible for stocks with many voussoirs, for smaller stocks this could result in small voussoirs being placed in the foundation while larger voussoirs would be suspended in the air. This could be changed to place larger and thicker voussoirs on the bottom to improve the structural capacity of the foundation, which experiences the largest loads. Note that this issue exists also for the “decreasing” sort in cases where the deployment is allowed to run across the entire structure and reach the other boundary curves at the end. Such a deployment was not demonstrated in this thesis. On top of this, the thickest voussoirs could be placed in locations that under variable loading would experience the greatest variations in the thrust surface. This is because the thicker voussoirs would have a thicker kern that could better support these adjustments in the thrust surface without the risks of hinging and concrete cracking.

Another way to improve the algorithm is by examining how voussoirs from different deployments are seamed together. Currently, the interfaces are manually processed. This however occasionally leads to interfaces that are not staggered or aligned with the force flow. Therefore, options should be explored on how to guarantee a staggered and force-aware interface between voussoirs from different deployments.

Finally, even though details of construction are out of the scope of this thesis, the construction of such structures is made more complicated due to the many bespoke voussoirs. Even though marking and digital tracking could ease this, another option is to investigate strategies of how to maximally standardize the voussoir geometry. On top of that, these structures give little room for tolerances, which due to the automated cutting might not be too big, yet, nevertheless, the room for error is small. Interestingly, these points are reflective of how much the construction influences design and fabrication. This bolsters the point that digital fabrication brings involved parties closer in the design phases but also makes it apparent that perhaps exact construction techniques should have been a part of the scope of this thesis.

6

Conclusions

The objective of this thesis was to investigate how to use reclaimed concrete in designing double-curved, compression-only structures. To do so, a novel workflow was suggested and a stacking algorithm was created using COMPAS. In total, 12 different shell structures were generated using a variation of three different shapes, a regular and an irregular shape voussoirs, three alternative methods of sorting the stock, and three different algorithm deployment strategies. All of the structures are held together in compression without any adhesives or mechanical joints and their stability was validated using the Rigid-Block Equilibrium method.

It was found that the average relative retained volume of each voussoir in all structures was 46.7%. Voussoirs of regular dimensions retained 48.8% of the volume while structures using irregular voussoirs retained 43.8%. This discrepancy was attributed to the force flow which locally is mostly parallel and therefore favours voussoirs with parallel sides. Next, no difference was found in the retained volume when stocks of different dimensions were used. However, almost twice as many smaller voussoirs were required, but they used 18.6% less volume and, thus, resulted in a lighter structure. Further, a mixed deployment strategy resulted in the Bowtie shell retaining 51.2% of volume whereas the separate symmetric and stacked strategies resulted in 46.1% and 45.6 respectively. This indicated that deployment strategies can be used for improved stacking. Even more, the ability to use various deployment strategies demonstrated the scalability of the algorithm in being able to tessellate complex geometries such as the pillow shell. Finally, a post-processing analysis estimated that 70-85% of the used concrete can be retained if offcuts are used for creating other voussoirs or returned to the stock for future placement.

The obtained results were used to devise an iterative design workflow that can influence the architectural design of the structure, processing of the stock, and the mode of building disassembly. More specifically, it is outlined how a user can identify locations on the shell where voussoirs retain less volume, and how they can rectify this by modifying the supports and geometry. On top of that, results can be used to inform how a certain stock should be used and how carefully a contractor should disassemble a building.

Finally, suggestions were made to improve the stacking algorithm. More specifically, the algorithm should account for the curvature of the shell, distance to staggering, distance to the previous voussoir's top transverse face, and local curvature at all sides of the voussoir when searching for a voussoir of best-fit.

6.1. Reflections: complete not compete

To conclude this thesis, a broader reflection is made to further highlight the importance of the suggested workflow and position it among other relevant innovations.

First of all, the interactive design process highlights a trend associated with the proliferation of new computational tools and digital fabrication methods. That is, fabrication stands in between design and construction – since many of the computational methods rely on the design being fabrication-aware, a designer is brought closer to the construction processes, which in the past have existed in more distinguished silos. This is relevant especially due to the fragmented nature of architects, engineers,

contractors, consultants, and clients, who are all naturally interested in their own profit, which, therefore, makes it difficult to align incentives. This thesis has highlighted an approach and benefits to bringing fabrication constraints to an earlier design stage, which requires a cross-disciplinary approach.

Simultaneously, the advancement of new design tools and methods poses a great economic opportunity. As suggested by the Paulson curve seen in Figure 6.1, project costs are lower at the beginning of any project, which is also when decisions have a high influence on the outcome [48]. Because the designer must now make decisions related to the construction in greater detail much earlier, decision-making can occur at a stage when costs are still low.

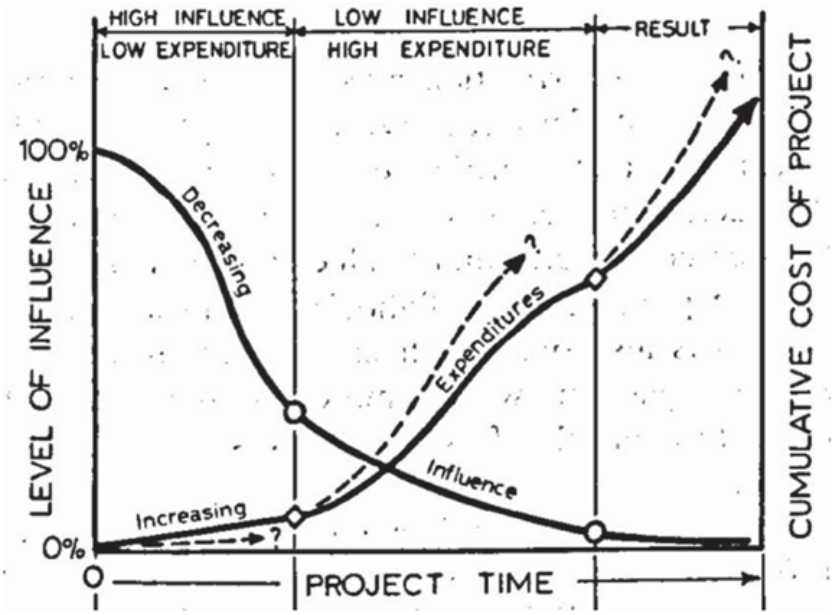

Figure 6.1: Paulson curve of level of influence & project costs over time [48]

The economic benefits could also stem from the untapped potential that is created by the lag in digitization and productivity rates of the construction industry. For instance, the voussoirs created in this thesis are all automatically generated and with minor adjustments could be ready for fabrication. This automation could minimize the cost overruns that could come from human errors. Even more, the voussoirs could all maintain their digital passports that provide information about their previous lifespan, material properties, and the processing performed on them, which can simplify any future maintenance works and disassembly of the structures. On top of that, as a digital twin of the structure is available, voussoir assembly would be simplified. This would be enabled by the ability to clearly visualize each voussoir's placement location and sequence as well as simplifying site logistics by delivering voussoirs to the site only when they are scheduled for placement. Overall, it is clear that digital fabrication methods have the potential to achieve both economic and environmental benefits.

Other methods for achieving a construction industry's transition to a more circular economy must be devised in parallel with the advancement of digital tools. They can range from governmental action, industry shifts, and individual actions. They are briefly mentioned in the following paragraphs.

For governmental action, regulations and tax-based approaches must be devised that guide the industry toward sustainability. For instance, clients could be required to pay a material deposit in taxes, which could be regained if the material is entered back into the circular economy by the end of the service lifespan of the structure. Furthermore, governing bodies should enforce the establishment of updated design codes that clearly assist designers in the design process and simplify the approval of buildings constructed with reclaimed materials. This would streamline the process, reduce costs that are currently higher due to the research nature of such projects, and significantly improve the trust in the safety of structures built with reclaimed materials. Additionally, projects such as Recreate must be funded to stimulate research [33]. Finally, public procurement should require companies to demonstrate a level of digitization and commitment to sustainability to be eligible for applying such as the case stipulated in Latvia's BIM Road-map to require BIM usage in all government procurement.

As for the industry, not only should digital fabrication methods be introduced in the existing business models, but digital fabrication methods could give rise to new business models. For instance, deconstruction could phase out demolition. This could be done by creating an incentive to reclaim the materials, which could be shared not only by the owner of the structure but also by the company that created it. In this approach, construction materials would shift from an economy of ownership and could become a part of the service economy through a performance contract according to which materials are not sold to the client but rather leased and reclaimed by the manufacturer at the end of the lifespan of a structure. This could, first of all, create an active incentive for both the manufacturing company and the owner of the structure to better maintain the structure since it still has monetary value and, second, lower the overall costs for all parties. The lowered prices would come from the fact that the material's value at the end of the lifespan could be subtracted from the costs that the client has to pay initially since the company will reclaim the materials.

Finally, individual action could incentivize environmental shifts in the previously discussed domains. A rising social demand for sustainability can influence the zeitgeist that drives the priorities of the industry. Possibly, pioneering structures could have a facilitating role in the strengthening of such a zeitgeist. For instance, the designed structures in this thesis depict ideas of sustainability and structural geometry in their design as the interfaces between voussoirs are dominating the aesthetic. In fact, the hope is that they can represent all three vitruvius values of great architecture of utilitas, firmitas, venustas (usable, durable, beautiful). Thus proliferation of digitally fabricated structures serve a purpose of starting a conversation of how things could be and imagining cityscapes that are not necessarily rectilinear.

These shifts in the governmental, industry and individual domains must also be bolstered by keeping the design tools open source and democratized. This is why COMPAS was chosen for this thesis. Similarly, configurators can play a great role in diminishing technical boundaries that otherwise separate clients from sustainable design options and tools.

In fact, it is because of the recency and currently still infancy of the computational tool proliferation in the built environment that deliberate steps must be taken now to shape the culture of how such tools are used. Otherwise, a risk exists of implementing the new tools in the old business models and thought processes that have resulted in the current environmental burden which the built industry carries. It is important to emphasize that innovation with the discussed results lies both with the materials and also the modeling techniques.

To conclude, using reclaimed concrete as suggested in this thesis is proposed to be only a single strategy in the larger scene of transitioning the construction industry to a circular economy. With that in mind, the suggested solutions are presented as a way to complete and compliment other solutions as opposed to competing against them. For instance, further research could explore how such structures could obtain local tensile strength by applying local reinforcements. Similarly, the extensive formwork needed to create such structures could perhaps be simplified by using textile formwork that has been solidified with initial layers of pasted concrete. Understanding that the building stock is set to grow, methods for creating structures in circular ways from new materials must be devised, too, for one reason being to simplify a potential reclaiming process. Ultimately, engineers, architects, consultants and other parties involved in the design process must be challenged to find more sustainable ways and build structures that barely stand.

Bibliography

[1] Robbie M. Andrew. “Global CO2 emissions from cement production”. In: *Earth System Science Data* 10.1 (Jan. 2018), pp. 195–217. ISSN: 18663516. DOI: 10.5194/essd-10-195-2018.

[2] Johanna Lehne and Felix Preston. *Making Concrete Change: Innovation in Low-carbon Cement and Concrete*. Tech. rep. Chatham House: The Royal Institute of International Affairs, June 2018. URL: www.chathamhouse.org.

[3] Statista and Aaron O’Neill. *Global population 10,000BCE-2100*. Sept. 2020. URL: https://www.statista.com/statistics/1006502/global-population-ten-thousand-bc-to-2050/.

[4] Alex Muresan et al. “Sustainability through reuse: a reconfigurable structural system for residential and office buildings”. In: *IOP Conference Series: Earth and Environmental Science* 588 (2020).

[5] Tom Van Mele et al. “COMPAS: A framework for computational research in architecture and structures”. In: (2017).

[6] Gene Ting Chun Kao et al. “Understanding the rigid-block equilibrium method by way of mathematical programming”. In: *https://doi.org/10.1680/jencm.20.00036* 174.3 (Sept. 2021), pp. 143–157. ISSN: 1755-0777. DOI: 10.1680/JENCM.20.00036. URL: https://www.icevirtuallibrary.com/doi/10.1680/jencm.20.00036.

[7] *AR6 Synthesis Report: Climate Change 2023 — IPCC*. URL: https://www.ipcc.ch/report/sixth-assessment-report-cycle/.

[8] Statista Research Department. *Global share of people living in cities since 1950*. Apr. 2011. URL: https://www.statista.com/statistics/274520/global-share-of-people-living-in-cities/.

[9] Bill Gates. *Buildings are bad for the climate*. Oct. 2019. URL: https://www.gatesnotes.com/Energy/Buildings-are-good-for-people-and-bad-for-the-climate.

[10] McKinsey Global Institute and McKinsey’s Capital Projects & Infrastructure Practice. *Reinventing Construction: a Route to Higher Productivity, Executive Summary*. Tech. rep. Feb. 2017. URL: www.mckinsey.com/mgi..

[11] *World Economic Forum*. URL: https://initiatives.weforum.org/digital-transformation/climate-scenarios.

[12] *Mission Possible: Reaching Net-Zero Carbon Emissions - ETC*. Tech. rep. Nov. 2018. URL: https://www.energy-transitions.org/publications/mission-possible/#download-form.

[13] *COMPAS*. URL: https://compas.dev/.

[14] *RV2 | Food4Rhino*. URL: https://www.food4rhino.com/en/app/rv2.

[15] P Block. *Thrust Network Analysis Exploring Three-dimensional Equilibrium Submitted to the Department of Architecture in Partial Fulfillment of the Requirements for the Degree of*. Tech. rep. 2009.

[16] *Karamba3D*. URL: https://karamba3d.com/.

[17] *What is a circular economy? | Ellen MacArthur Foundation*. URL: https://www.ellenmacarthurfoundation.org/topics/circular-economy-introduction/overview.

[18] *The Butterfly Diagram: Visualising the Circular Economy*. URL: https://www.ellenmacarthurfoundation.org/circular-economy-diagram.

[19] E MacArthur - Journal of Industrial Ecology and undefined 2013. “Towards the circular economy”. In: *werktrends.nlE MacArthurJournal of Industrial Ecology, 2013•werktrends.nl* (). URL: https://www.werktrends.nl/app/uploads/2015/06/Rapport_McKinsey-Towards_A_Circular_Economy.pdf.

[20] Chunbo Zhang et al. “An overview of the waste hierarchy framework for analyzing the circularity in construction and demolition waste management in Europe”. In: *Science of The Total Environment* 803 (Jan. 2022), p. 149892. ISSN: 0048-9697. DOI: 10.1016/J.SCITOTENV.2021.149892.

[21] Betonakkoord Voor. *Betonakkoord voor duurzame groei*. Tech. rep. July 2018.

[22] Christof Knoeri, Esther Sanyé-Mengual, and Hans-Joerg Althaus. “Comparative LCA of recycled and conventional concrete for structural applications”. In: (). DOI: 10.1007/s11367-012-0544-2.

[23] Francesco Colangelo et al. “Comparative LCA of concrete with recycled aggregates: a circular economy mindset in Europe”. In: *International Journal of Life Cycle Assessment* 25.9 (Sept. 2020), pp. 1790–1804. ISSN: 16147502. DOI: 10.1007/S11367-020-01798-6. URL: https://www.popsci.com/science/reuse-concrete-bridge/.

[24] S Huuhka et al. “Architectural potential of deconstruction and reuse in declining mass housing estates”. In: (2019). URL: https://trepo.tuni.fi/handle/10024/126244.

[25] S. Huuhka et al. “Reusing concrete panels from buildings for building: Potential in Finnish 1970s mass housing”. In: *Resources, Conservation and Recycling* 101 (Aug. 2015), pp. 105–121. ISSN: 0921-3449. DOI: 10.1016/J.RESCONREC.2015.05.017.

[26] M. Coenen, G. Lentz, and N. Prak. “De kop is eraf: Evaluatie van de aftopping van een flat in Middelburg”. In: (1990).

[27] Jorn Van Der Steen et al. *Computational Reuse Optimisation for Stadium Design*. Tech. rep. 2015. URL: https://www.researchgate.net/publication/283258420.

[28] Julie Devènes et al. “Re:Crete – Reuse of concrete blocks from cast-in-place building to arch footbridge”. In: *Structures* 43 (Sept. 2022), pp. 1854–1867. ISSN: 2352-0124. DOI: 10.1016/J.ISTRUC.2022.07.012.

[29] J. Warmuth, J. Brütting, and C. Fivet. *Phoenix3D*. 2021. URL: https://www.epfl.ch/labs/sxl/phoenix3d/.

[30] Corentin Fivet and Jan Brütting. *Nothing is lost, nothing is created, everything is reused: structural design for a circular economy*. Tech. rep. 2020, pp. 74–81.

[31] Jan Brütting, Gennaro Senatore, and Corentin Fivet. “Form follows availability -designing structures through reuse”. In: *Journal of the international association for shell and spatial structures: J. IASS* (2019).

[32] *Waste Framework Directive*. URL: https://environment.ec.europa.eu/topics/waste-and-recycling/waste-framework-directive_en.

[33] *ReCreate*.

[34] *Building : 3000 years of design engineering and construction : Addis, William, 1949- : Free Download, Borrow, and Streaming : Internet Archive*. URL: https://archive.org/details/building3000year0000addi.

[35] Robert Hooke. *A description of helioscopes and some other instruments*. 1676.

[36] Christian Meyer and Michael H. Sheer. “Do Concrete Shells Deserve Another Look?” In: *Concrete International* 27.10 (Oct. 2005), pp. 43–50.

[37] Matthias Rippmann et al. “The Armadillo Vault: Computational design and digital fabrication of a freeform stone shell”. In: *Advances in Architectural Geometry 2016* (2016), pp. 344–363. DOI: 10.3218/3778-4{_}23.

[38] Matthias Rippmann. *Funicular Shell Design: Geometric approaches to form finding and fabrication of discrete funicular structures*. 2016. URL: https://www.researchgate.net/publication/305316560_Funicular_Shell_Design_Geometric_approaches_to_form_finding_and_fabrication_of_discrete_funicular_structures.

[39] Shajay Bhooshan et al. “The Striatus bridge”. In: *Architecture, Structures and Construction 2022 2:4* 2.4 (June 2022), pp. 521–543. ISSN: 2730-9894. DOI: 10.1007/S44150-022-00051-Y. URL: https://link.springer.com/article/10.1007/s44150-022-00051-y.

[40] naaro. *Striatus - 3D concrete printed masonry bridge*. URL: https://www.block.arch.ethz.ch/brg/project/striatus-3d-concrete-printed-masonry-bridge-venice-italy-2021.

[41] *Konstruktives Recycling: Ein sicherer Übergang auf Re-Use Beton*. URL: https://www.architektur-aktuell.at/news/konstruktives-recycling-ein-sicherer-uebergang-auf-re-use-beton.

[42] Robin Oval et al. “A path towards the off-site automated fabrication of segmented concrete shells for building slabs”. In: *Proceedings of the IASS Annual Symposium 2020/21 and the 7th International Conference on Spatial Structures*. Guilford, Aug. 2021.

[43] David López López et al. *Prototype of an ultra-thin, concrete vaulted floor system*. Tech. rep. 2014. URL: https://www.researchgate.net/publication/272357567.

[44] *New concrete vaulted floor suggests path to cutting carbon emissions*. URL: https://www.dezeen.com/2022/03/04/concrete-vaulted-floor-suggests-path-to-cutting-carbon-emissions/.

[45] Gursans Guven et al. “A construction classification system database for understanding resource use in building construction”. In: *Scientific Data* 9.1 (Dec. 2022). ISSN: 20524463. DOI: 10.1038/S41597-022-01141-8.

[46] Daniele Panozzo, Philippe Block, and Olga Sorkine-Hornung. “Designing unreinforced masonry models”. In: *ACM Transactions on Graphics (TOG)* 32.4 (July 2013). ISSN: 07300301. DOI: 10.1145/2461912.2461958. URL: https://dl.acm.org/doi/abs/10.1145/2461912.2461958.

[47] A Borgart, M Leuw, and JP Hoogenboom. *The relationship of form and force in (irregular) curved surfaces*. 2005. URL: https://research.tudelft.nl/en/publications/the-relationship-of-form-and-force-in-irregular-curved-surfaces.

[48] Boyd C. Paulson. “Designing to Reduce Construction Costs”. In: *Journal of the Construction Division* 102.4 (Dec. 1976), pp. 587–592. ISSN: 0569-7948. DOI: 10.1061/JCCEAZ.0000639. URL: https://ascelibrary.org/doi/abs/10.1061/JCCEAZ.0000639%20https://ascelibrary.org/doi/10.1061/JCCEAZ.0000639.

[49] Yue Wu et al. “Structural analysis and construction quality assessment of a free-form ice composite shell”. In: *Structures* 27 (Oct. 2020), pp. 868–878. ISSN: 2352-0124. DOI: 10.1016/J.ISTRUC.2020.06.032.

[50] *The Ice Shell Project*. URL: https://vimeo.com/channels/iceshellproject/.

7

Appendix A: Physical prototyping

To acquire an apt feel for compression-only structures, a physical model inspired by the ice models created by Heinz Isler [49] as well as “The Ice Shell Project” [50] was prototyped. More specifically, a wet towel was hung from four corners and allowed to freeze. Once frozen, it was flipped upside down and placed in a rig that prevents the towel’s legs from sliding outwards as shown in Figure 7.1 below.

(a) Wet towel allowed to freeze

(b) Frozen towel inverted and fixed in a rig

Figure 7.1: Formation of the towel-shell

To test its structural capacity, bricks were stacked atop the towel until the structure collapsed. During the process, the legs of the structure buckled and began to unwind after four bricks were placed. Nevertheless, the top part of the shell, which exhibits double curvature as opposed to curvature in only a single direction like the legs, only caved after nine bricks were placed. As each brick weighed approximately two kg, the towel-shell structure held up 16kgs as shown in Figure 7.2.

(a) Loaded with five bricks (b) Legs buckled; middle holds (c) Collapse at nine bricks

Figure 7.2: Loading process of the towel-shell

For comparison purposes, the experiment was repeated with a flat towel that was supported at each end at an equally spaced distance as in the rig used for the towel-shell. A half-brick was placed in the middle of the flat towel and it caved in immediately. While rigorous qualitative conclusions, of course, cannot be derived, the towel seemed to carry 16 times more weight when it was curved than when it was flat, which gives rise to a qualitative appreciation of shell structures. On top of that, if the same weight had been applied uniformly across the towel and not as a point load, it is reasonable to expect that the towel-shell could have carried even more weight. For a more comprehensive study of ice shell structures, the reader is directed to the work of [49].

Aside from the towel-shell prototype, which was studied in the initial stages of this thesis, a small-scale model of the Bowtie pedestrian bridge was created once the algorithm was finished. More specifically, small plastic elements were 3D printed and a model was glued together as shown in Figure 7.3. In this way, the model differs from the proposed structures as those have no adhesives or mechanical connections present in the voussoir interfaces. Nevertheless, the small-scale model greatly demonstrated the challenges associated with assembling the voussoirs. As seen in Figure 7.3b, gaps have formed between voussoirs despite voussoir interfaces being aligned in the digital model. This calls upon a further study of the proposed workflow to understand ways of handling geometric imprecision and create guides on the voussoirs that help with alignment.

(a) Perspective view (b) Top view

Figure 7.3: Prototype of the Bowtie shell

8

Appendix B: Retained voussoir volume

The following section compliments the Results chapter and provides plots in Figure 8.1 for the relative retained volumes for each voussoir in all of the studied results.

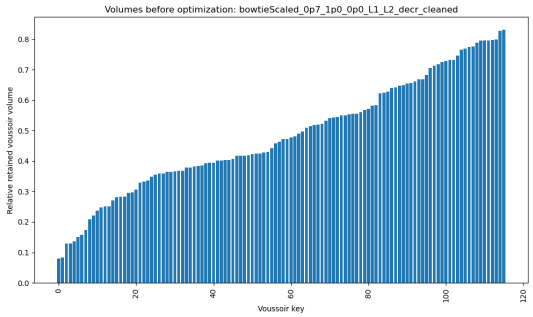

(a) 0p7-1p0-0p0-decr-symmetric-bowtie

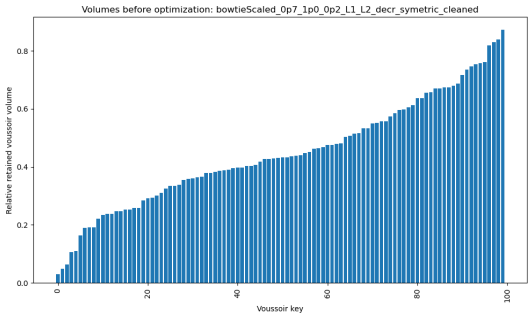

(b) 0p7-1p0-0p2-decr-symmetric-bowtie

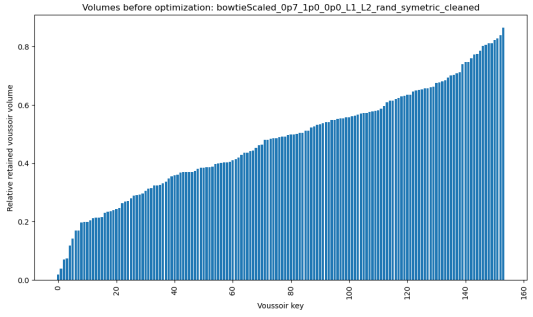

(c) 0p7-1p0-0p0-rand-symmetric-bowtie

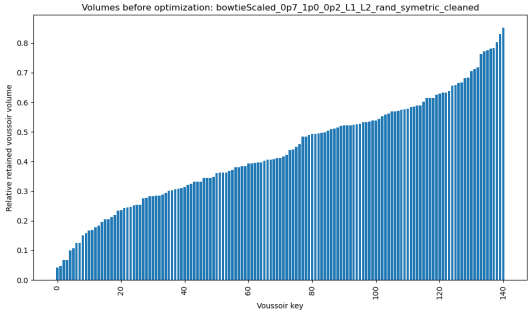

(d) 0p7-1p0-0p2-rand-symmetric-bowtie

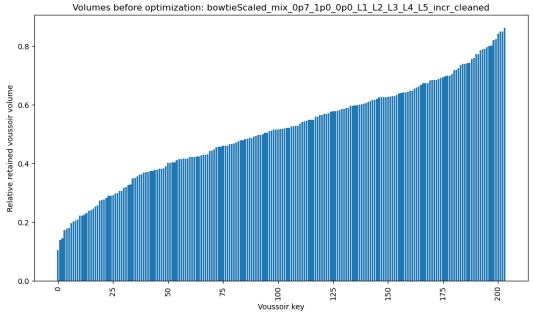

(e) 0p7-1p0-0p0-incr-symmetric-bowtie

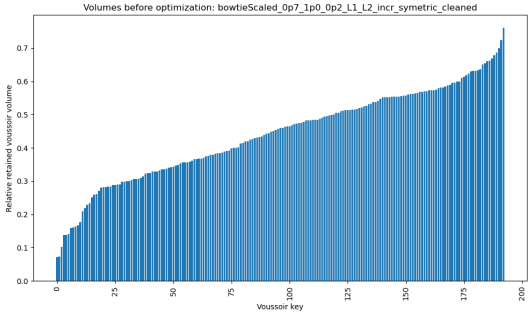

(f) 0p7-1p0-0p2-incr-symmetric-bowtie

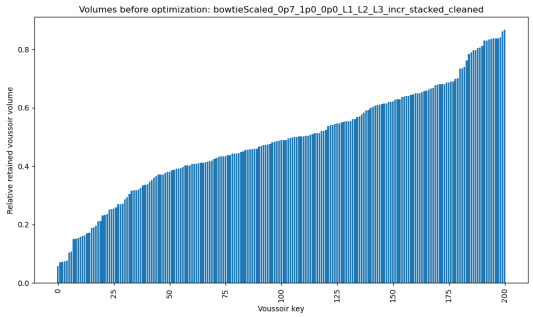

(g) 0p7-1p0-0p0-incr-stacked-bowtie

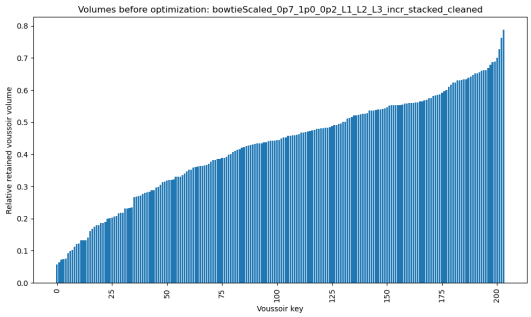

(h) 0p7-1p0-0p2-incr-stacked-bowtie

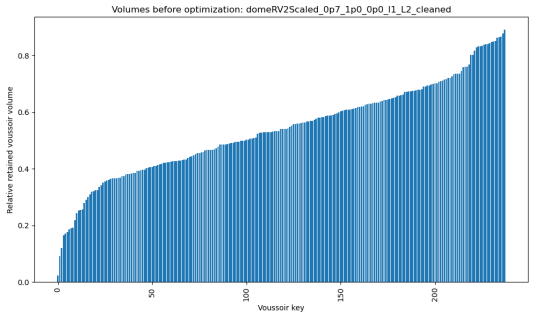

(i) 0p7-1p0-0p0-decr-between-dome

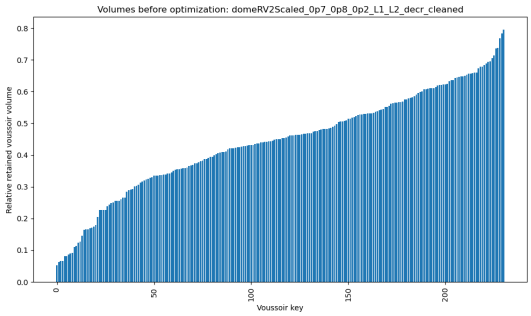

(j) 0p7-0p8-0p2-decr-between-dome

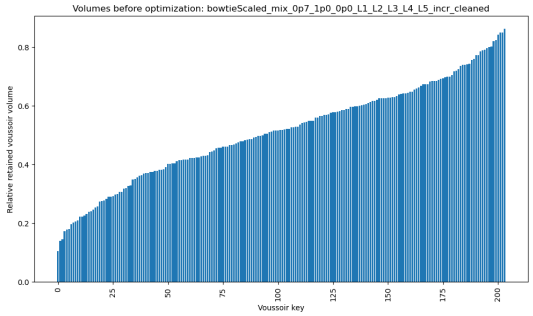

(k) 0p7-1p0-0p0-incr-mixed-bowtie

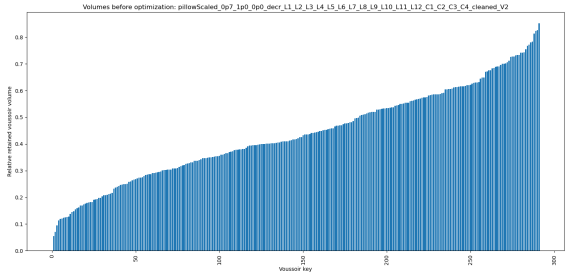

(l) 0p7-1p0-0p0-decr-mixed-pillow

Figure 8.1: Relative retained volumes for all tested tessellations before waste minimization

The following Figure 8.2 shows the relative retained voussoir volume when fudge factor equals 0.2.

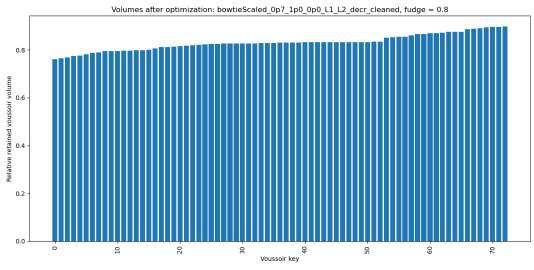

(a) 0p7-1p0-0p0-decr-symmetric-bowtie

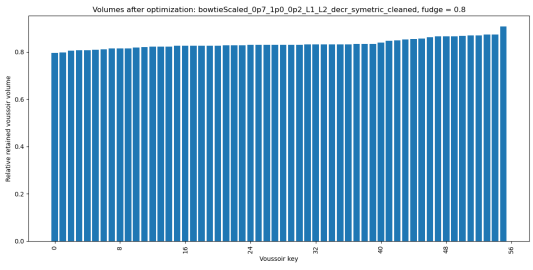

(b) 0p7-1p0-0p2-decr-symmetric-bowtie

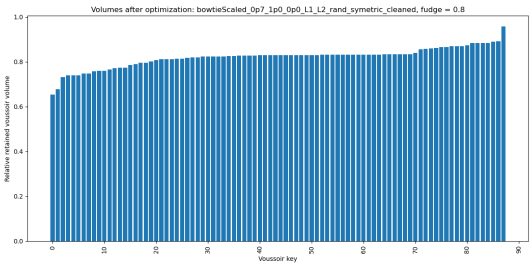

(c) 0p7-1p0-0p0-rand-symmetric-bowtie

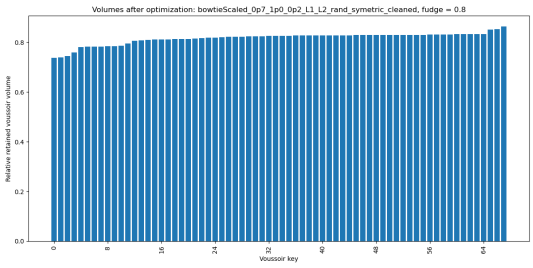

(d) 0p7-1p0-0p2-rand-symmetric-bowtie

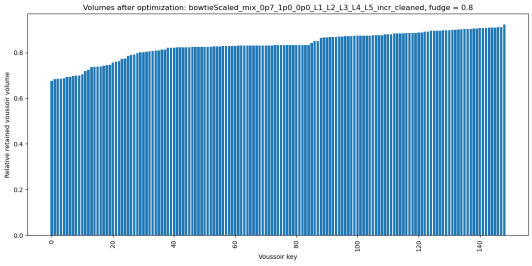

(e) 0p7-1p0-0p0-incr-symmetric-bowtie

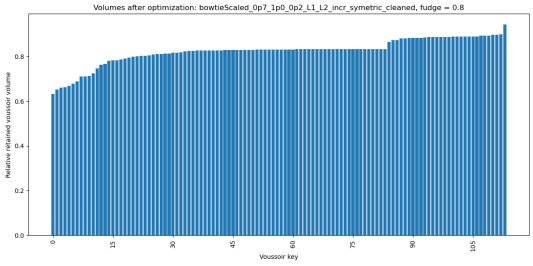

(f) 0p7-1p0-0p2-incr-symmetric-bowtie

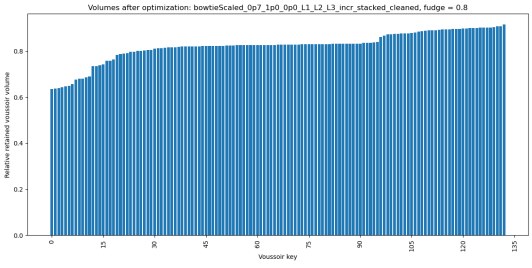

(g) 0p7-1p0-0p0-incr-stacked-bowtie

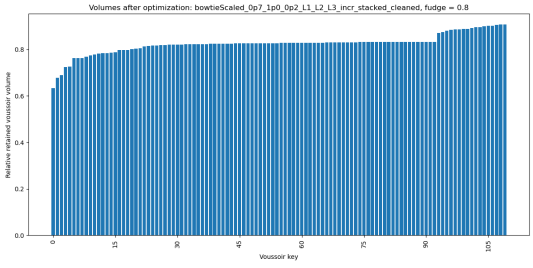

(h) 0p7-1p0-0p2-incr-stacked-bowtie

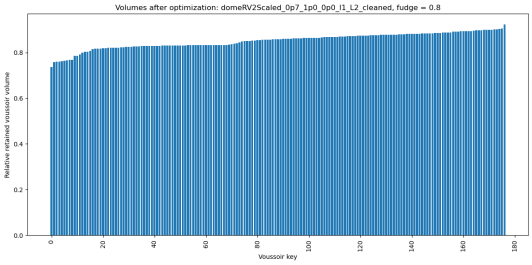

(i) 0p7-1p0-0p0-decr-between-dome

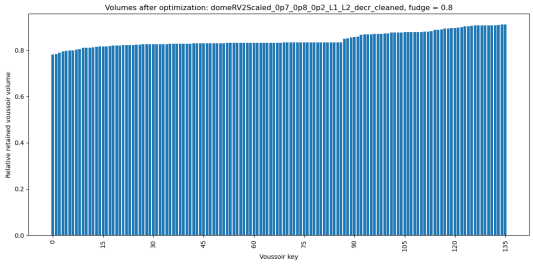

(j) 0p7-0p8-0p2-decr-between-dome

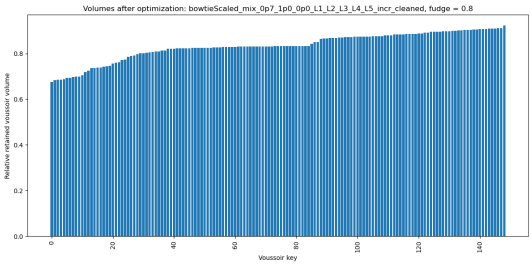

(k) 0p7-1p0-0p0-incr-mixed-bowtie

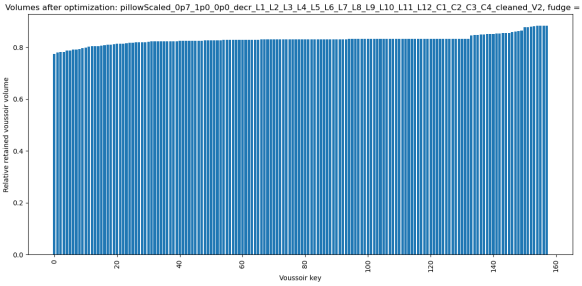

(l) 0p7-1p0-0p0-decr-mixed-pillow

Figure 8.2: Relative retained volume of each voussoir placed in a bowtie after optimization with a fudge factor of 0.2 for various stocks

The Figure 8.3 shows the relative retained voussoir volume when fudge factor equals 0.5.

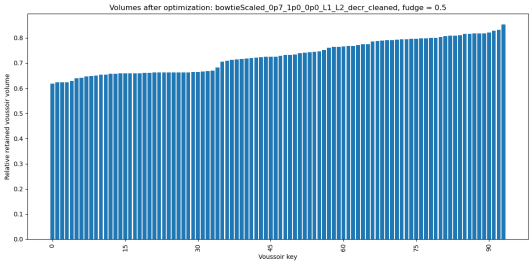

(a) 0p7-1p0-0p0-decr-symmetric-bowtie

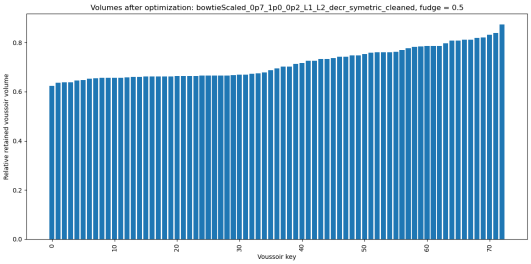

(b) 0p7-1p0-0p2-decr-symmetric-bowtie

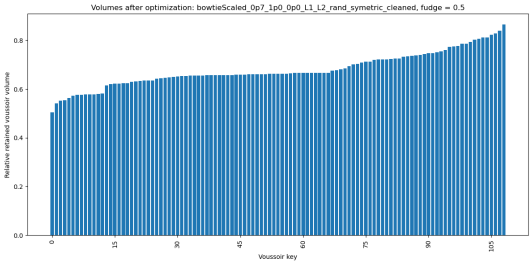

(c) 0p7-1p0-0p0-rand-symmetric-bowtie

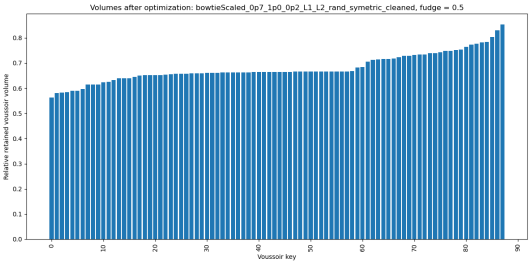

(d) 0p7-1p0-0p2-rand-symmetric-bowtie

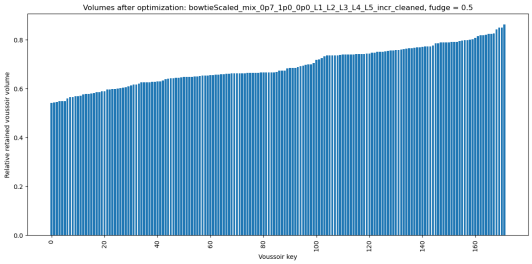

(e) 0p7-1p0-0p0-incr-symmetric-bowtie

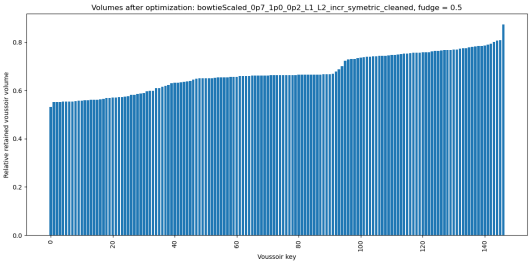

(f) 0p7-1p0-0p2-incr-symmetric-bowtie

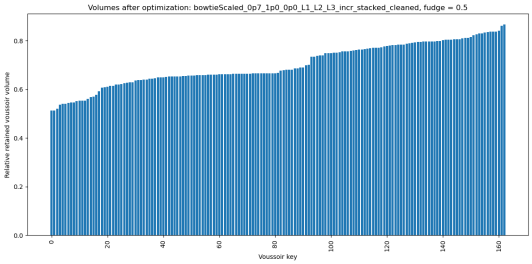

(g) 0p7-1p0-0p0-incr-stacked-bowtie

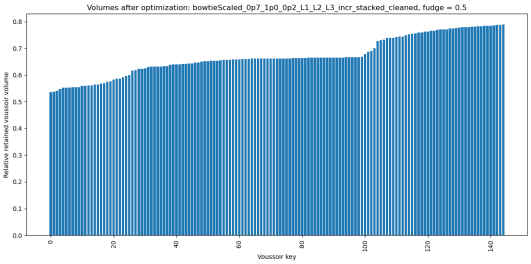

(h) 0p7-1p0-0p2-incr-stacked-bowtie

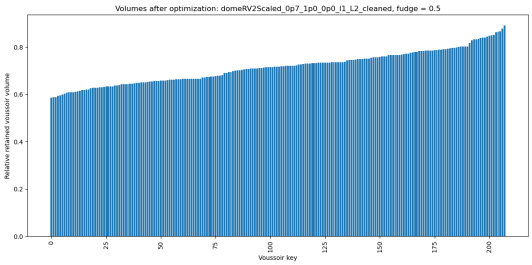

(i) 0p7-1p0-0p0-decr-between-dome

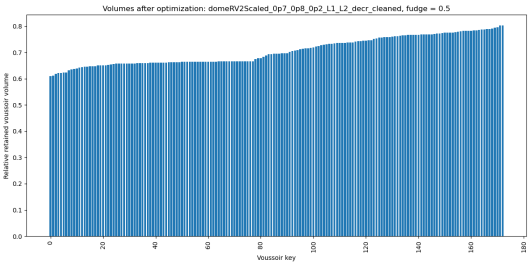

(j) 0p7-0p8-0p2-decr-between-dome

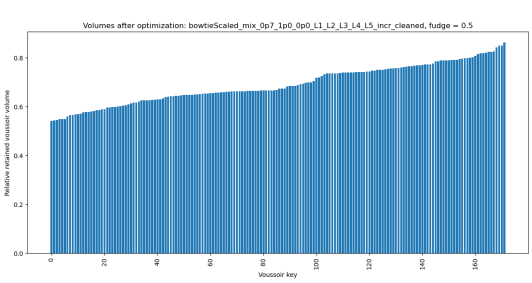

(k) 0p7-1p0-0p0-incr-mixed-bowtie

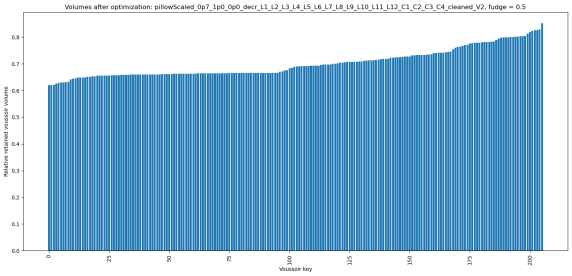

(l) 0p7-1p0-0p0-decr-mixed-pillow

Figure 8.3: Relative retained volume of each voussoir placed in a bowtie after optimization with a fudge factor of 0.5 for various stocks

Bibliography

[1] Robbie M. Andrew. “Global CO2 emissions from cement production”. In: *Earth System Science Data* 10.1 (Jan. 2018), pp. 195–217. ISSN: 18663516. DOI: 10.5194/essd-10-195-2018.

[2] Johanna Lehne and Felix Preston. *Making Concrete Change: Innovation in Low-carbon Cement and Concrete*. Tech. rep. Chatham House: The Royal Institute of International Affairs, June 2018. URL: www.chathamhouse.org.

[3] Statista and Aaron O’Neill. *Global population 10,000BCE-2100*. Sept. 2020. URL: https://www.statista.com/statistics/1006502/global-population-ten-thousand-bc-to-2050/.

[4] Alex Muresan et al. “Sustainability through reuse: a reconfigurable structural system for residential and office buildings”. In: *IOP Conference Series: Earth and Environmental Science* 588 (2020).

[5] Tom Van Mele et al. “COMPAS: A framework for computational research in architecture and structures”. In: (2017).

[6] Gene Ting Chun Kao et al. “Understanding the rigid-block equilibrium method by way of mathematical programming”. In: *https://doi.org/10.1680/jencm.20.00036* 174.3 (Sept. 2021), pp. 143–157. ISSN: 1755-0777. DOI: 10.1680/JENCM.20.00036. URL: https://www.icevirtuallibrary.com/doi/10.1680/jencm.20.00036.

[7] *AR6 Synthesis Report: Climate Change 2023 — IPCC*. URL: https://www.ipcc.ch/report/sixth-assessment-report-cycle/.

[8] Statista Research Department. *Global share of people living in cities since 1950*. Apr. 2011. URL: https://www.statista.com/statistics/274520/global-share-of-people-living-in-cities/.

[9] Bill Gates. *Buildings are bad for the climate*. Oct. 2019. URL: https://www.gatesnotes.com/Energy/Buildings-are-good-for-people-and-bad-for-the-climate.

[10] McKinsey Global Institute and McKinsey’s Capital Projects & Infrastructure Practice. *Reinventing Construction: a Route to Higher Productivity, Executive Summary*. Tech. rep. Feb. 2017. URL: www.mckinsey.com/mgi..

[11] *World Economic Forum*. URL: https://initiatives.weforum.org/digital-transformation/climate-scenarios.

[12] *Mission Possible: Reaching Net-Zero Carbon Emissions - ETC*. Tech. rep. Nov. 2018. URL: https://www.energy-transitions.org/publications/mission-possible/#download-form.

[13] *COMPAS*. URL: https://compas.dev/.

[14] *RV2 | Food4Rhino*. URL: https://www.food4rhino.com/en/app/rv2.

[15] P Block. *Thrust Network Analysis Exploring Three-dimensional Equilibrium Submitted to the Department of Architecture in Partial Fulfillment of the Requirements for the Degree of*. Tech. rep. 2009.

[16] *Karamba3D*. URL: https://karamba3d.com/.

[17] *What is a circular economy? | Ellen MacArthur Foundation*. URL: https://www.ellenmacarthurfoundation.org/topics/circular-economy-introduction/overview.

[18] *The Butterfly Diagram: Visualising the Circular Economy*. URL: https://www.ellenmacarthurfoundation.org/circular-economy-diagram.

[19] E MacArthur - Journal of Industrial Ecology and undefined 2013. “Towards the circular economy”. In: *werktrends.nlE MacArthurJournal of Industrial Ecology, 2013•werktrends.nl* (). URL: https://www.werktrends.nl/app/uploads/2015/06/Rapport_McKinsey-Towards_A_Circular_Economy.pdf.

[20] Chunbo Zhang et al. “An overview of the waste hierarchy framework for analyzing the circularity in construction and demolition waste management in Europe”. In: *Science of The Total Environment* 803 (Jan. 2022), p. 149892. ISSN: 0048-9697. DOI: 10.1016/J.SCITOTENV.2021.149892.

[21] Betonakkoord Voor. *Betonakkoord voor duurzame groei*. Tech. rep. July 2018.

[22] Christof Knoeri, Esther Sanyé-Mengual, and Hans-Joerg Althaus. “Comparative LCA of recycled and conventional concrete for structural applications”. In: (). DOI: 10.1007/s11367-012-0544-2.

[23] Francesco Colangelo et al. “Comparative LCA of concrete with recycled aggregates: a circular economy mindset in Europe”. In: *International Journal of Life Cycle Assessment* 25.9 (Sept. 2020), pp. 1790–1804. ISSN: 16147502. DOI: 10.1007/S11367-020-01798-6. URL: https://www.popsci.com/science/reuse-concrete-bridge/.

[24] S Huuhka et al. “Architectural potential of deconstruction and reuse in declining mass housing estates”. In: (2019). URL: https://trepo.tuni.fi/handle/10024/126244.

[25] S. Huuhka et al. “Reusing concrete panels from buildings for building: Potential in Finnish 1970s mass housing”. In: *Resources, Conservation and Recycling* 101 (Aug. 2015), pp. 105–121. ISSN: 0921-3449. DOI: 10.1016/J.RESCONREC.2015.05.017.

[26] M. Coenen, G. Lentz, and N. Prak. “De kop is eraf: Evaluatie van de aftopping van een flat in Middelburg”. In: (1990).

[27] Jorn Van Der Steen et al. *Computational Reuse Optimisation for Stadium Design*. Tech. rep. 2015. URL: https://www.researchgate.net/publication/283258420.

[28] Julie Devènes et al. “Re:Crete – Reuse of concrete blocks from cast-in-place building to arch footbridge”. In: *Structures* 43 (Sept. 2022), pp. 1854–1867. ISSN: 2352-0124. DOI: 10.1016/J.ISTRUC.2022.07.012.

[29] J. Warmuth, J. Brütting, and C. Fivet. *Phoenix3D*. 2021. URL: https://www.epfl.ch/labs/sxl/phoenix3d/.

[30] Corentin Fivet and Jan Brütting. *Nothing is lost, nothing is created, everything is reused: structural design for a circular economy*. Tech. rep. 2020, pp. 74–81.

[31] Jan Brütting, Gennaro Senatore, and Corentin Fivet. “Form follows availability -designing structures through reuse”. In: *Journal of the international association for shell and spatial structures: J. IASS* (2019).

[32] *Waste Framework Directive*. URL: https://environment.ec.europa.eu/topics/waste-and-recycling/waste-framework-directive_en.

[33] *ReCreate*.

[34] *Building : 3000 years of design engineering and construction : Addis, William, 1949- : Free Download, Borrow, and Streaming : Internet Archive*. URL: https://archive.org/details/building3000year0000addi.

[35] Robert Hooke. *A description of helioscopes and some other instruments*. 1676.

[36] Christian Meyer and Michael H. Sheer. “Do Concrete Shells Deserve Another Look?” In: *Concrete International* 27.10 (Oct. 2005), pp. 43–50.

[37] Matthias Rippmann et al. “The Armadillo Vault: Computational design and digital fabrication of a freeform stone shell”. In: *Advances in Architectural Geometry 2016* (2016), pp. 344–363. DOI: 10.3218/3778-4{_}23.

[38] Matthias Rippmann. *Funicular Shell Design: Geometric approaches to form finding and fabrication of discrete funicular structures*. 2016. URL: https://www.researchgate.net/publication/305316560_Funicular_Shell_Design_Geometric_approaches_to_form_finding_and_fabrication_of_discrete_funicular_structures.

[39] Shajay Bhooshan et al. “The Striatus bridge”. In: *Architecture, Structures and Construction 2022 2:4* 2.4 (June 2022), pp. 521–543. ISSN: 2730-9894. DOI: 10.1007/S44150-022-00051-Y. URL: https://link.springer.com/article/10.1007/s44150-022-00051-y.

[40] naaro. *Striatus - 3D concrete printed masonry bridge*. URL: https://www.block.arch.ethz.ch/brg/project/striatus-3d-concrete-printed-masonry-bridge-venice-italy-2021.

[41] *Konstruktives Recycling: Ein sicherer Übergang auf Re-Use Beton*. URL: https://www.architektur-aktuell.at/news/konstruktives-recycling-ein-sicherer-uebergang-auf-re-use-beton.

[42] Robin Oval et al. “A path towards the off-site automated fabrication of segmented concrete shells for building slabs”. In: *Proceedings of the IASS Annual Symposium 2020/21 and the 7th International Conference on Spatial Structures*. Guilford, Aug. 2021.

[43] David López López et al. *Prototype of an ultra-thin, concrete vaulted floor system*. Tech. rep. 2014. URL: https://www.researchgate.net/publication/272357567.

[44] *New concrete vaulted floor suggests path to cutting carbon emissions*. URL: https://www.dezeen.com/2022/03/04/concrete-vaulted-floor-suggests-path-to-cutting-carbon-emissions/.

[45] Gursans Guven et al. “A construction classification system database for understanding resource use in building construction”. In: *Scientific Data* 9.1 (Dec. 2022). ISSN: 20524463. DOI: 10.1038/S41597-022-01141-8.

[46] Daniele Panozzo, Philippe Block, and Olga Sorkine-Hornung. “Designing unreinforced masonry models”. In: *ACM Transactions on Graphics (TOG)* 32.4 (July 2013). ISSN: 07300301. DOI: 10.1145/2461912.2461958. URL: https://dl.acm.org/doi/abs/10.1145/2461912.2461958.

[47] A Borgart, M Leuw, and JP Hoogenboom. *The relationship of form and force in (irregular) curved surfaces*. 2005. URL: https://research.tudelft.nl/en/publications/the-relationship-of-form-and-force-in-irregular-curved-surfaces.

[48] Boyd C. Paulson. “Designing to Reduce Construction Costs”. In: *Journal of the Construction Division* 102.4 (Dec. 1976), pp. 587–592. ISSN: 0569-7948. DOI: 10.1061/JCCEAZ.0000639. URL: https://ascelibrary.org/doi/abs/10.1061/JCCEAZ.0000639%20https://ascelibrary.org/doi/10.1061/JCCEAZ.0000639.

[49] Yue Wu et al. “Structural analysis and construction quality assessment of a free-form ice composite shell”. In: *Structures* 27 (Oct. 2020), pp. 868–878. ISSN: 2352-0124. DOI: 10.1016/J.ISTRUC.2020.06.032.

[50] *The Ice Shell Project*. URL: https://vimeo.com/channels/iceshellproject/.